TECHNISCHE UNIVERSITÄT MÜNCHEN
Lehrstuhl für Biochemische Pflanzenpathologie

Development of a novel TCR avidity assay for human CD8$^+$ T cells

Magdalena Nauerth

Vollständiger Abdruck der von der Fakultät Wissenschaftszentrum Weihenstephan für Ernährung, Landnutzung und Umwelt der Technischen Universität zur Erlangung des akademischen Grades eines

Doktors der Naturwissenschaften

genehmigten Dissertation.

Contents

List of Figures

Abbreviations

ACT	Ammoniumchloride/Tris
Ag	Antigen
α-MM	α-Methylmannopyranoside
APC	Allophycocyanin
APC	antigen presenting cell
APL	altered peptide ligand
APS	Ammoniumpersulfate
ATCC	American type culture collection
β_2m	beta-2-microglobuline
BSA	bovine serum albumin
CCR	receptor for CC-type chemokines
CD	cluster of differentiation
CDR	complementarity determining region
CFU	colony forming unit
CMV	Cytomegalovirus
ConA	Concanavalin A
^{51}Cr	Chromium-51
CTL	cytotoxic T lymphocyte
d	day
dH$_2$O	distilled, deionized water
DNA	Deoxyribonucleic acid
DTT	Dithiothreitol
EBV	Epstein-Barr virus
EDTA	Ethylendiaminetetraacetate
ELISPOT	enzyme linked immunospot technique
EMA	Ethidiummmonazidebromide
FACS	fluorescence activated cell sorting
FCS	fetal calf serum
FITC	Fluoresceinisothiocyanate
FPLC	fast protein liquid chromatography
h	hour
h	human
HIV	human immunodeficiency virus
HLA	human leukocyte antigen
HSCT	hematopoetic stem cell transplant
IC$_{50}$	peptide concentration mediating 50% IFN-γ production in ICCS
ICCS	intracellular cytokine staining
IFN	Interferon
Ig	Immunoglobulin
IL	Interleukin
IPTG	Isopropyl-β-D-thiogalactopyranoside
kDa	kilodalton
LB	Luria Bertoni medium
Lck	leukocyte-specific protein tyrosine kinase

LFA	leukocyte function-associated antigen
L.m.	*Listeria monocytogenes*
LSM	laser scanning microscope
m	murine
M	molar
MHC	major histocompatibility complex
min	minutes
OD	optical density
PAGE	polyacrylamide gel electrophoresis
PBMC	peripheral blood mononuclear cell
PCR	polymerase chain reaction
PBS	phosphate-buffered saline
PE	Phycoerythrin
PFA	Paraformaldehyde
pMHC	peptide loaded MHC molecule
PTLD	post-transplant lymphoproliferative disease
RNA	Ribonucleic acid
rpm	rounds per minute
RT	room temperature
RU	response unit
SDS	Sodiumdodecylsulfate
SPR	surface plasmon resonance
TAA	tumor-associated antigen
TBE	Tris/Borate/EDTA buffer
T_{CM}	central memory T cell
TCR	T cell receptor
TdT	terminal deoxynucleotide transferase
T_E	effector T cell
T_{EM}	effector memory T cell
TEMED	N,N,N,N-Tetramethylethylendiamine
T_H	T helper cell
TNF	tumor necrosis factor
Tris	Tris-(hydroxylmethyl)-aminomethane
$V\alpha/V\beta$	V alpha/V beta region of the TCR
ZAP-70	ζ-associated protein of 70 kDa

Chapter 1

Introduction

1.1 T cell immunity

The adaptive immune system has developed versatile response mechanisms against
the different life styles of pathogens. Lymphocytes can recognize defined structures
(antigens) of infectious agents, which in most cases results in their elimination and
life long protection against reinfection. Antibodies produced by B cells bind free
antigen and therefore primarily target extracellular pathogens and their toxic prod-
ucts. In contrast, antigens of intracellular pathogens or tumor cells have to be
processed and presented in the context of MHC molecules to be recognized by the
antigen receptor of T cells, called T cell receptor (TCR). The effector mechanisms
how T cells combat infected or abnormal cells and the interaction between the TCR
and its ligand will be elucidated in the next sections [1].

1.1.1 Cytotoxic T cells

T cells of the cellular immune system can be distinguished by the expression of the
cell surface molecules CD4 and CD8. $CD4^+$ T cells, also called T helper cells, acti-
vate macrophages (Th1 cells) or B cells (Th2 cells) that present the cognate antigen
on MHC II molecules and enable these cells to fight the infection. Besides Th1 and
Th2 cells, a third subset of T helper cells producing IL-17 has been recently discov-
ered. This so-called Th17 cells exhibit effector functions distinct from Th1 and Th2
cells and are therefore believed to clear pathogens that are insufficiently handled by
Th1 and Th2 cells. In addition, Th17 cells are potent inducers of tissue inflamma-
tion and could be shown to be involved in many experimental autoimmune diseases
and human inflammatory conditions [2]. The control of intracellular pathogens or
tumors on the other hand depends on the direct interaction of $CD8^+$ T cells and the
cells presenting the antigen on their surface. Upon antigen encounter, naive $CD8^+$
T cells proliferate and differentiate into effector cells, so-called cytotoxic T cells [1].
At the contact area between the $CD8^+$ T cells and the target cell, cell surface
molecules of T cell and antigen presenting cells are recruited into a highly organized
interface, the **immunological synapse**. Thereby, the surface receptors segregate
into three concentric compartments, the central, peripheral and distal supramolecu-
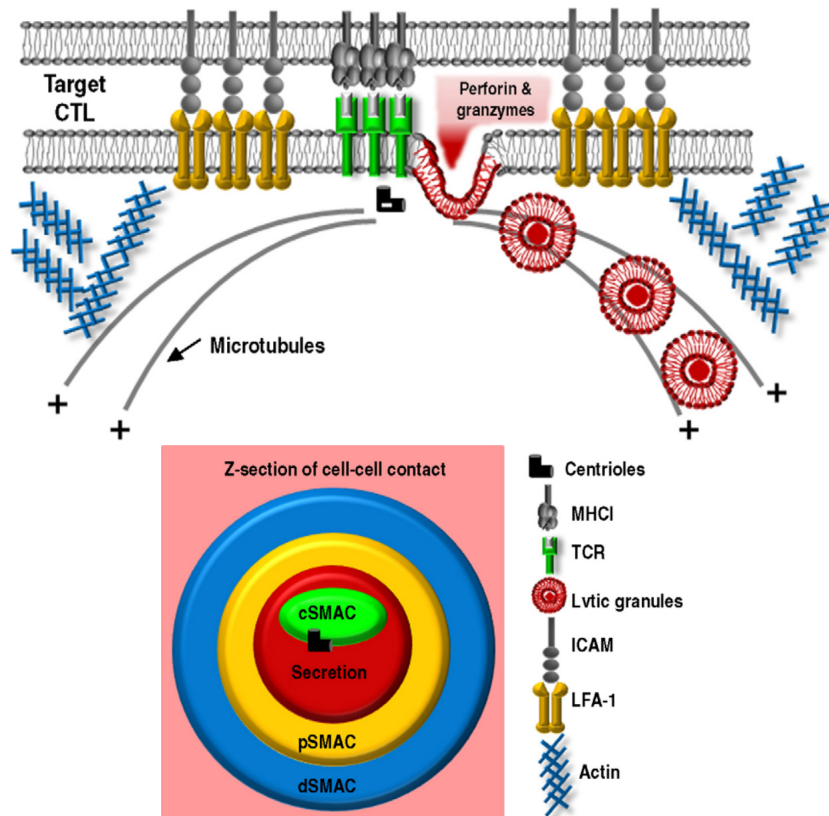
Figure 1.1: **Composition of the immunological synapse:** The schematic Z-section of the CTL-target cell contact area is shown in a lateral view (upper panel) and as top view with illustration of the ring-like assembly of the participating molecules (lower panel). Modified from [4]

lar activation complexes (SMACs)[3]. In the distal SMAC occurs actin accumulation and in the peripheral SMAC the binding between the antigen non specific adhesion molecules leukocyte function associated antigen 1 (LFA-1) on the T cell and the intracellular adhesion molecule (ICAM) on the target cell (Figure 1.1). However, the main site of TCR signaling is believed to be located in the central SMAC (cSMAC), as there TCRs and TCR associated signaling proteins including TCRζ, Lck, Zap-70 and PKCθ are enriched [4].

After signaling has occurred, polarization of the actin and microtubule cytoskeleton towards the synapse is a crucial step for cytotoxicity, as the release of effector molecules is focused at the site of contact with the target cell. The polarization is initialized by local reorganization of the actin cytoskeleton at the site of contact, which in turn causes the reorientation of the microtubule organizing center (MTOC) and of the Golgi apparatus (GA). Lytic granules derived from the GA migrate specifically towards the MTOC, which always contacts the plasma membrane at the cSMAC. Forming a secretory domain, the cytotoxic effector molecules contained in the granules are subsequently released at the plasma membrane, initiating the so called **"lethal hit"**[5, 6].

One of these cytotoxic effector molecules is perforin, which polymerizes in the membrane of the target cell to form pores. Water and salts can pass trough these pores, leading to osmotic lysis of the cell. However, for effective cell killing, another class of cytotoxic proteins called granzymes is necessary. The granzymes belong to the family of serine proteases and enter the target cell through the pores built by perforin and induce apoptosis of the cell. Besides perforine-mediated cytotoxicity, a perforine independent mechanism of T cell cytotoxicity exists. For example, the transmembrane receptor Fas-ligand (CD95L) that is also released from lytic granules, leads to the induction of apoptosis by binding to Fas (CD95) on the target cell [1, 6].

Also the release of cytokines by cytotoxic T cells contributes to host defense. Interferonγ (IFNγ) inhibits viral replication and acitvates other immune cells like macrophages and recruits them to the site of infection. Tumor necrosis factors α and β (TNFα and TNFβ) act in synergy with IFNγ to activate macrophages or to kill cells by binding to the surface receptor TNFR-I [1].

After elimination of a pathogen, most of the effector T cells rapidly die to prevent an overload of the immune system with a mass of "useless" cells. However, a small proportion of the T cells survives to become long-lived **memory T cells** that persists in the absence of antigen. In case of a secondary infection, memory T cells are immediately activated after antigen encounter followed by a rapid proliferation of specific T cells, resulting in protection against new expansion of the pathogen [7, 8]. Two subsets of memory T cells that can be distinguished by expression of different surface markers have been reported [9]. Central memory T cells (T_{CM}) show a high expression for the lymphoid homing receptors CCR7 and CD62L, whereas effector memory T cells (T_{EM}) show only a low expression of both receptors. T_{CM} are believed to be crucial for the long-lasting protective immunity, as they demonstrate a high proliferation potential after reinfection. However, the transition of T_{CM} into effector cells is often not quickly enough to confer protection, especially after infection with rapidly proliferating pathogens like Listeria monocytogenes [10, 11]. Hence, for immediate protective capacity against rapidly proliferating pathogens, T_{EM} have to be present in sufficient number at the site of infection [12, 13]. To answer the question, if the different T cell memory subsets have a common progenitor or developed independently, a single, naive antigen-specific CD8$^+$ T cell was transferred into a mouse followed by microbial challenge [14]. This led to clonal expansion and development of both effector and central memory T cell subsets, revealing the single naive T cell as common progenitor.

In summary, cytotoxic T cells recognize infected or abnormal cells specifically and are able to kill them efficiently and directed without causing damage to non infected cells. Persisting memory T cells are able to confer protection after re-challenge with the same pathogen. However, prerequisite for the effector functions is the successful binding of the T cell receptor to its ligand, the peptide loaded MHC complex.

1.1.2 TCR ligand interaction

The question how T cells recognize antigens and participate in the immune response had been basis for different theories and discussions in the history of immunological discoveries. After it had been shown that cells derived from the thymus, called

T cells, raised the efficiency of B cells in producing antibodies, T cells were thought to act in cell cooperation with B cells, recognizing one determinant of the antigen and then helping B cells to develop antibodies against a second determinant of the same molecule [15, 16]. However, this left the role of the major histocompatibility complex (MHC) unexplained, which was identified to be responsible for immune reactions against grafts or tumors. In addition, experiments revealed that T cells recognized antigens that were associated with cells rather than soluble [17]. The break-trough in the understanding of T cell antigen recognition came along with cell lysis experiments by Zinkernagel and Doherty in 1974. They found that T cells were only able to lyse infected cells *in vitro*, if the T cells and the target cells shared at least on set of H-2 antigenic specificities. This led them to the conclusion that T cells had to recognize both the antigen and the MHC molecule because probably "only in this situation, the necessary intimacy of contact" was achieved [18]. If two different T cell antigen receptors were involved in the recognition or if one single receptor bound both the antigen and the MHC was clarified with a dual TCR T cell hybrid experiment in 1981. T cells bearing two TCRs, specific for two different combinations of antigen (antigen a + MHC A and antigen b + MHC B) were not able to react with the mixed combinations (antigen a + MHC B and antigen b + MHC A), which showed that a single TCR had to react to a specific combination of antigen and MHC [19]. Since the first crystal structure of a TCR in 1996 was published, the architecture of TCR and MHC and their molecular interaction have been explored in detail.

1.1.2.1 TCR structure

Years before the first crystal structures, sequence analyses predicted that the TCR would resemble a membrane bound Fab-fragment of an antibody molecule [20, 21]. X-ray cystallographic analyses then confirmed that the structure of a TCR and a Fab-fragment share several common features [22, 23]. The TCR consists of two different transmembrane polypeptide chains, the T cell receptor α (TCRα) and the T cell receptor β (TCRβ) chain, linked by a disulfide bond. Both chains contain a variable (V) region and a constant (C) region, which show homology to the immunoglobulin V and C domain respectively (Figure 1.2). One motif, however, in the C region of the TCRα chain, shows unusual folding. Instead of the β sheet sandwich contained in antibodies or the Cβ region, where a disulfide bond connects two β sheets, the disulfide bond in the TCRα chain creates a helical structure, unlike that of any other immunoglobuline like domain. Adjacent to the C region follows a short hinge region that contains a cysteine residue to form the disulfide bond between α and β chain. Finally, each chain spans the lipid bilayer by a hydrophobic transmembrane region that ends in a short cytoplasmic tail [1]. Unusually, positively charged aminoacids are contained in the transmembrane region that serve to interact with the transmembrane regions of the invariant signaling chains CD3 and ξ to form the TCR complex [24].
The V regions of the α and β chain pair similarly to antibodies and form a region with high variability between different TCRs. Each chain contains three hypervariable loops, called complementarity-determining-regions (CDRs) which are located

(a)

(b)
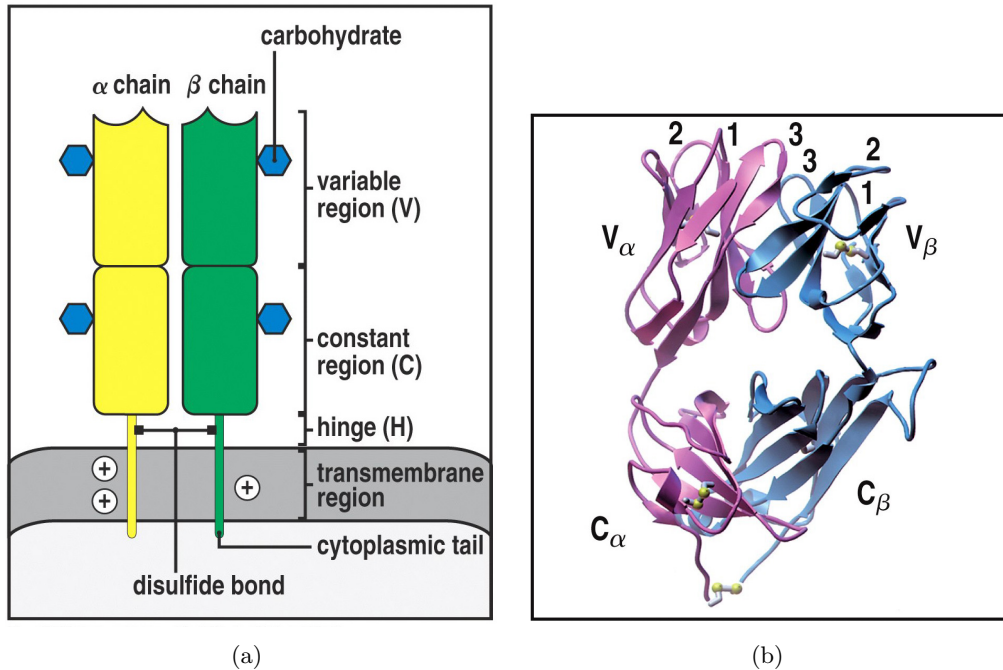
Figure 1.2: **Structure of the $\alpha\beta$T cell receptor:**(a) Schematic illustration of the different TCR domains and (b) crystal structure of an $\alpha\beta$T cell receptor resolved at 2.5Å. CDR loops are indicated by the numbers 1-3. (Modified from [1])

on a relatively flat top and form the antigen binding site. **Diversity** of the TCR repertoire is generated by somatic recombination of multiple gene segments for the α and β chain during maturation of a T cell. CDR1 and CDR2 of the human α and β chain are encoded by 42 Vα and 46 Vβ genes, the CDR3 is assembled after the joining of V- and J- gene segments in case of the α chain and after the joining of V-, D- and J-gene segments in case of the β chain. Beside the combination of different gene segments, the diversity is enhanced by the insertion of P- and N- nucleotides in the joining reactions. Thereby, the CDR3 region exhibits the highest diversity. This is in line with the structural models that propose the binding of the highly variable CDR3 to the (also highly variable) peptide, and the binding of the less variable CDR1 und CDR2 to the relatively less variable MHC molecule [20, 21, 25, 26].

1.1.2.2   MHC structure

The major histocompatibility complex (MHC) was originally identified in mice as the locus responsible for the acceptance or the rejection of transplants. It was shown in inbred strains of mice that differences in a single gene locus caused the rapid rejection of skin grafts, leading to the term "histocompatibility genes". Several closely linked and highly polymorphic genes turned out to be the main determinant for histocompatibility and are summarized in the term major histocompatibility complex [1]. Two classes of MHCs can be distinguished that are expressed on different cell types and bind different types of peptides.

MHC class I molecules are expressed on all body cells and present peptides from proteins degraded in the cytosol to CD8$^+$ T cells. The foreign cytosolic proteins originate from intracellular bacteria or viruses, and recognition of the peptide loaded MHC results in killing of the infected cell [27, 28]. MHC class II molecules are expressed on a more limited subset of cells, mainly antigen presenting cells that interact with CD4$^+$ T cells. In contrast to MHC I molecules, they bind peptides derived from extracellular antigens that were e.g. engulfed by macrophages. The recognition by CD4$^+$ T cells results amongst others in the activation of B cells and macrophages [28]. Besides the described classical MHC molecules, which show a highly polymorphic distribution, there are also nonclassical MHCs with little polymorphic variation. As the focus of this PhD work is on cytotoxic T cells, the next paragraphs will only describe the structure of MHC I molecules.

The human MHC I molecule consists of a transmembrane heavy chain glycoprotein of about 44kD, a soluble protein of 16kD, called the β_2-microglobulin (β_2m), and a peptide of 8-10 residues derived from cytosolic proteins. The binding site for the antigenic peptide consists of two α helices, the α1 and α2 domain, in the heavy chain, building a solvent exposed groove [29]. The α3 domain is located beneath the α1 and α2 and connects the heavy chain to the plasma membrane via its transmembrane region [27]. The association of the β_2m to the MHC occurs via noncovalent bindings to the heavy chain. It could be shown that the binding of the peptide to the binding groove is important to maintain the MHC I molecule stably assembled [30, 31], which is an essential requirement for the recognition by the specific TCR.

1.1.2.3 Molecular interaction of TCR and pMHC

The interaction between a TCR and its cognate pMHC ligand is crucial for different kinds of cell-cell encounters. As already discussed, the binding of TCR to pMHC is an important step for the initialization of T cell effector functions. Furthermore, TCR/pMHC interaction determines the TCR repertoire during T cell development in the thymus by positive and negative selection. In the periphery, TCR pMHC contacts are required to maintain T cell survival. Crystallographic studies revealed the precise structure of the TCR/peptide/MHC complex and elucidated e.g. the principles of viral antigen recognition, agonist and antagonist ligand recognition and mechanism of alloreactivity in graft rejection[32]. After the first crystal structure of an $\alpha\beta$ TCR with its cognate pMHC ligand in 1996, a sizable database of class I and class II TCR/pMHC complexes could be generated [33].

The **TCR/pMHC orientation** of different TCRs bound to pMHC I or pMHC II show slight variations, with the TCR positioned over the pMHC surface in an angle between 45° and 80° [32]. Differences in orientation depend on global parameters like the twist, tilt and shift of the TCR over the pMHC surface [34], the different angles between the Vα and the Vβ domains and the conformation and length of the CDR loops. However, there is a common docking mode for both murine and human TCR/pMHC complexes. The Vα domain of the TCR is always located closer to the N-terminal end of the antigenic peptide, whereas the Vβ domain is closer to the C-term of the peptide. This results in a diagonal orientation of the TCR over the pMHC surface. The diagonal orientation serves apparently to generate

distance to the N-terminal regions of the antiparallel αhelices of the MHC, which represent the highest point of the pMHC surface. As the TCR surface is relatively flat, binding between these highpoints of the MHC α helices allows for a large interface between TCR and pMHC [23, 28]. The hypothetical structure of the $\alpha\beta$ TCR/pMHC/CD3$\epsilon\delta$/CD3$\epsilon\gamma$/CD8 complex is illustrated in Figure 1.3. The CDR2 regions of the TCR α and β chains only contact the MHC molecule, while the CDR1 and CDR3 loops bind both to the MHC molecule and the peptide. As the CDR3 loop shows the highest variability (s.1.1.2.1), it was already suspected to bind to the most variable part of the pMHC complex, the antigenic peptide. Later this could be verified for the most structures where the centrally located CDR3 loop dominates the interaction with the pMHC complex.

Even if there is a known **TCR footprint** on the pMHC surface, it is not possible to predict, which aminoacids of the pMHC complex are actually contacted. From the crystal structures of TCR/pMHC complexes, 31 aminoacids are known to be potential binding partners. However, only about half of them are actually involved in the interaction in each single complex, and this pattern is changed to only one common amino acid even in contacts between the same pMHC molecule and different TCRs [23, 35]. This effect is caused by differences in orientation of the TCR towards the pMHC complex (see paragraph above). To predict these global parameters or the details of binding based on the sequences of the TCR and the pMHC complex is not possible at present, although common features have been found between different structures [36, 37].

The apparent paradox that MHC complexes contain conserved residues but the binding of the TCRs is not conserved led to the development of different hypotheses. The theory of a **combinatoral mechanism** suggests that different TCRs contact different subsets of MHCs, as there are many different conserved MHC residues and many different genes encoding for TCRs [32]. However, even TCR with identical CDR1 and CDR2 loops were shown to interact differently with MHC molecules [22, 34, 35]. An alternative theory proposes that a **selection of signaling competent TCRs** occurred in the coevolution of TCRs and MHCs. Any binding mode necessary to initiate signaling would be preserved, independent of the amino acid sequence. Huseby et al. showed that TCRs have to interact with certain 'hot spots' of TCR binding on the MHC side chains to escape negative selection in the thymus. Furthermore, some pMHC residues contributed to TCR specificity, even when the side chain did not contribute to binding affinity. These 'interruptive side chains' give a hint why TCRs preferentially bind a subset of amino acids in a given pMHC position [38].

The **recognition of foreign antigen** by the TCR is limited to about one-third of the whole peptide, as the other parts of the MHC bound peptide are buried and not accessible for TCR binding. In some cases, the TCR contacts the peptide side chain over a relatively flat surface. In other cases, residues of the peptide are surrounded by a a central cavity in the TCR built by the CDR3 loops of the Vα and the Vβ chains [39]. As the number of contacts between TCR and antigenic peptides is limited, **crossreactivity** could occur by the binding of one identical TCR to different peptides bound to the same MHC. The effect on the outcome of the signaling was tested with altered peptide ligands (APL), i.e. peptides with

single amino acid substitutions. It could be shown that minor changes in the peptide sequence, even in amino acids not directly involved in TCR binding, could turn a strong agonist pMHC ligand into a weak agonistic or even an antagonistic ligand [40]. Minor structural changes in the TCR/peptide interface, also termed **induced fit**, could be observed in structural studies of three TCR/APL/MHC complexes [41]. These changes had no effect on the outer surface of the TCR, and the magnitude of the structural refitting and the signaling outcome could not be correlated [42]. These results are in line with suggestions that the tightness and duration of TCR binding and not different conformations in the TCR/pMHC complexes are responsible for different signaling outcome [43].

As mentioned at the beginning of this section, grafted cells expressing foreign MHC molecules are quickly rejected by the immune system. This reactions is executed by **alloreactive T cells**, i.e. T cells recognizing foreign MHCs. Remarkably, up to 10% of peripheral T cells take part in such an alloreaction, an impressive amount compared to about 1% of peripheral T cell responding normally to viral challenge [44]. Two models have been proposed to explain this high reactivity. One explanation is that the TCR binds in an alloreaction mainly to the polymorphic and conserved residues of the allo-MHC molecule. An alternative model suggests that many new self-peptide MHC ligands are generated, as the allo-MHC is able to bind new constellations of self peptides. Because the allo-MHCs is not present during thymic selection, T cells would not have been eliminated by negative selection against these new complexes. Crystal structures of TCRs bound to allo MHCs showed that the TCR binds both to the peptide and to the MHC complex and thus favor the second model [45]. Also other models support the conclusion that the principle of allo-recognition is similar to other TCR reaction, and the higher frequency of recruited T cells is just caused by the generation of novel peptide/allo-MHC complexes [36, 46].

1.1.2.4 Assembly of the TCR complex

Beside the interaction between TCR and its cognate pMHC ligand, several further interactions take place to assemble the immunological synapse (s. chapter 1.1.1). Thereby, a signaling competent complex is initialized by the interaction of TCRs, its coreceptors CD4 or CD8 and additional signaling molecules like CD3. The following section will summarize our current knowledge on the role of CD3 and CD8 in the TCR-ligand interaction of CD8$^+$ T cells.

The TCR is able to recognize and bind its pMHC ligand, but cannot signal to the cell. To achieve signal transduction, the $\alpha\beta$ TCR chains are associated with six accessory chains, called the **CD3 signaling module**. The subunits δ, ϵ, γ and ζ are non covalently associated to form the $\zeta\zeta$ homodimer and the heterodimers CD3$\epsilon\delta$ and CD3$\epsilon\gamma$ [33, 47, 48]. Each CD3 chain contains one, each ζ chain three ITAMs (immunoreceptor tyrosine-based activation motifs), that serve for the intracellular signal transduction [1]. Conformational changes in the CD3ϵ subunit are assumed to be critical for early TCR signaling events [49]. Furthermore, normal development of the $\alpha\beta$ TCR and its stable expression on the cell surface depend on the presence of CD3 components [50, 51]. The hypothetical structure of the $\alpha\beta$

Figure 1.3: **Hypothetical TCR/pMHC/CD3$\epsilon\delta$/CD3$\epsilon\gamma$/CD8 complex:** The TCR/pMHC-CD8$\alpha\alpha$ and putative CD8$\alpha\beta$ interaction is modeled by superimposing two structures, the HLA-A2/CD8$\alpha\alpha$ complex and the TCR A6/HLA-A2/Tax P6A complex on their MHC residues α1180, with TCR (green), MHC (darkblue), peptide (red) and CD8 (yellow and orange). The CD3 $\epsilon\delta$ (pink and blue) and CD3$\epsilon\gamma$ (gold and blue) are shown docked at the top of the figure, with the common ϵ-chains colored in blue. Lines are drawn in to depict tethers connecting the different subunits to the TCR cell membrane (top, green) or the antigen-presenting cell membrane (brown, bottom). (Modified from [33])

TCR/pMHC/CD3$\epsilon\delta$/CD3$\epsilon\gamma$/CD8 complex is illustrated in Figure 1.3.

The interaction of **the CD8 coreceptor** with the pMHC complex is a critical step for the development and function of cytotoxic T cells. Cell surface expressed CD8 is either assembled as the homodimer CD8$\alpha\alpha$ or the heterodimer CD8$\alpha\beta$ [52, 53]. Crystal structures of CD8$\alpha\alpha$ with pMHC complexes revealed the binding of the CD8 homodimer to the α_3 domain of the MHC molecule in an antibody-like fashion [54, 55]. The determination of a crystal structure of the CD8$\alpha\beta$ heterodimer turned out to be more difficult [33]. The Ig-like domains of mouse CD8$\alpha\alpha$ and CD8$\alpha\beta$ are similar in size, shape and electrostatical potential of their pMHC I binding regions, suggesting a similar interaction of both CD8 variants with pMHC I [56, 57]. However, despite the structural similarity, CD8$\alpha\alpha$ and CD8$\alpha\beta$ show remarkable differences concerning tissue distribution, ligand specificity and efficiency of antigen presentation [58, 59]. CD8$\alpha\alpha$ shows a broad expression, including $\alpha\beta$ TCR$^+$ and $\gamma\delta$ TCR$^+$ intestinal lymphocytes, natural killer cells and dendritic cells, whereas CD8$\alpha\beta$ is mainly expressed on the surface of $\alpha\beta$ TCR$^+$ T cells and can be considered as the true $\alpha\beta$ TCR coreceptor [33, 56]. The enhancing effect of CD8$\alpha\beta$ to early T cell acitivation is mediated by different mechanisms [60, 61]: (1) CD8$\alpha\beta$ localizes the TCR to membrane domains that are believed to be privileged site for TCR signal transduction [62], (2) it recruits essential signaling molecules to the intracellular site

of the TCR/CD3/ζ complex [63, 64] and (3) it stabilizes the TCR-pMHC interaction at the cell surface approximately tenfold [65–67]. Furthermore, CD8 was shown to influence both the on-rate (k_{on})and the off-rate (k_{off}) of TCR-pMHC binding [68–70]. Studies demonstated that those kinetic parameters determine the consequences of antigen engagement on the functional level [71–73], also termed T cell avidity.

1.2 T cell avidity

As summarized in the previous sections, CD8$^+$ T cells recognize their targets specifically by binding with the TCR to their cognate pMHC ligand. An intracellular signaling cascade is initialized, leading to effector functions of the T cells. Thus, CD8$^+$ T cells play a crucial role in clearing viral infections or combating malignant cells. But not only the quantity of specific T cells seems to be important. A growing number of studies supports the assumption that the quality of the CD8$^+$ T cells plays a decisive role for the efficacy of the T cell response [74–78].

1.2.1 Definition

The quality of a T cell is often described as T cell avidity, which can be defined as the efficiency how a T cell reacts to antigen encounter. The avidity is mostly measured by determining the amount of peptide ligand required to induce T cell proliferation or effector functions. Thereby, T cells that recognize target cells presenting low amount of peptide are termed high avidity, T cell responding only to high amounts of peptide are termed low avidity T cells [79]. The knowledge of the different peptide sensitivity has changed the way to elicit and expand cytotoxic T cells: before, increasing amounts of peptide were used to yield stronger CTL responses. But these strong responses relied mainly on the activation of large numbers of peptide-specific T cells [80]. After it could be shown that not only the number but also the quality of the induced T cells played an important role for the efficiency of the CTL response, the differential sensitivity of T cells to peptide ligand has been used to expand cells of defined avidity *in vitro* [74, 81]. A greater efficacy of high avidity T cells has been shown ever since both in viral [74, 82, 83] and in tumor systems [77, 84].

1.2.2 T cell avidity and tolerance

While highly reactive T cells are believed to be beneficial for immune responses against pathogens or malignant cells, they can become harmful when recognizing components of the host, leading to severe tissue damage and autoimmunity. To prevent this, several mechanisms have evolved to induce T cell tolerance to body tissue.

1.2.2.1 Central tolerance

The development of $\alpha\beta$ T cells relies on the interaction with self-MHC molecules in the thymus. Self-antigen MHC complexes are presented by bone marrow derived
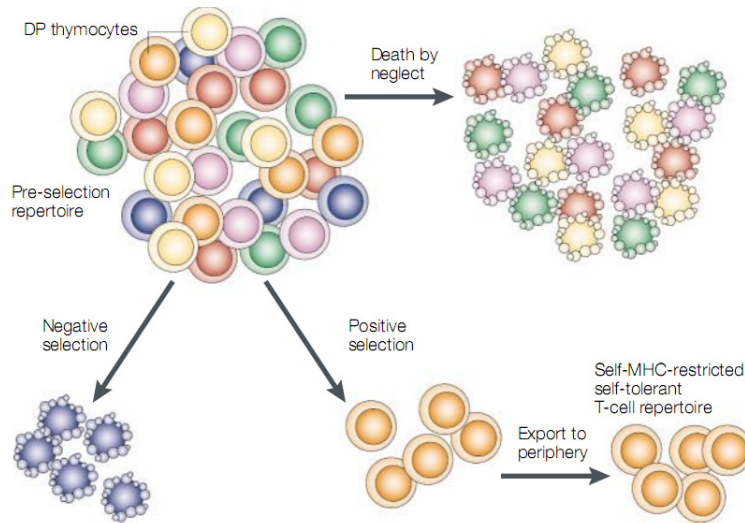
Figure 1.4: **Selection of mature T cells from thymocytes:** CD4$^+$CD8$^+$ double positive (DP) thymocytes expressing a TCR with high affinity for self-peptideMHC ligands undergo apoptosis (negative selection), DP cells recoginzing self-peptideMHC ligands with low affinity differentiate into CD4$^+$ or CD8$^+$ single positive (SP) thymocytes (positive selection). The repertoire of peripheral T cells that has survived both positive and negative selection is both self-MHC restricted and self-tolerant [86].

antigen presenting dendritic cells (DC). Those cells are able to present both endogenously and exogenously expressed antigens on their surface, using a mechanism called cross-presentation to aquire antigens from phagocytic compartments [85]. In addition to DCs, also thymic epithelial cells (TECs) play an important role in presenting antigen in the thymus. TECs express the autoimmune regulator (AIRE) gene, which enables them to synthesize and express many peripheral tissue antigens that would otherwise not be available in the thymus [86, 87].

In the so-called positive selection, thymocytes have to recognize antigens bound to self-MHC molecules to ensure that these cells will be able to mount an immune response. This interaction both rescues thymocytes from apoptosis and induces their differentiation into mature T cells [1]. In a further step, called clonal deletion, T cells with self-reactive receptors have to be eliminated to prevent the maturation of autoreactive T cells (negative selection) (Figure 1.4) [88–90]. These two pathways of self-MHC restriction and self-tolerance are both initiated by the engagement of the TCR with MHC:self:peptide complexes, but lead to totally different outcomes. How can these superficially similar events be distinguished?

Two hypothesis have been proposed to explain these differences [1]: in the **qualitative signaling hypothesis**, the nature of the signal delivered by the TCR is decisive. Positive and negative selection are induced by different pMHC complexes, leading to qualitative different signals evoked by conformational or spatial changes in the TCR or modulation of the signal transduction by associated molecules [91, 92]. In contrast, the **avidity hypothesis** claims that the outcome of pMHC binding by the TCR is dependent on the strength of the signal delivered by the receptor and

coreceptor. This binding strength in turn depends on the affinity of the TCR to the pMHC complex and the density of the complex on thymic cortical epithelial cells [1]. A weak signal will rescue the thymocyte from apoptosis and positively select it, a strong signal accordingly to apoptosis and thus negative selection. It could be shown that very small differences in the affinity of the TCR to the presented pMHC are sufficient to alter the fate of the developing thymocyte [93]. Affinity models for signal transduction are e.g. the kinetic proofreading [94] and the discrimination model [72]. In these models, small differences in affinity are able to induce large differences in outcome due to the complexity of the signaling process [94] or the ratio of complete (positive) to incomplete (negative) signals [72].

1.2.2.2 Peripheral tolerance

Central tolerance mechanisms lead to the elimination of T cells that recognize self pMHC complexes with high avidity. But for several reasons, additional tolerance mechanisms in the periphery are necessary to fully prevent autoimmunity. First, immune responses to harmless environmental antigens that are acquired over the diet or the environment have to be avoided [95]. Second, central tolerance is not complete, as not all antigens are expressed by the activity of AIRE in the thymus. And third, T cells that recognize self pMHC complexes with low avidity are not depleted by negative selection and should remain ignorant in the periphery [96]. Changes in the stimulatory milieu, however, can stimulate those T cells and break their ignorance [97]. The induction of tolerance to potentially autoreactive T cells depends on different mechanisms: the suppression by regulatory T cells (T_{reg}), the activation status of antigen-presenting DCs and the persistence of antigen [87, 98]. Naturally occurring T_{reg}s were shown to express beside CD4 the high-affinity IL-2 receptor α chain (CD25), as their growth and survival is strictly dependent on the presence of IL-2. $CD4^+CD25^+$ T_{reg}s develop in the thymus and show a diverse TCR repertoire. During thymic selection, the development of $CD4^+CD25^+$ T_{reg}s requires a higher avidity interaction of their TCR with self pMHC molecules expressed on cortial epithelial cell than required for normal positive selection. This led to the suggestion that low avidity interaction in the thymus would lead to T cell survival, high avidity interactions to negative selection and intermediate interactions to the development of regulatory T cells [99]. T_{reg}s are suggested to act over the secretion of cytokines, including TGF-β and IL-10, and over direct cell-cell-contact. Thereby, T_{reg}s act on T cells that bind with high avidity to pMHCs on the same APC as the T_{reg} [100–102]. Finally, it could be shown that T_{reg}s are also able to modify APC function and make them unable to activate T cells [103].

Dendritic cells acquire antigen in the periphery and present it subsequently to T cells circulating in secondary lymphoid organs. T cells with high avidity for the presented antigen can be thereby activated. In the absence of pathogens, however, DC express only low levels of costimulatory molecules like B7.1 or B7.2, which interact with CD28 on T cells [104, 105]. High avidity recognition of Ag by T cells without the costimulation through CD28 results only in a short proliferation period and diminished effector functions [106, 107]. In the end, T cell tolerance is induced either by deletion or anergy of the T cell.
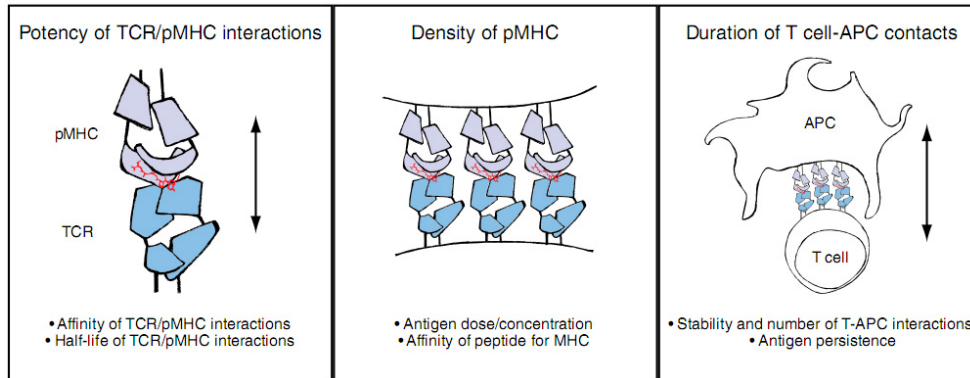
Figure 1.5: **Variables influencing the strength of TCR activation:** Several parameters contribute to the strength of TCR stimulation: biochemical parameters of TCR-pMHC interactions, such as affinity and $t_{1/2}$, density of pMHC ligand, and temporal components, including duration of T cell-APC interactions and Ag persistence [116].

1.2.3 T cell avidity in immune responses

To undergo positive selection in the thymus, the TCR has to bind to a MHC complex with sufficient affinity. In the periphery, the T cell is activated by recognition of an antigenic pMHC by the TCR and an immune response is elicited. This demonstrates that the TCR-ligand binding is different from the common scheme of most protein-protein interactions, as a single TCR can bind to many different ligands [108]. Variants of antigenic peptide/MHC ligands can induce drastically different T cell responses, which leads to the classification of those ligands as TCR partial agonistis or antagonists [109–111]. In most of the cases, the spectrum of biological and clinical processes is correlated with the binding strength between the TCR and the cognate pMHC ligand. Thereby, a ligand with a higher affinity to the TCR is superior in inducing immune responses [112, 113]. The next sections will summarize our current knowledge on the impact of T cell avidity on different aspects of the T cell response.

1.2.3.1 T cell activation and recruitment

Whether TCR-pMHC interaction leads to complete T cell activation seems to be strongly dependent on the affinity of the ligand to the TCR. As already mentioned in section 1.2.2.1, the kinetic proofreading and the kinetic discrimination model try to explain how subtle differences in TCR-ligand affinities can lead to different outcomes. They refer to the duration of TCR-ligand interaction that is necessary for a T cell to commit to complete activation events [72, 94, 109, 114, 115]. Several factors that influence the strength of TCR-pMHC interaction are illustrated in Figure 1.5.

According to those kinetic models, ligands exhibiting low affinity for the TCR, and thereby fast off-rates of the TCR, would only be able to provoke early T cell activation events, but would not allow the T cell to commit to later activation events. Hence, low avidity TCR-ligand interactions would only lead to an incomplete T cell response or even totally inhibit it. A longer TCR interaction, however, would pro-

mote a complete T cell activation and thereby a successful T cell response. The basic concept of this assumption is that a minimum time is required for the formation of fully functional signaling complexes, which could allow the T cell to discriminate between low and high affinity ligands.

Several studies have examined the differences in early activation events in detail [116]. One way to monitor early T cell activation is to measure the concentration of intracellular Ca^{2+} after TCR-ligand interaction. If this interaction is relatively short, the increase in Ca^{2+} concentration is delayed [117]. In a more detailed study with tumor-reactive T cells, interaction with high affinity ligands induced continuous Ca^{2+} efflux and complete usage of the Ca^{2+} stored in the endoplasmatic reticulum. However, low affinity TCR-ligand interaction resulted in oscillating Ca^{2+} efflux and only partial emptying of the stored Ca^{2+} [118]. Also the recruitment of CD3ζ to the immunological synapse is an indicator for early T cell activation. This recruitment was shown to be delayed after shorter TCR-ligand interaction. However, if the synapse was observed over a longer time period, similar levels of CD3ζ were accumulated [119]. Also other studies indicate that weak pMHC ligands interaction lead to delayed but often comparable response if enough time was given [116, 120].

in vivo studies with different pathogen doses revealed how the differences in T cell activation affect the recruitment of T cell clones with different avidities to the immune response. During the early stage of the immune response, the TCR diversity of the activated T cells was comparable to the naive repertoire [121, 122]. However, at the peak of the immune response, the TCR repertoire shifted towards higher affinity clones [121]. Confirming these findings, further data could show that low affinity TCR-ligand interactions results in early T cell activation *in vivo*, but undergo premature contraction [120]. In addition, Busch and Pamer showed in the Listeria monocytogenes infection model that the functional avidity of antigen-specific T cells was higher in a secondary infection compared to primary infection. This effect was correlated with a focusing of the T cell repertoire to higher affinity TCRs in the secondary infection [123]. Taken together, these studies suggest that immune system maximizes its reactivity to invading pathogens by favoring the complete recruitment of high affinity T cell clones. Remarkably, this participation of high affinity clones was highly efficient even at low pathogen doses [124].

1.2.3.2 Peptide specificity

To result in any T cell activation (complete or incomplete), the TCR-pMHC interaction has to achieve a minimum threshold for TCR binding. The peptide specificity of a TCR can strongly influence the outcome of this interaction, as minor changes in the peptide sequence could lower the binding affinity and result in an interaction energy below the minimum threshold [108, 125]. In this context, T cells with low affinity TCRs seem to be more specific, as minor alterations in the peptide sequence could result in complete loss of T cell activation. T cells with higher affinity TCRs, however, would be able to get activated even after stronger reduction of the interaction energy and therefore tolerate more changes in the peptide sequence. Hence, high affinity TCRs show a reduced peptide specificity [126]. In primary immune responses, the low affinity TCRs show the advantage to be very peptide specific,

but are not able to recognize and eliminate peptide variant arising e.g. after virus mutations. After immunization, an increase of the overall T cell avidity can be observed, which could provide the immune system with the ability to react to peptide variants [126–128].

1.2.3.3 Protection

As discussed, high avidity T cells are more efficient in activating T cells and initiating immune responses. Several studies could show that this ability directly affects the capacity of the T cells to confer protection against viral infections [74, 83] or tumors [77, 84]. Thereby, high avidity CTL turned out to be much more effective in reducing viral load than the same number of low avidity CTLs, even though both were able to recognize the target [74]. Low avidity CTLs remained to be less capable of reducing viral burden, even when the number of transferred CTLs was increased 3fold or more time was given. Derby et al. found two complementary mechanisms underlying this increased efficiency: high avidity CTL both recognize their target cells earlier and initiate the lysis of those cells earlier [82]. The different effectiveness of low versus high avidity T cells *in vivo* could be due to the different amounts of viral antigen required for the recognition of target cells. It was postulated that CTLs that are able to recognize and lyse their target cells earlier in the course of infection might be more efficient in achieving viral clearance than CTLs that recognize their target cells when the infection is already progressed [129–131]. Consequently, if low avidity CTLs require high Ag densities on the infected cell that are only achieved shortly before the release of newly assembled virus, it is unlikely that the CTLs are able to control the infection. In addition, low avidity T cells exhibit a delay in the onset of their lytic activity, most probably due to inherent differences in the efficiency of TCR signaling. The rates of lysis are comparable, but as mentioned before, the delayed initiation allows the infection to progress and makes it therefore harder to control. The differences in the onset of lytic activity of low versus high avidity T cells can be explained with differences in TCR affinity. The onset might require some threshold of TCR molecules that have to be engaged or aggregated [132], or serially triggered [133, 134]. Since it can be assumed that the TCR-pMHC interaction of low avidity T cells has a much shorter average dwell time, the encounter of the TCR with its ligand might not be long enough to provoke productive TCR signaling. In conclusion, the early recognition and elimination of target cells by high avidity T cells prevents the accumulation of virus in the cells and enables the T cell to control the progress of the infection.

1.2.4 Measuring T cell avidity

The previous sections have demonstrated that T cell avidity is an important parameter for judging T cell quality, as it strongly affects the outcome of a T cell response. However, the term T cell avidity often describes the results of completely different readout systems. The so-called 'functional avidity' is mostly determined by measuring the sensitivity of antigen recognition, i.e. the amount of peptide required to provoke T cell proliferation or effector functions. However, T cell avidity can be also

described as 'structural avidity', which is defined by the affinity of the TCR to the pMHC molecules combined with the affinities of the coreceptors CD8 or CD4. For the measurement of the functional and the structural avidity, respectively, several different methods exist.

1.2.4.1 Functional avidity assays

The functional avidity of a T cell is influenced by a variety of different factors. Thus, it can be altered by change of the expression of adhesion molecules, components in the T cell signaling cascade or TCR coreceptors. It could be shown that the functional avidity of a T cell is controlled by the expression of CD8$\alpha\alpha$ versus CD8$\alpha\beta$. On high avidity T cells, higher expression of the CD8$\alpha\beta$ heterodimer was found, which promoted the increased colocalization of CD8 with the TCR in lipid rafts [135, 136]. Besides CD8, also the expression levels of other molecules as LFA, ZAP-70, Lck or the TCR, have the potential to influence the functional avidity of a T cell. However, to take part in successful T cell activation, the right localization in the immunological synapse is of great importance for all mentioned molecules. Hence, optimal localization of membrane molecules, achieved by their recruitment into lipid rafts, leads to high functional avidity of the T cell [135].

The determination of functional avidity is mostly done *in vitro* by stimulating T cells with APCs that are loaded with graded concentrations of peptide. As a readout, effector functions like IFNγ production or lysis of peptide pulsed cells is measured [74].

Intracellular cytokine staining

Among the diverse methods to determine the cytokine production of a T cell, the intracellular cytokine staining (ICCS) is one of the most commonly used assays beside ELISA and the ELISpot assay. The detection of antigen-specific T cells by ICCS is based on the combination of a fixation and permeabilization method with the use of directly labeled monoclonal anti-cytokine antibodies [137]. In the first step, the target cells are stimulated in an antigen-specific manner, e.g. by incubation with peptide pulsed APCs to induce cytokine production. After two hours, Brefeldin A is added to the cells. Brefeldin A interferes with the retrograde transport of proteins from the golgi apparatus to the endoplasmatic reticulum (ER), which leads to accumulation of proteins in the ER. This means for the ICCS that cytokines are enriched in the stimulated T cell. The stimulation is continued for additional 3h, followed by staining the T cells for surface markers with fluorescence labeled antibodies. The cells are subsequently fixed, permeabilized and stained with fluorescence-labeled antibodies against intracellular accumulated cyokines like IFNγ, TNFα or IL-2. After the staining, the surface and the cytokine staining of the T cells can be analyzed by flow cytometry. To determine the functional avidity of a T cell population, the amount of peptide used for stimulation is titrated and subsequently the percentage of cytokine producing cells is displayed versus the peptide concentration. To obtain a comparable parameter, the peptide concentration needed to stimulate 50% of all reacting T cells, defined as IC$_{50}$, is calculated.

^{51}Chromium release assay

Another broadly applied method to determine the functional avidity is the ^{51}Chromium release assay. This assay measures the direct effector functions of the T cells by detection of the antigen specific lysis of peptide pulsed target cells [138], which were labeled with the γ radiating isotope ^{51}Cr and loaded with peptide. T cells and target cells are incubated together in a defined effector:target ratio for 4-5 hours, which leads to lysis of the target cells and thereby release of ^{51}Cr into the supernatant. The amount of released ^{51}Cr can be quantified with a γ counter and is proportional to the number of lysed target cells. Hence, the efficiency of target cell killing and thereby the extent of effector functions of the T cell population can be analyzed. By titrating the amount of peptide used to load the target cells, the functional avidity of the T cell population can be calculated analogous to the approach described for the ICCS. The extent of ^{51}Cr release is plotted as 'percentage of maximal lysis' versus the peptide concentration used to load the target cells and 50% of specific lysis (EC_{50}) are calculated as a comparable parameter.

A major advantage of the described methods to determine the functional avidity of T cells is that they are easy to standardize and transferable into different laboratories. Hence, the obtained results provide good worldwide comparability. However, it is not possible to measure the functional avidity of a single cell, as whole populations are needed to perform the described peptide titrations. Furthermore, as the functional avidity of a T cell is influenced by many factors and can be changed e.g. due to culturing conditions, it might be of interest to measure a parameter, which is hard-wired within the T cell.

1.2.4.2   Assays for structural avidity

The structural avidity of a T cell depends on the binding strength between TCR, pMHC and the coreceptors CD8 or CD4. These components interact by electrostatic forces, hydrogen bonds, van der Waals forces and hydrophobic interactions, i.e. physical parameters that are hard wired in the structures of the proteins and thus invariant. T cell transfer experiments suggest that an important part of T cell functionality is hard wired within the structure of the TCR. However, it is challenging to exactly measure these physical parameters on living T cells. Using different methods it has been attempted to get information about the structural avidity of a T cell.

Biacore assay

To study the biomolecular interactions between TCR and pMHC, the Biacore system has been widely used. It is based on the principle of surface plasmon resonance (SPR) [139, 140] and allows to characterize binding events of samples of different nature like proteins, nucleic acids, lipid vesicles, bacteria etc. [141]. With Biacore, among others the specificity, strength, k_{on}-rate and k_{off}-rate of protein interactions can be analyzed. The Biacore optical biosensors are built of three core components: an optical detector systems that monitors the changes in the SPR signal, a sensor chip which can be coated with one of the interacting molecules, and a microfluidic system that controls the buffer and sample flow over the sensor chip. To understand

(a)   (b)
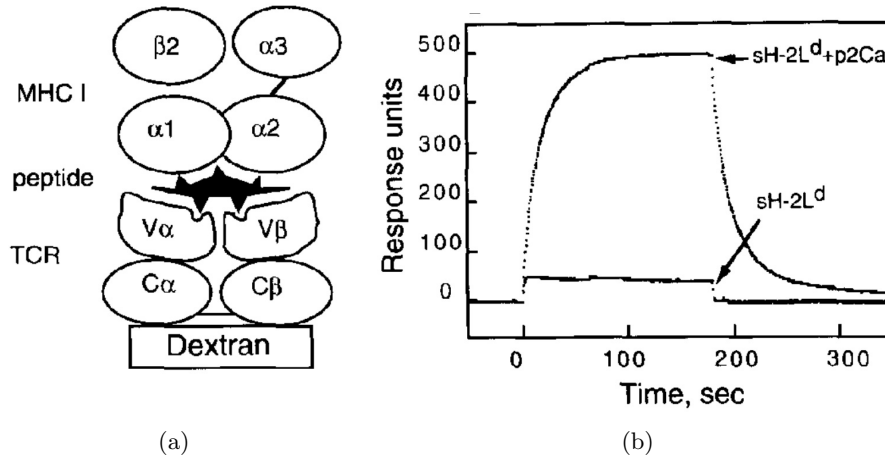
Figure 1.6: **Binding of MHC I-peptide complexes to TCR-coupled biosensor surface:** (a) Schematic illustration of the interaction of a TCR covalently coupled to the surface with its cognate MHC-peptide complex. (b) Typical SPR binding curve using the example of sH-2Ld complexed with or without p2Ca peptide binding to the 2C TCR immobilized on the surface. [142]

the basic mechanisms of this method, the principle of SPR will be explained in the following. Surface plasmon resonance is an optical phenomenon that occurs in general in thin conducting layers at the interface between two media with different refractive indices. For the Biacore setup, a thin gold layer on the sensor chip is located between the glass surface of the sensor chip and the sample solution flowing through the microfluidic system. Polarized light traveling through the glass surface of the chip is totally reflected at the interface to the sample solution, as the optical density of this medium is reduced compared to that of the glass surface. The intensity of the reflected light is monitored by a diode array detector. The evanescent wave, a electromagnetic component of the light, however, can pass across the gold layer into the sample/buffer solution. At a defined angle, the evanescent wave is able to excite electrons in the gold layer, resulting in electron charge density waves, so called surface plasmons. Concomitantly, the light intensity at this angle (SPR angle) is reduced. Binding between the interaction partner and the sample immobilized on the sensor chip surface changes the mass on the surface and thereby provokes a shift in the SPR angle of the reflected light. Those changes are measured in resonance units (RU) with 1 RU corresponding to $0.0001°$ shift in SPR angle. 1000 RU correspond to the surface concentration change of about 1 ng/mm^2 of an average protein, which means that the method is quite sensitive and allows for the analysis of weak macromolar interactions. The gold layer is covered with a hydrogel matrix, on which one of the interacting components is covalently immobilized whereas the other component is passed over the chip in solution. As the changes of the SPR angle are monitored in real time, association, duration and dissociation of the interaction are visualized (Figure 1.6 [140]).

Due to its high sensitivity for low affinity events, the Biacore assay has often been used to analyze the interaction of purified TCR with its pMHC ligand [142]. Corr

et al. used SPR for the first time to analyze the specificity, kinetics and affinity of the interaction of the 2C TCR with H2Ld peptide complexes [143]. For these experiments, the TCR was covalently coupled to the biosensor surface, which could be shown to maintain the integrity and specificity of the TCR structure. Among different tested H2Ld peptide complexes, the 2C TCR turned out to bind only to H2Ld complexed with p2Ca peptide, derived from 2-oxoglutarate dehydrogase. Dissociation kinetics done with this setup revealed a high k_{off}-rate ($0.026s^{-1}$) of the TCR pMHC complex, which corresponds to a half life time of $\sim 27s$, and a K_d of $\sim 10^{-7}$M. Another study analyzing the binding of the 2C TCR to its different ligands H2-K^b/dEV8, H-2K^{bm3}/dEV8, H2-K^b/SIYR and H-2L^d/p2Ca found affinities in the range of $K_d= 10^{-4}$ to 10^{-6} for the syngeneic (H2-K^b) and allogeneic (H-2K^{bm3}, H-2L^d) ligands [144]. To correlate the immunological activity of a T cell with the affinity of the TCR to its cognate pMHC complex, studies were done on a large set of synthetic peptides that contained single aminoacid mutations based on the p2Ca sequence. The mutated peptides were analyzed for H-2L^d binding stability, induction of lysis of target cells expressing H-2L^d and the respective peptide variant and binding of the H-2L^d peptide complexes to the purified soluble 2C TCR [145]. Although for most of the peptides, a clear correlation between the ability to sensitize 2C T cells for cytolysis and the affinity of the 2C TCR to the respective H-2L^d peptide complex could be found, there was one p2Ca peptide variant (L4) that was able to induce lysis but failed to bind to the TCR in the SPR assay. These data suggested that TCR affinity was not the only critical parameter for the activation of the T cells. Other SPR studies, examining agonist and antagonist ligands of TCRs could show that the agonist ligand was bound with higher affinity and had thus a slower dissociation rate [114, 146]. Also the discovery of an affinity window for positive selection in the thymus was done by analysis of positively and negatively selecting ligands with SPR [93].

SPR application in the Biacore assay offers a very sensitive method to determine TCR affinity and generated important findings, but also entails severe disadvantages. For every SPR affinity measurement, not only the MHC molecules but also the TCRs have to be expressed recombinantly, whereupon the latter is technically challenging. Different approaches have been developed to generate soluble TCRs including the replacement of the transmembrane region with signal sequences for glycolipid linkage [147], deletion of the transmembrane region [22] or cysteine mutation and Escherichia coli expression [23]. However, no method is suitable for all TCRs, turning the TCR production into a time consuming and difficult process. Furthermore, it could be shown that especially for fast reactions diffusion of the soluble binding partner into the hydrogel matrix can decrease its overall transport significantly and therefore introduce many unknown factors into the binding progress curve [148]. Finally, the setting of the macromolecular interaction in the SPR setup is far away from physiological conditions. In the case of the analysis of TCR affinity, both the TCR and the pMHC complex have to be recombinantly expressed and one binding partner is immobilized on the surface, the other in solution. In contrast to cell-cell interactions, where both binding partners are able to move in two dimensions within the cell membrane, in the SPR setting only one of the binding partners is allowed to move, but this in three dimensions. These differences are suggested to

influence the binding kinetics. In addition, the contribution of the CD8 coreceptor is not taken into account in the SPR measurements, which could be shown to stabilize the TCR pMHC complex [66].

Multimer based avidity assays

Structural avidity assays based on multimer techniques allow for the measurement of TCR-pMHC interaction on the surface of living T cells. In the beginning of the MHC multimer techniques it could be shown that tetrameric complexes of pMHC molecules, so called MHC tetramers, were able to bind stably to T cells expressing their specific TCR on the surface [149]. Two different types of tetramer based avidity assays have been used in the past [150]. With the first assay, several groups revealed a correlation between the tetramer staining intensity and the avidity of a T cell [75, 77, 151–153]. As the generation and analysis of data with this methods is not complicated and easy to standardize, the assay seems to be suitable to produce comparable data on T cell avidity. However, other studies found a missing correlation between the tetramer staining intensity and the T cell avidity, suggesting that the staining intensity is also dependent on other parameters and thus not suitable to provide reliable information on T cell avidity [145, 154–156].

In the other tetramer based approach, tetramer dissociation kinetics have been used to quantify T cell avidity [123, 128, 157–161]. However, the way how the experiments were performed in the mentioned studies differs strongly, especially in one variable, the blocking reagent. Thereby, the use of a blocking reagent at all and, if used, the nature of the blocking reagent varies between the studies. Following variants were used: No blocking reagent [123, 160], intact anti-MHC antibodies [128, 157], unlabeled tetramer [159, 161] and Fab-fragments [158]. As it seems necessary to use a blocking reagent to prevent rebinding of dissociated tetramers, Wang and Altman examined the effect of a different blocking reagent on the dissociation kinetics [150]. Using MHC antibodies as blocking reagent complicates the interpretation of kinetic data, as the bivalent antibodies are able to interact with tetramer stained cell in different ways, e.g. by crosslinking two tetramers together or by linking a tetramer to a MHC I molecule expressed on the surface of the labeled T cell. Indeed, Wang and Altman found faster tetramer dissociation using Fab fragments as blocking reagent in comparison to MHC antibodies. In addition, without blocking reagents, no significant dissociation could be observed [150]. In a further step, they analyzed the effect of the concentration of the blocking reagent on the tetramer dissociation rate. They found that above a certain threshold, the dissociation rate was independent of the concentration of the blocking Fab-fragments. However, the dissociation rate was influenced by change in concentrations of blocking MHC antibodies and saturation was only reached at very high concentrations. Consequently, this study recommends Fab fragments as suitable blocking reagent for tetramer dissociation assays (Figure 1.7). Besides the problem of the suitable blocking reagent, is has to be taken into account that tetramer based T cell avidity assays do not allow for the analysis of monomeric TCR pMHC interaction. The interpretation of the data is based on the assumption that differences in tetramer binding correlate to different TCR affinity. However, due to the multimeric nature of the MHC tetramers, the level and the dissociation rate of binding could be influenced by additional factors
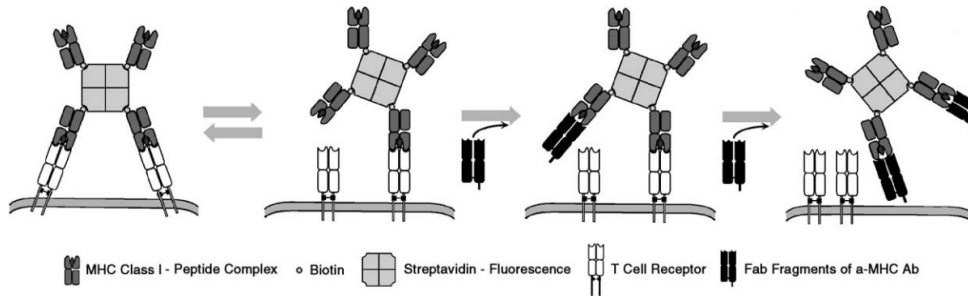
Figure 1.7: **Model of using Fab fragments of the blocking antibody as competitors in the tetramer dissociation assay:** MHC Class I tetramer binds to the TCRs on the T cells surface (left panel). Dissociation of one MHC molecule and blockage of rebinding by a competitor Fab-fragment (middle panels). Complete dissociation of the tetramer after dissociation and blockage of all engaged MHC molecules in the presence of Fab competitor (right panel) [150].

like organization of the TCR in the membrane [79, 152, 162]. Furthermore, the level of multimerization, i.e. the actual number of MHC molecules in one multimer is hard to control, but influences the dissociation kinetics of the multimer. Therefore, multimer dissociation assays are very difficult to standardize.

In conclusion, even if several studies could reveal a correlation between MHC dissociation and T cell avidity, the multimeric nature of the tetramers interferes with a correct examination of the TCR pMHC interaction. Dissociation of the tetramer requires first the detachment of all MHCs. However, due to their close proximity to the T cell surface and thus high local concentration, newly detached MHCs might rebind to the TCR, creating difficult higher order kinetics [150]. Some reports postulate that MHC tetramer dissociation underlie first order dissociation kinetics [128, 157, 163], but others report more complicated higher order kinetics, especially when blocking reagents are used [150].

While Biacore assays allow for the correct calculation of monomeric TCR pMHC affinity but in a quite artificial environment, MHC tetramer based avidity assays measure dissociation kinetics from the surface of living T cells, but are not able to correctly determine the binding strength between a monomeric pMHC molecule bound to the TCR. An improved assay system would thus ideally measure monomeric pMHC TCR interactions on the surface of living T cells.

k_{off}-rate assay for murine T cells

To meet those needs for an improved T cell avidity assay, a novel k_{off}-rate assay was designed in the laboratory of Prof. Busch and established for the measurement of murine T cells during the PhD work of Robert Knall. As the k_{off}-rate assay for murine and for human T cells, with the latter established in this PhD work, share the same principle, the assay is described in detail in section 4.1. The k_{off}-rate assay is based on reversible multimers, so called *Strep*tamers and allows to determine accurately the dissociation of monomeric pMHC from the TCRs on a living T cell, with the dissociation kinetics independent of the level of multimerization or the nature of
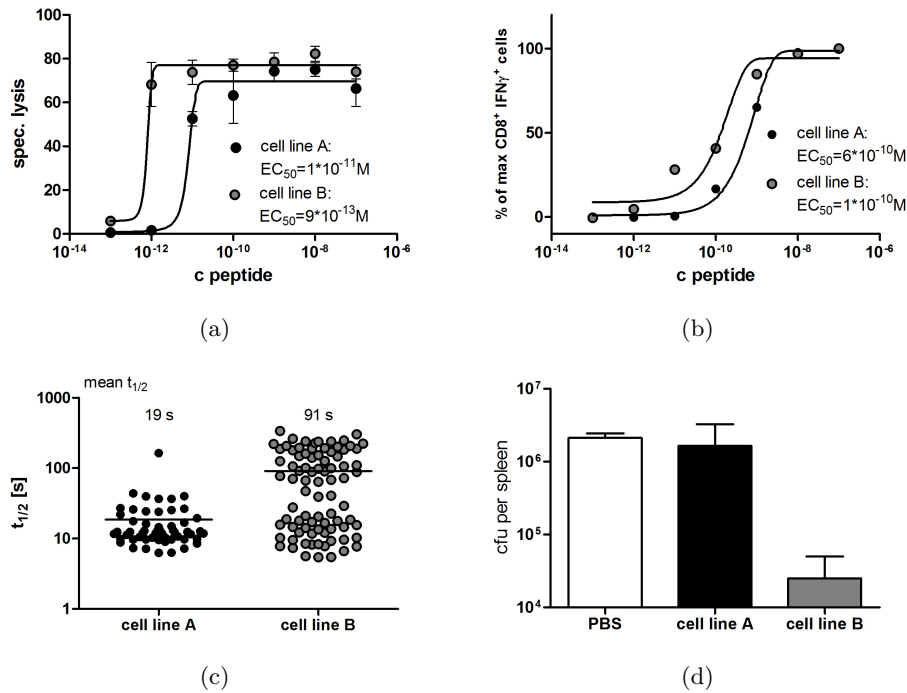
Figure 1.8: **Long half-life time correlates with high functional avidity and protectivity of T cell lines in *L.m.* infection**: LLO_{91-99} specific T cell lines were generated from sorted LLO_{91-99} specific $CD8^+$ T cells of *L.m.* infected Balb/c mice by restimulation with 10^{-6}M peptide (cell line A, black circles) and 10^{-9}M peptide respectively (cell line B, gray circles). (a) Analysis of the functional avidity of the T cell lines with (a) ICCS and (b) ^{51}Cr release assay . (c) k_{off}-rate assay of the two T cell lines A and B. Numbers indicate the mean $t1/2$ of all measured cells. (d) $5*10^6$ T cell line cells were transferred into Balb/c mice i.v. and mice were infected i.v. with $2*10^4$ CFU *L.m.* one hour later. After 3 days, mice were sacrificed and bacterial load analyzed in the spleen. [164]

a blocking reagent. Robert Knall analyzed two murine T cells lines specific for the Listeria monocytogenes epitope LLO_{91-99}. The T cell lines were restimulated with different peptide concentrations and therefore exhibited different functional avidity (Figure 1.8 (a), (b)). Robert Knall could show in his experiments a direct correlation between the k_{off}-rate and the functional avidity of the T cell clones (Figure 1.8(c)). Most importantly, when T cells of those lines were transferred into mice, which were subsequently infected with Listeria, only the T cell line with the low k_{off}-rate was able to protect the mice from bacterial burden (Figure 1.8(d)). This superior protective capacity of T cells with low k_{off}-rate pointed to the fact that T cells with a high structural avidity would be superior for adoptive T cell therapy.

1.3 Adoptive T cell therapy

Adoptive cellular therapy is defined as the infusion of effector cells for the treatment and/or prevention of diseases [165]. Cytotoxic T cells have the ability to lyse target

cells with high efficiency and have a well documented role in the elimination of viral infections [82]. Therefore, they are promising candidates for adoptive T cell therapy and have been already applied in different studies for the treatment of viral diseases as well as cancer.

1.3.1 T cell therapy in viral infections

Adoptive immunotherapy with specific T cells has shown promising results for the treatment of CMV, EBV, LCMV and HIV infection [133, 166–168]. It could be shown that the transferred T cells were able to reduce the viral load in infected patients and to persist after the transfer for some time. In the following, the different possible strategies for T cell therapy of viral infections will be discussed for infections with CMV.

CMV infection or reactivation is often the cause of morbidity or even mortality in immunocompromised patients after allogenic stem cell transplantation (SCT). Prophylactic or preemptive antiviral treatment is able to control the early onset of CMV disease during the first 100 days after transplantation. However, late onset of CMV disease later than 100 days after the transplantation can cause severe complications. Hence, several strategies have been developed to reconstitute CMV-specific T cell responses in the patients. The transfer of CMV-specific CD8$^+$ T cell clones could protect patients at risk from CMV related complications [167, 169]. The administered T cells were detectable in the blood of treated patients for at least 8 weeks. However, if the patients failed to develop a concomitant CMV-specific CD4$^+$ T$_H$ response, the count of the transferred cells declined progressively. In another approach, polyclonal T cell lines instead of T cell clones were infused into patients that did not respond to anitviral chemotherapy after allogeneic SCT. Einsele and colleagues generated CD4$^+$ CMV-specific T cell lines and achieved virus clearance in 5/8 patients after the transfer of ~1-5*10^6 T cells [170]. Also CD8$^+$ CMV-specific T cell lines could be shown to control CMV infection in patients after allogeneic SCT [171]. Generating polyclonal T cell lines has an essential benefit in time compared with the generation of specific T cell clones and therefor provides a more flexible application without the loss of specificity or safety of the T cells [172]. However, a more sophisticated approach might be the direct isolation and infusion of CMV-specific CTLs using HLA multimers. Based on the multimer-technology described in section 1.2.4.2, specific T cells are visualized and subsequently sorted. Using reversible multimers, so called *Strep*tamers, nearly untouched antigen specific CTL can be obtained that still show a good viability, proliferative capacity and functionality [173]. A major advantage of directly isolated T cells in comparison to *in vitro* expanded T cells is that *in vitro* expansion might increase the expression of the pro-apoptotic FAS molecule and reduce the telomere length of specific T cells, leading to a shorter survival of the T cells after adoptive transfer [172]. In addition, also the risk of contamination and finally the costs of the immunotherapy are increased by cultivating T cells *in vitro*.

Hence, adoptive T cell therapy has shown to lead to viral control without apparent side effects. Because of different methods to generate T cells it has to be further examined which T cell subpopulations are best suited for antiviral therapy, which

differentiation stages should be applied and which dose is optimal depending on viral load and immunosuppression of the patient [172].

1.3.2 T cell therapy in cancer

Different studies revealed that virus-associated diseases in immuno-compromised patients could be efficiently prevented and treated with adoptive T cell transfer. As this treatment turned out to be safe, effective and protective *in vivo*, the use of adoptive T cell transfer should be extended to cancer therapy in immuno-competent patients [174]. But compared to the treatment of viral infections, tumor specific T cell therapy turned out to be more challenging and less effective. The development of a successful T cell therapy for patients with malignancies is hampered by several reasons. First, it is difficult to isolate and culture T cells with high avidity TCRs specific for self-antigens expressed selectively or preferentially by tumor cells [175]. Second, tumor cells have evolved several mechanisms to escape detection both by innate and adaptive immunity. These include e.g. down-modulation of MHC I and costimulatory molecules, expression of Fas-Ligand and other pro-apoptotic molecules on the cell surface, production of inhibitory factors such as TGF-β and IL-10 and recruitment of regulatory T cells. Another factor that complicates cancer therapy with T cells is the short *in vivo* persistence of transferred T cells caused by factors of the tumor environment and the attributes of isolated and expanded T cells [174, 175]. The first study to treat metastatic solid cancer with adoptively transferred T cells were done in 1988 with patients with metastatic melanoma. Tumor infiltrating lymphocytes (TILs) were grown from resected tumor nodules of patients. The transfer of autologous TILs in combination with high dose IL-2 achieved an overall response rate of 34% in 86 patients. Thereby, T cells were transferred in two cycles of treatment two weeks apart. TILs were administered irrespective of their *in vitro* activity. A retrospective analysis, however, revealed a clear correlation between the ability of the TILs to lyse tumor cells *in vitro* and the clinical outcome. This initial study demonstrated also the short persistence of the transferred lymphocytes and emphasized the need of modifications to improve the *in vivo* survival of administered T cells [176].

The longest persistence of adoptively transferred virus-specific T cells was observed when T cells were transferred into immunodeficient allogenic hematopoetic stem cell recipients early after transplantation [169, 177]. At this time point, lymphopenia was present, which reduced the competition of transferred T cells for IL-2 and IL-15 and eliminated CD4$^+$ CD25$^+$ regulatory T cells and other cells with suppressor function. Rosenberg et. al could demonstrate direct evidence for the benefit of lymphopenia for the survival of transferred T cells. Lymphopenia was induced in melanoma patients using chemotherapy alone or in combination with total body irradiation before the transfer of melanoma specific T cells. In 56% of patients, T cells expanded *in vivo*, persisted long term and infiltrated into tumors and induced tumor regression [178–180]. In further studies, improved antitumor efficacy of transferred T cells could be correlated with prolonged persistence *in vivo*, pointing out the depletion of endogenous lymphocytes as effective treatment to improve efficacy of adoptively transferred tumor specific T cells.

1.3.3   Optimizing T cells for adoptive transfer

Diverse studies demonstrated that adoptive T cell transfer for the treatment of viral infections and cancer offers the possibility for a specific and safe therapy. With lymphodepletion, T cell persistence and thereby antitumor efficacy could be improved. Nevertheless, often high numbers of T cells were necessary, and survival and efficacy of the transferred cells were still limited. Thus, it seems reasonable not only to transfer T cells with the desired specificity but with optimal characteristics for adoptive T cell transfer. But which characteristics account for an optimal T cell for T cell therapy? Some of the aspects will be discussed in the next paragraph.

An important step in the generation of a T cell response with the required magnitude, duration and quality is the selection of the optimal $CD8^+$ T cell subset (s. Figure 1.9). Highly activated effector T cells show rapid cytotoxic function, high cytokine production and are able to infiltrate into tumor tissue. Therefore, they seem to be optimal candidates for adoptive T cell therapy. However, they exhibit decreased proliferative potential and adoptive transfer of terminally differentiated effector cells into mice demonstrated poor proliferation, poor IL-2 production and only short survival of the transferred cells [181]. Less differentiated memory T cells that bear longer telomeres and express costimulatory and homing receptors demonstrated longer persistence both in murine models and in human immunotherapy trials [174]. Which subset of memory T cells, effector memory T cells T_{EM} or central memory T cells T_{CM}, is better suited for adoptive T cell therapy, is still matter of debate. T_{EM} exhibit a more activated phenotype than T_{CM} and are recruited to effector lymphoid tissue and site of inflammation due to their expression of adhesion molecules and chemokine receptors. Therefore, T_{EM} are important in fighting localized infections [182, 183], whereas T_{CM} have been shown to be crucial for the protection against systemic infections with high pathogens loads [184]. Studies can be found where either T_{CM} or T_{EM} showed longer persistence and survial [185–187]. Hence, research has to continued at this field to examine in more detail which subpopulation is each better suited for a certain treatment.

As already discussed, high avidity T cells could be shown to be superior in clearing viral infections and in inducing tumor regression after adoptive transfer. Especially in adoptive immunotherapy of cancer, it is in many cases not possible to isolate T cell with high affinity for tumor associated antigen (TAA). Most TAAs are self proteins and therefore T cells with high avidity against the antigens are deleted during tolerance induction. To optimize both the specificity and the functionality of transferred T cells, different approaches have been developed to genetically modify T cells. In a procedure called TCR gene transfer, genes that encode the α and β chains from T cells with known specificity and functionality are cloned and subsequently introduced into recipient T cells. These cells then endow both the specificity and the avidity of the donor T cell and show *in vitro* IFNγ production and lysis of target cells after antigen recognition. TCR gene transfer has been applied to melanoma antigens [189–191], minor histocompatibility antigens [192, 193] and common oncoproteins [194, 195]. One problem arising in this approach is the potential mispairing of the introduced TCR chains with endogenous TCR chains of the recipient cell. This would create new specificities and could lead e.g. to autore-
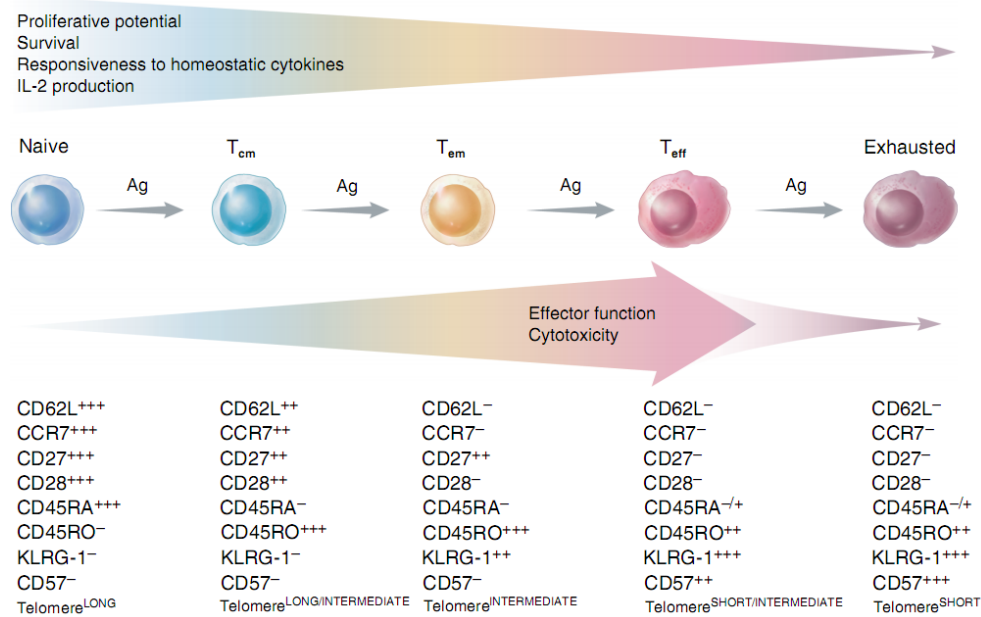
Figure 1.9: **Phenotype and functional properties of CD8$^+$ T cell subsets:** Chronic or repetitive antigen stimulation drives naive T cells to a terminally differentiated effector state and results finally in exhaustion. The phenotypic changes during differentiation are illustrated as low expression (+), intermediate expression (++), and high expression (+++) of different cell surface markers.[188]

activity of transferred T cells. This problem is addressed by diverse attempts to modify the transmembrane association domains of the introduced TCR chains that allow no longer for the dimerization with endogenous chains [174].

Another important approach focuses on the optimization of the safety of transferred T cells. T cells that are redirected against antigens that are expressed both on target and normal cells or T cells that are modified to confer improved functionality could cause side effects and toxicity. The introduction of a conditional suicidal gene into T cells would allow for the quick elimination of transferred T cells in the case of adverse events and therefore enhance the safety of the T cell therapy. Several suicide switches have been developed and tested the last years [196–199]. The introduction of a gene encoding the herpes simplex virus thymidine kinase (HSV-TK) allows for the elimination of modified T cells by administration of the drug ganciclovir. Other strategies are to induce FAS expression, leading to elimination of modified T cells by the endogenous apototic pathway, fusion of a myc-tag to the TCR or expression of CD20 or human tEGFR on T cells. Elimination of infused T cells that were modified with the last three suicide switches is done through the administration of the respective specific monoclonal antibodies. However, it is of great advantage if the applied antibody is already clinically approved (as the case for αCD20 and αEGFR) to prevent potential complications.

In conclusion, adoptive T cell transfer has proven to be a promising therapy both for viral infections and cancer. Deeper knowledge of optimal characteristics of trans-

ferred T cells and the possibility of genetic modification allow for the generation of T cells that are optimal suited for adoptive transfer. Additional introduction of suicide switches offers the possibility to quickly eliminate infused T cells and therefore contributes to the safety of adoptive T cell therapy.

Chapter 2

Aim of this PhD thesis

$CD8^+$ T cells play a crucial role in the identification and elimination of infected or abnormal cells. The T cell receptor recognizes foreign peptides presented on MHC I molecules and T cell activation is triggered with the additional help of different coreceptors and costimulatory molecules. The quality how a T cell recognizes its MHC peptide ligand is mostly described as T cell avidity. T cells with high avidity could be shown to be more efficient in clearing viral infections and inducing tumor regression. The T cell avidity can be measured by functional readouts (assessing "functional avidity") or by the determination of the binding strength of the TCR to its ligand, the so called "structural avidity". A crucial parameter of structural avidity is the k_{off}-rate, the dissociation rate of pMHC molecules from TCRs. A novel k_{off}-rate assay that was recently developed for measurement of murine T cells allows for the exact determination of this parameter and overcomes several drawbacks of hitherto existing methods to assess the k_{off}-rate. Studies with preclinical mouse models showed a remarkable correlation between the k_{off}-rate and the functional avidity of T cells and, most importantly, with the protective capacity. This led to the assumption that the k_{off}-rate might also provide an important parameter for T cell quality for adoptive transfer in humans. Therefore, the aim of the PhD thesis was to transfer the k_{off}-rate assay setup established for murine cells to the measurements of human T cells. First data indicated that it was not possible to directly transfer the murine k_{off}-rate assay to human T cells. Hence, first objective was to find a position in the recombinant MHC-steptag fusion protein, where dye conjugation would not alter binding abilities of the MHC molecule to the TCR or the *Strep*-Tactin backbone. Second, a fluorescent dye had to be found that was small enough, and that showed bright staining and resistance to photobleaching. After technical establishment of the k_{off}-rate assay for human T cells, T cells with relevance for adoptive transfer were analyzed. For this purpose, the k_{off}-rate assay was performed directly ex vivo (no cell culture step involved) with different CMV specific populations. Furthermore, T cell clones generated from the ex vivo populations were analyzed and compared to the originating populations to examine the reproducibility and the reliability of the k_{off}-rate assay. Finally, T cell receptor transfer experiments were conducted to reveal if the k_{off}-rate was determined by the structure of the TCR or depended on other cell specific factors.

Chapter 3

Material and methods

3.1 Material

3.1.1 Chemicals and reagents

Reagent	Supplier
Alexa-488-maleimide	Molecular Probes, Leiden, The Netherlands
α-Methylmannopyranoside (α-MM)	Calbiochem, Darmstadt, Germany
Ammoniumchloride (NH_4Cl)	Sigma, Taufkirchen, Germany
Ampicillin	Sigma, Taufkirchen, Germany
Atto-565-maleimide	ATTO-TEC GmbH, Siegen, Germany
BCA assay reagents	Interchim, Montlucon, France
β-Mercaptoethanol	Sigma, Taufkirchen, Germany
Biocoll Ficoll solution	Biochrom, Berlin, Germany
Bovine serum albumin (BSA)	Sigma, Taufkirchen, Germany
Carbenicillin	Roth, Karlsruhe, Germany
Cytofix/Cytoperm	BD Biosciences, Heidelberg, Germany
d-Biotin	Sigma, Taufkirchen, Germany
Dimethylformamid (DMF)	Sigma, Taufkirchen, Germany
Dimethyl sulfoxid (DMSO)	Sigma, Taufkirchen, Germany
Ethanol	Klinikum rechts der Isar, Munich, Germany
Ethidium-monazide-bromide (EMA)	Molecular Probes, Leiden, The Netherlands

Reagent	Supplier
Fetal calf serum (FCS)	Biochrom, Berlin, Germany
Gentamycin	GibcoBRL, Karlsruhe, Germany
Gluthathione (oxidized)	Sigma, Taufkirchen, Germany
Gluthathione (reduced)	Sigma, Taufkirchen, Germany
Golgi-Plug	BD Biosciences, Heidelberg, Germany
Guanidine-HCl	Sigma, Taufkirchen, Germany
HCl	Roth, Karlsruhe, Germany
HEPES	GibcoBRL, Karlsruhe, Germany
Human serum	in-house production, Institut für Medizinische Mikrobiologie, Immunologie und Hygiene
IPTG	Sigma, Taufkirchen, Germany
L-Arginine	Roth, Karlsruhe, Germany
L-Glutamine	GibcoBRL, Karlsruhe, Germany
Leupeptin	Sigma, Taufkirchen, Germany
Lysozym	Sigma, Taufkirchen, Germany
NaOH	Roth, Karlsruhe, Germany
Penicillin	Roth, Karlsruhe, Germany
Pepstatin	Sigma, Taufkirchen, Germany
PermWash	BD Biosciences, Heidelberg, Germany
pET3a expression vectors	Novagen, Darmstadt, Germany
Phosphate buffered saline (PBS)	Biochrom, Berlin, Germany
Propidiumjodide (PI)	Molecular Probes, Invitrogen, UK
RPMI 1640	GibcoBRL, Karlsruhe, Germany
Sodiumacetate	Sigma, Taufkirchen, Germany
Sodiumazide (NaN_3)	Sigma, Taufkirchen, Germany
Sodiumchloride (NaCl)	Roth, Karlsruhe, Germany
Sodium-EDTA (Na-EDTA)	Sigma, Taufkirchen, Germany
*Strep*tomycin	Sigma, Taufkirchen, Germany
Strep-Tactin-APC	IBA, Göttingen, Germany
Strep-Tactin-PE	IBA, Göttingen, Germany
Tris-hydrochloride (Tris-HCl)	Roth, Karlsruhe, Germany
Trypan Blue solution	Sigma, Taufkirchen, Germany
T-Stim culture supplement	BD Biosciences, Heidelberg, Germany

3.1.2   Buffers and Media

Buffer	Composition
Buffer	**Composition**
FACS buffer	1x PBS 0.5% (w/v) BSA pH 7,45
RP10+ cell culture medium	1x RPMI 1640 10% (w/v) FCS 0.025% (w/v) L-Glutamine 0.1% (w/v) HEPES 0.001% (w/v) Gentamycin 0.002% (w/v) *Strep*tomycin 0.002% (w/v) Penicillin
Ammoniumchloride-Tris	0.17 M NH_4Cl 0.17 M Tris-HCl mix NH_4Cl and Tris-HCl at a ratio of 9:1
Refolding buffer	100 mM Tris-HCl 400 mM L-Arginin 2 mM NaEDTA 0.5 mM ox. Gluthathione 5 mM red. Gluthathion ad 1 L H_2O, pH 8.0
Guanidine solution	3M Guanidine-HCl 10 mM NaAcetate 10 mM NaEDTA ad 100 ml H_2O, pH4.2
FPLC buffer	20 mM Tris-HCl 50 mM NaCl ad 1 L H_2O, pH 8.0 or pH 7.3
d-biotin	10 M stock solution 244.31 g d-biotin ad 100 ml H_2O, pH was brought to $\approx$ pH 11 to facilitate solution of d-biotin, then back down to pH 7
complete freezing medium (CFM)	FCS 10% DMSO

3.1.3 Peptides

All peptides were purchased from IBA, Göttingen, Germany
$\mathrm{IE1}_{199-207K}$ (ELRRKMMYK)
$\mathrm{IE1}_{88-96}$ (QIKVRVDMV)
$\mathrm{pp65}_{417-426}$ (TPRVTGGGAM)
$\mathrm{pp65}_{495-503}$ (NLVPMVATV)
$\mathrm{Ova}_{257-264}$ (SIINFEKL)
SIY (SIYRYYGL)

3.1.4 Antibodies

Antibody	clone	supplier
Fcblock (rat anti-mouse CD16/CD32)	2.4 G2	BD Bioscience, Heidelberg, Germany
Rat anti-mouse CD3 APC	145-2C11	BD Bioscience, Heidelberg, Germany
Rat anti-mouse CD8αAlexa-488	CT-CD8α	Caltag Laboratories, Hamburg, Germany
Rat anti-mouse CD8αFITC	CT-CD8α	Caltag Laboratories, Hamburg, Germany
Rat anti-mouse CD8αPE	CT-CD8α	Caltag Laboratories, Hamburg, Germany
mouse anti-human CD3 APC	UCHT1	Beckman Coulter, Marseille, France
mouse anti-human CD3 PE	UCHT1	Beckman Coulter, Marseille, France
mouse anti-human CD8 PB	B 9.11	Beckman Coulter, Marseille, France
mouse anti-human CD8 FITC	DK25	Dako, Glostrup, Denmark
mouse anti-human CD8 PE	DK25	Dako, Glostrup, Denmark

3.1.5 MHC *Strep*tamers

HLA B8 *Strep*-tagIII/hβ_2m Cys-67 Alexa488/$\mathrm{IE1}_{199-207K}$ *Strep*-Tactin-PE
HLA B8 *Strep*-tagIII mutIII Alexa488/hβ_2m /$\mathrm{IE1}_{199-207K}$ *Strep*-Tactin-PE
HLA B8 *Strep*-tagIII mutIII Atto488/hβ_2m /$\mathrm{IE1}_{199-207K}$ *Strep*-Tactin-PE
HLA B8 *Strep*-tagIII mutIII Atto532/hβ_2m /$\mathrm{IE1}_{199-207K}$ *Strep*-Tactin-PE
HLA B8 *Strep*-tagIII mutIII Atto633/hβ_2m /$\mathrm{IE1}_{199-207K}$ *Strep*-Tactin-PE
HLA B8 *Strep*-tagIII mutIII Atto594/hβ_2m /$\mathrm{IE1}_{199-207K}$ *Strep*-Tactin-PE
HLA B8 *Strep*-tagIII mutIII Atto647N/hβ_2m /$\mathrm{IE1}_{199-207K}$ *Strep*-Tactin-PE
HLA B8 *Strep*-tagIII mutIII Atto565/hβ_2m /$\mathrm{IE1}_{199-207K}$ *Strep*-Tactin-APC
HLA B8 *Strep*-tagIII/hβ_2m /$\mathrm{IE1}_{199-207K}$ *Strep*-Tactin-APC

HLA B8 *Strep*-tagIII mutIII Atto565/hβ_2m /IE1$_{88-96}$ *Strep*-Tactin-APC
HLA B8 *Strep*-tagIII/hβ_2m /IE1$_{88-96}$ *Strep*-Tactin-APC

HLA B7 *Strep*-tagIII mutIII Atto565/hβ_2m /pp65$_{417-426}$ *Strep*-Tactin-APC
HLA B7 *Strep*-tagIII/hβ_2m /pp65$_{417-426}$ *Strep*-Tactin-APC

HLA A2 *Strep*-tagIII mutIII Atto565/hβ_2m /pp65$_{495-503}$ *Strep*-Tactin-APC
HLA A2 *Strep*-tagIII/hβ_2m /pp65$_{495-503}$ *Strep*-Tactin-APC

H2-k^b *Strep*-tagIII/mβ_2m -cys67 Alexa-488/Ova$_{257-264}$ *Strep*-Tactin-PE
H2-k^b *Strep*-tagIII mutIII Atto565/mβ_2m / Ova$_{257-264}$ *Strep*-Tactin-APC
H2-k^b *Strep*-tagIII/mβ_2m / Ova$_{257-264}$ *Strep*-Tactin-APC/PE

H2-k^b *Strep*-tagIII/mβ_2m -cys67 Alexa-488/SIY *Strep*-Tactin-PE
H2-k^b *Strep*-tagIII mutIII Atto565 /mβ_2m /SIY *Strep*-Tactin-APC
H2-k^b *Strep*-tagIII/mβ_2m /SIY *Strep*-Tactin-APC/PE

3.1.6   Gels

SDS-PAGE running gel	7 ml dH$_2$O
	4.38 ml 1.5 M Tris-HCl pH 8.8
	5.8 ml 30% Acrylamide 1% Bisacrylamide
	170 μl 10% SDS
8.8 μl TEMED	
170 μl 10% APS	
SDS-PAGE stocking gel	6.2 ml dH$_2$O
	2.5 ml 0.5 M Tris-HCl pH 6. 8
	1.2 ml 30% Acrylamide 1% Bisacrylamide
	100 μl 10% SDS
	5 μl TEMED
	100 μl 10% APS
Agarose gel	0.45 g Agarose
	40 ml TBE buffer
	1 μl Ethidium bromide

3.1.7   Microscope and equipment for TCR k$_{off}$-rate measurements

Zeiss LSM 510	confocal microscope (Zeiss, Jena, Germany)
Leica SP5	confocal microscope (Leica, Bensheim, Germany)
Zeiss temperable insert P	cooling device (Zeiss, Jena, Germany)
Huber Minichiller	peltier cooler (Huber Kältemaschinenbau, Offenburg, Germany)
Metal inserts for cooling device	(Locksmithery, Klinikum rechts der Isar, Munich, Germany)
Polycarbonate membranes	pore size 5 μ,(Millipore, Bergisch-Gladbach, Germany)
Metal shims	(Schneider + Klein, Landscheid, Germany)

3.1.8   Equipment

Leica SP 5 confocal microscope	Leica, Bensheim, Germany
FACSCalibur flow cytometer	BD Bioscience, Heidelberg, Germany
FPLC System	Amersham, Munich, Germany
Varifuge 3.0RS centrifuge	Thermo, Schwerte, Germany
Multifuge 3S-R centrifuge	Thermo, Schwerte, Germany
Biofuge fresco table top centrifuge	Thermo, Schwerte, Germany
Biofuge 15 table top centrifuge	Thermo, Schwerte, Germany
RC26 Plus ultra-centrifuge	Sorvall, Langenselbold, Germany
HE33 agarose gel casting system	Hoefer, San Francisco, USA
Mighty Small SE245 gel casting system	Hoefer, San Francisco, USA
NanoDrop spectrophotometer	NanoDrop, Baltimore, USA
Gel Imaging System	BioRad, Munich, Germany

3.1.9   Software

FlowJo	Treestar, Ashland, USA
Microsoft Office	Microsoft, Redmond, USA
MetaMorph Offline	Molecular Devices, Downingtown, USA
Analyzer.nt	Sebastian Nauerth, Department of Physics, LMU München
GraphPad Prism 5	GraphPad Software, La Jolla, USA

3.2 Methods

3.2.1 Generation of a new conjugation site in the MHC heavy chain

For the generation of a new conjugation site for a fluorescent dye in the MHC heavy chain, a cysteine residue had to be introduced to allow for a maleimide reaction of the dye with the free -SH group of the cysteine. To achieve this, first suitable primers for the mutagenesis at the chosen site had to be generated. Then, a mutagenesis PCR had to be performed and the products had to be checked for correct sequence. Successfully mutated vectors were used for proteine expression and expressed proteins analyzed for correct size.

3.2.1.1 Primerdesign

To introduce a mutation with PCR, primers have to be designed which contain the DNA bases coding for the aminoacid(s) that should be inserted. To ensure a stable binding to the template DNA, regions flanking the mutation site should be of about 10 bases. PrimerX, a free online program from Bioinformatics.org was used to design optimal primers. Primers with high melting temperatures and GC content as low as possible to create optimal conditions for the following mutagenesis PCR. Successful mutagenesis PCRs with the respective MHC molecules were performed using following primers:

Primers for mutagenesis of the *Strep*-tagIII of HLA B8 (also used for the mutagenesis of HLA B7 and H2-k^b):

HLA B8 MutI forward	CTCCTCCgTCTggATgCTCCAgCgCTTggTCTCAC
HLA B8 MutI reverse	gTgAgACCAAgCgCTggAgCATCCAgACggAggAg
HLA B8 MutII forward	CggAggTggATCgTgCggAggTggATCgTg
HLA B8 MutII reverse	CACgATCCACCTCCgCACgATCCACCTCCg
HLA B8 MutIII forward	CCCgCAgTTCgAAAAAggAggTTCCTgCTAATAAgCTTgATCCgg
HLA B8 MutIII reverse	CCggATCAAgCTTATTAgCAggAACCTCCTTTTTCgAACTgCggg

Primers for mutagenesis of the *Strep*-tagIII HLA A2:

HLA A2 MutI forward	gCCgggCCATggAggTTCCTgCggTAgCTggAgCCAC
HLA A2 MutI reverse	gTggCTCCAgCTACCgCAggAACCTCCATggCCCggC
HLA A2 MutIII forward	CgCAgTTCgAgAAAggAggTTCCTgCTAggATCCggCTgC
HLA A2 MutIII reverse	gCAgCCggATCCTAgCAggAACCTCCTTTCTCgAACTgCg

3.2.1.2 Mutagenesis-PCR

The mutagenesis was performed using a Stratagene QuikChange Lightning Site-Directed Mutagenesis Kit. All reagents used were products from the kit, and the product guidelines were followed closely. In brief, 50ng DNA vector were mixed with 100ng of the respective primers and the components of the mutagenesis kit including an enzyme blend featuring a Pfu Fusion DNA polymerase. Thermal cycling steps for denaturation of the template DNA, annealing of the mutagenic primers and extension were chosen as follows:

	temp	time	←	#
1	95°C	1 min 30 sec		
2	95°C	45 sec		
3	55°C	1 min		
4	68°C	5 min 30 sec	2	18
5	68°C	20 min		
6	4°C	pause		

After the PCR, template DNA was digested by incubation with DpnI endonuclease, which is specific for methylated abd hemimethylated DNA. $10\mu l$ of the PCR samples were loaded on an agarosegel to check for the existence and the size of PCR products. The agarose gel was made with 40 ml TAE buffer, 0.45 g agarose and 5 μl EtBr. A 1 kB DNA ladder was used as marker, and 2 μl 6x DNA loading dye was added to the samples for staining.

3.2.1.3 Transformation and plasmid preparation

10 μl of the reaction mixture were used to transform DH5αbacteria with the mutated plasmids. Therefor, 100 μl competent cells were cautiously thawed on ice and then 10 μl pcr product was added. The mixture was incubated on ice for 30 min, then heat shocked in a 42 °C water bath for 30 sec. After 2 min incubation on ice, 150 μl SOC-medium was added to each reaction mixture and incubated for 1 h at 37 °C. The mixtures were then plated on ampicillin-containing agar plates to select only colonies containing the vector in 10, 50 and 2x100 μl doses and incubated over night at 37 °C. One colony was picked from every transformation plate and inoculated into reaction tubes containing 6 ml LB-medium and 6 μl ampicillin. The cultures were incubated over night at 37 °C and subsequently 1 ml bacteria sample was mixed 1:1 with glycerol for glycerol stocks and frozen at -20 C. For the plasmid preparation the Qiagen Plasmid Miniprep Kit was used. The preparation was performed according to protocol, and the isolated DNA was eluted with 50 μl ddH$_2$O. DNA concentrations were measured with NanoDrop. Following plasmid preparation all samples were sent to GATC Biotechnologies Ltd. for sequencing to confirm successful mutations.

3.2.1.4 Protein expression

10 μl heat competent BL21 (DE3)cells were mixed with 1 μl DNA and transformed using the same protocol as the first transformation. The transformation products were plated on amp-containing agar plates and incubated over night at 37 °CC.

To test the expression of the protein in a small scaled preparation, cell culture bottles containing 20 ml LB-medium, 200 μl 40% glucose and 20 μl ampicillin were inoculated with 4-5 colonies from each agar culture plate. The cultures were shaken at 37 °C until OD600 reached 0,3 and 1 ml glycerol stocks were taken. At OD600 0,7 a 0h sample was taken before induction and the cultures were induced using 1 μl IPTG per ml culture. The cultures were shaken for further 3 h and a 3 h sample was taken after induction. The 0- and 3 h samples were centrifuged at 9000 rpm for 3 min, the pellets washed with PBS and frozen at -20 °C or directly loaded on a SDS gel to check the expression and the size of the proteins. 15% SDS-PAGE gel was produced according to hte common protocol. The sample pellets were dissolved in 100 μl water, 13 μl mixed with 2x SB and boiled at 96 °C for 5 min 10 μl was run on the gel.

If the small scaled approach revealed a sufficeint expression of the protein, a large scale protein expression was started. 2 l culture flasks containing 1 l LB-medium, 50 ml DMEM and 1 ml carbenicillin were inoculated with 1 ml of bacterial solution consisting of 20 μl bacteria in 7 ml LB-medium. The flasks were shaken at 180 rpm, 37 °C for 8 hours and at OD600 0,7 protein expression was induced with 1 ml IPTG. After 3 h the mixtures there transferred to 500 ml centrifugation tubes and centrifuged for 10 min at 5 000 rpm (SLA 1500 rotor). The pellets were then frozen at -80 °C.

For the purification of inclusion bodies the bacterial pellets were thawed on ice. The pellets were resuspended in 13 ml solution buffer and transferred to 50 ml centrifuge tubes. The pellets were homogenized using a sonicator. 100 μl lysosome (50 mg/ml solution), 250 μl DNAse I (2 mg/ml) and 50 μl MgCl2 (0,5 M) was added and gently mixed. 12,5 ml lysis buffer was then added and mixed. The tubes were incubated at rt for 1 h. Then the tubes were frozen at -80 °C for 25 min and subsequently transferred to a 37 °C water bath for 30 min. 50 μl MgCl2 was added and incubated another 30 min at rt until viscosity decreased. Then 350 μl NaEDTA (0,5 M) was added and the tubes centrifuged at 11 000 rpm, 4 °C for 20 min (Rotor SA 300, Sorvall). The supernatant was discarded and the pellets resuspended in 10 ml washing buffer with Triton X on ice. The suspension was homogenized using the sonicator. Again the tubes were centrifuged, resuspended in 10 ml washing buffer without Triton X, and homogenized. The tubes were once more centrifuged and the supernatants discarded. The pellets were resuspended in 200 μl urea and shaken over night at 4 °C. The next day the urea solution was transferred to ultracentrifugation tubes and centrifuged at 45 000 rpm for 20 min at 20 °C (Rotor Ti 70.1). The supernatants were pooled into a 15 ml falcon tube. The 0 h and 3 h samples were centrifuged at 9000 rpm for 3 min, washed with PBS, centrifuged again and the pellets frozen at -20 °C or directly loaded on a SDS gel to check the expression and the size of the proteins.

3.2.2   Generation of *Strep*tamers

To generate *Strep*tamers for the k_{off}-rate assay, first the MHC heavy chain has to be refolded with β_2m and the peptide of interest to build the complete and stable MHC complex. Subsequently, the purified complex has to be conjugated with a fluorescent dye and finally, the dye conjugated MHC molecules are multimerized on a *Strep*-Tactin backbone.

3.2.2.1   Refolding and purification of MHC molecules

Heavy chain and β_2m proteins in 8 M Urea were diluted into refolding buffer containing high concentrations of the respective synthetic peptide epitope (60μ/ml). Aliquots of the proteins were first diluted in 3 M guanidine buffer, injected directly into 200 ml refolding buffer every 8 h while vortexing heavily and incubated under constant agitation for 48 h at 10C. The refolding buffer contained a gluthathion redox system to facilitate optimal formation of disulfide-bridges. After 48 h, the protein solution was concentrated to a volume of 10-20 ml over a 10 kDa membrane (Millipore, Eschborn, Germany), then further reduced to 1 ml using 10 kDa concentrator columns (Millipore, Eschborn, Germany). The flowthrough of the first concentration step still contained large amounts of peptide and could be used for a second refolding. Correctly folded MHC I molecules were purified by gelfiltration (Superdex 200HR, Amersham, Munich, Germany) over a FPLC system (FPLC basic, Amersham, Munich, Germany), pooled and incubated over night in a buffer containing NaN$_3$, protease inhibitors(1 mM NaEDTA, Leupeptin, Pepstatin) and 0,1 mM DTT to keep the free cysteine in a reduced state. The next day, the buffer was exchanged against PBS pH 7.4 and the protein concentration determined by a standard BCA-assay.

3.2.2.2   Dye-conjugation and purification

MHC complexes prepared as described in 3.2.2.1 were incubated with the respective fluorescent dye containing a maleimide group in a molar ratio of 1:10 for 2h, RT and in the dark. To separate unbound dye from dye-conjugated MHC molecules, illustra NAP-25 gravity flow columns (GE Healthcare, Buckinghamshire, UK) were used, pre-packed with Sephadex G-25 DNA grade resin. After columns were equilibrated with PBS pH 7.3, the protein dye reaction mix was pipetted on top of the column and waited until the mixture had entered the gel bed completely. 500 μl PBS pH7.3 were added and allowed to enter the gel bed completely. Subsequently, 3ml PBS pH8.0 are added to elute the protein. During elution, the separation of the dye conjugated MHC molecules (first, lighter colored band) from the unbound dye (second, deeper colored band) becomes visible. The first band was collected in a 10 kDa concentrator column (Millipore, Eschborn, Germany) and PBS pH 8 added to 4ml volume. After concentration to 250 μl, 3750 μl PBS pH 8 containing NaN$_3$ and protease inhibitors (1 mM NaEDTA, Leupeptin, Pepstatin) were added, concentrated again to 250 μl and the protein stored in liquid nitrogen after measuring its concentration.

3.2.2.3 Multimerization

For each staining (up to 5 x 10^6 cells), 1 μg of dye-conjugated MHC I and 5 μg *Strep*-Tactin-PE or *Strep*-Tactin-APC respectively were diluted in a final volume of 50 μl FACS buffer and incubated over night or for at least 1 h.

3.2.3 FACS analysis

3.2.3.1 Antibody and *Strep*tamer staining

For *Strep*tamer and/or antibody staining, 5 x 10^6 or less cells per staining were used. Usually, the stainings were performed in 96-well plates. Murine cells were first incubated in 50 μl Fc block (1:500, stock at 2.5 μg/μl) and EMA (1:1000, stock at 2 μg/μl) for 20 min under light, to block Fcγ receptors and to stain dead cells. Cells were then washed once with FACS buffer in a total volume of 200 μl, pelleted for 2 min at 460 x g and resuspended in 50 μl *Strep*tamer solution. Human cells were directly pelleted and resuspended in 50 μl *Strep*tamer solution. Cells were incubated on ice in the dark for 45 min. Antibodies at the appropriate dilution were added for the last 20 min of the staining. The samples were then washed three times in FACS buffer, resuspended in FACS containing propidium iodide to stain dead cells and subsequently analyzed by flowcytometry.

3.2.3.2 Conjugation of *Strep*-Tactin beads to MHC molecules

To test the dye conjugation on MHC molecules in a cell-free setup, 7 μl of magnetic beads coated with *Strep*-Tactin (IBA, Göttingen, Germany)were incubated with 1 μg dye-conjugated MHC molecules for 1h. Beads with multimerized MHC molecules were analyzed for fluorescence By flowcytometry.

3.2.3.3 FACS aquisition and analysis

For FACS analysis, at least 10^5 cells of the populations of interest were acquired on a Cyan flowcytometer (Beckman Coulter, California, USA). *Strep*-Tactin beads coupled with MHC molecules were analyzed in a FACSCalibur (Becton Dickinson, Heidelberg, Germany). Data analysis was performed using FlowJo software (Treestar, Ashland, USA).

3.2.4 k$_{off}$-rate assay

3.2.4.1 *Strep*tamerstaining and sorting

Human PBMCs were obtained by purification of PBS diluted blood over a Ficoll gradient. PBMCs were washed twice with FACS buffer and subsequently allowed to rest in a 96-well plate on ice for at least 1 h before staining, to minimize side effects of MHC multimer staining like internalization of the reagents. After that, the cells were spun down, resuspended in 50 μl *Strep*tamer solution and stained for 45 min on ice and antibodies were added for the last 20 min as described in 3.2.3.1. The cells were washed three times in ice-cold FACS buffer, resuspended in 100 μl FACS

containing propidium iodide (1:1000) and transferred to pre-cooled 1.5 ml tubes. The whole staining procedure was performed on ice and in a cooled centrifuge at all times.

Cells were sorted on a MoFlo II Cell Sorter (DakoCytomation, Glostrup, Danmark) for living, CD8$^+$, *Strep*tamer$^+$ cells. As the cells were sorted into a cooled tube containing FCS, to avoid physical damage, cells had to be washed three times after sorting in a volume of at least 5ml FACS buffer. Finally, cells were resuspended in a final concentration of 10^4 cells in 1 μl FACS.

3.2.4.2 Performance of the k$_{off}$-rate assay

All k$_{off}$-rate measurements were performed on a Leica SP5 confocal laser scanning microscope. Working with *Strep*tamer stained cells, low temperatures had to be assured, as binding of pMHC multimers can lead at temperature higher than 10C internalization of the multimer, which abrogates dissociation of the MHC molecules from the surface. 4C was chosen as optimal temperature for the assay. To guarantee constant cooling of 4C under the microscope, a water cooling device was used, connected to a peltier cooler. A customized metal insert, which fits exactly into the cooling device, was sealed with a cover slip at the bottom to build a reservoir. 1 μl cell suspension was pipetted to the glass slide an immediately covered with a polycarbonate membrane, weighed down with a small metal shim, and subsequently, cold buffer was added. Cells were efficiently arrested in a thin layer between the membrane and the cover slip while the 5 μm pores in the membrane still allowed for rapid diffusion of d-biotin to the cells. A time series was started on the microscope, taking one picture every 10 seconds. After the first picture d-biotin was added and the time series was run until the complete dissociation of the MHCs. The k$_{off}$-rate assay was performed with a confocal microscope due to its high sensitivity. To detect the fluorescence of a complete cell, the pinhole was opened until the thickness of the detected plane corresponded to the layer of the cells.

3.2.4.3 Data analysis

Images were analyzed using MetaMorph Offline image analysis software (Molecular Devices, Downingtown, USA). For each individual cell, integrated fluorescence intensity inside a gate containing the cell was measured over the whole time series that was acquired. The same gate was then put in close proximity to the cell, but not containing the cell, for measurement of background fluorescence intensity. Data were logged into Microsoft Excel (Microsoft, Redmond, USA). Further data analysis was done automatically by the Analyzer nt software (Sebastian Nauerth, LMU) as described in detail in section 4.4.4.

3.2.4.4 Bleaching measurements with beads

To obtain a cell free testing system for the fluorescence intensity and the photostability of fluorescent dyes under the microscope, 7 μl *Strep*-Tactin superflow beads

were incubated with 1μg dye conjugated MHC molecule to allow for their multi-merization on the bead surface. Beads were analogous to cells mounted under the microscope and exposed to the same laser intensities as used in the k_{off}-rate assays. As in the dissociation assay, fluorescence intensities of the beads were monitored by taking pictures every 10s. The bleaching constant k_{bleach} was obtained from the exponent of the curve fitted into the data points.

Chapter 4

Results

4.1 Principle of the k_{off}-rate assay

T cell avidity is believed to be an important parameter for T cell quality. Therefore, it is of special interest to analyze the binding kinetics of surface expressed TCRs in more detail.

Common methods used to assess the binding strength between TCR and pMHC are mainly based on pMHC multimer dissociation assays. However, with these methods it is not possible to accurately determine the binding strength between a monomeric pMHC and a TCR on the surface of a living T cell (s. section 1.2.4.2). Furthermore, it is hard to compare data obtained with different batches of multimers due to heterogeneity in the level of multimerization. In order to improve multimer based k_{off}-rate measurements, Robert Knall originally developed a novel assay for murine T cells based on the use of reversible multimers, so-called *Strep*tamers [173]. The design of this assay allows for accurate calculation of the dissociation kinetics of monomeric pMHC molecules bound to surface expressed TCRs.

The principle of the k_{off}-rate assay is based on fluorescently labeled pMHC molecules that are fused to a *Strep*-tag III sequence at the C-terminus. Several of these altered pMHCs can bind to *Strep*-Tactin via this *Strep*-tag III region and form multimers. Specific T cells can be stably labeled with those multimers (Figure 4.1(a)). As d-biotin has a higher affinity to *Strep*-Tactin than the *Strep*-tag III sequence, adding d-biotin results in a fast detachment of the *Strep*-Tactin backbone from pMHCs bound to surface expressed TCRs (Figure 4.1(b)). We hypothesize that the kinetics of subsequent dissociation of monomerized pMHCs correlates with the binding strength between pMHC and TCR. As the MHC molecules are labeled, the dissociation can be observed as the decay in fluorescence intensity by realtime microscopy (Figure 4.1(c)).

4.2 Setup of the k_{off}-rate assay for murine T cells

To generate a suitable pMHC ligand, the *Strep*-tag III sequence and a flexible Glycine-Serine (GS) linker were fused to the C-term of an MHC molecule, which had been truncated at the transmembrane region. In the murine k_{off}-rate assay setup
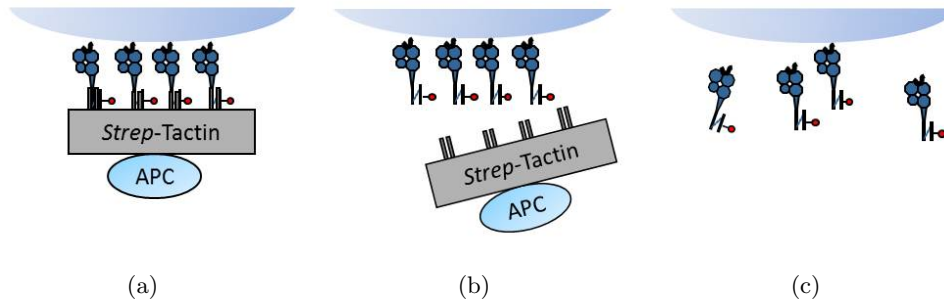
Figure 4.1: **Principle of the k$_{\text{off}}$-rate assay:** Several pMHC-*Strep*-tag fusion proteins can multimerize on *Strep*-Tactin, building a so-called *Strep*tamer. The *Strep*tamers can be used to specifically label pMHC specific CD8$^+$ T cells (a). Upon addition of d-biotin, the *Strep*-Tactin backbone is removed, leaving monomeric MHC molecules bound to surface bound TCRs (b), which dissociate from the T cell surface depending on the binding strength between pMHC and TCR (c). As both the pMHC proteins and the *Strep*-Tactin are conjugated with fluorophores, the dissociation of both molecules can be monitored by realtime microscopy.

the conjugation site for the fluorescent dye was located within the β_2 microglobulin. As iodation experiments revealed that the tyrosin at position 67 was surface accessible [200], Herman Eisen et al. exchanged the tyrosine by a cysteine. The free -SH group of the cysteine allowed for conjugation of different maleimide reactive substances [201]. Thus, a fluorescent dye fused to a maleimide group could be covalently linked to the free -SH group and should not interfere with the structure of the MHC molecule. As a major advantage of this setup, different MHC I heavy chains can be refolded with the mutated β_2 microglobulin, providing a system, which can be easily applied for different mouse MHC alleles. Alexa488-maleimide was chosen as the fluorescent dye, as it is very small and restistant to photobleaching.

The Alexa488 conjugated MHC molecules were multimerized on *Strep*-Tactin that were conjugated with phycoerythrin (PE). These dichromatic *Strep*tamers lead to a PE and Alexa 488 double staining of the *Strep*tamer stained T cells (Figure 4.3(a)). The PE fluorescence intensity of dichromatic *Strep*tamers and *Strep*tamers with unconjugated MHC molecules were comparable, whereas only the dichromatic *Strep*tamers showed a clear shift for Alexa488 (Figure 4.3(b)). Most importantly, both the PE and the Alexa488 fluorescence were nicely detectable by fluorescence microscopy (Figure 4.3(c)).

In conclusion, by conjugating a fluorescent dye to the murine β_2 microglobulin, dichromatic *Strep*tamers could be generated that showed a double staining of antigen-specific T cells. This double staining was clearly detectable by flow cytometry and fluorescence microscopy, and could be reversed by the addition of d-biotin (data not shown). Fulfilling these essential requirements, k$_{\text{off}}$-rate assays could be successfully performed with the described setup.
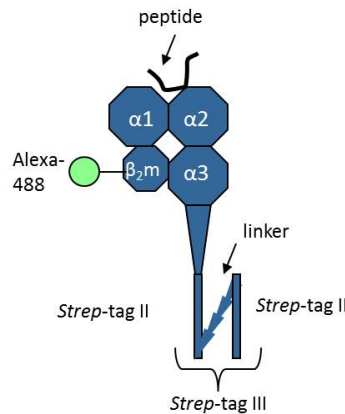
Figure 4.2: **Dye conjugated pMHC molecule in the murine setup:** The pMHC-*Strep*-tag fusion protein is composed of a pMHC molecule that was truncated at the transmembrane domain and fused to two *Strep*-tag II sequences, forming together the *Strep*-tag III. Several pMHC molecules can bind to one *Strep*-Tactin via the reversible *Strep*-tag-*Strep*-Tactin interaction, forming *Strep*tamers. For murine k_{off}-rate assays the tyrosine at position 67 in the murine β_2m was exchanged for a cysteine to allow for the conjugation to a fluorescent dye over a maleimide reaction. Alexa488 was used as the fluorescent dye in the murine k_{off}-rate assay setup.

4.3   Test of human β_2 microglobulin conjugated MHCs

The k_{off}-rate assay with murine T cells revealed a clear correlation between the functional avidity and the k_{off}-rate. Most importantly, Robert Knall could show in preclinical mouse models that only T cells with a high half-life time were able to confer protection after infection. This finding emphasizes the correlation between the k_{off}-rate and the protective capacity of a T cell [164].

This indicates the k_{off}-rate could also be an important predictive parameter for T cell quality, for example in the setting of adoptive T cell therapy in humans. Hence, it was of major interest to establish the k_{off}-rate assay for human T cells.

4.3.1   Insufficient *Strep*tamer staining after dye conjugation on human β_2 microglobulin

As the structures of the murine and the human MHC I molecules are very similar, it was expected that the setup of the murine k_{off}-rate assay could be directly transferred to human MHC I molecules. Analogue to the murine counterpart, Alexa488 was conjugated to the cys67 of the human β_2m. For initial experiments, the MHC I allele HLA B8 loaded with the CMV peptide Immediate Early $1_{199-207K}$ ($\text{IE1}_{199-207K}$) was tested with the described Alexa488 conjugation. This MHC-peptide combination was chosen, as T cells specific for this pMHC complex could be obtained from healthy individuals, which allowed for the easy testing of newly generated *Strep*tamers. Furthermore, CMV-specific T cells have a high impact in adoptive T cell therapy of immunocompromised patients after allogenic stem cell transplantation (SCT). It is thus very interesting to analyze these T cells in more detail.
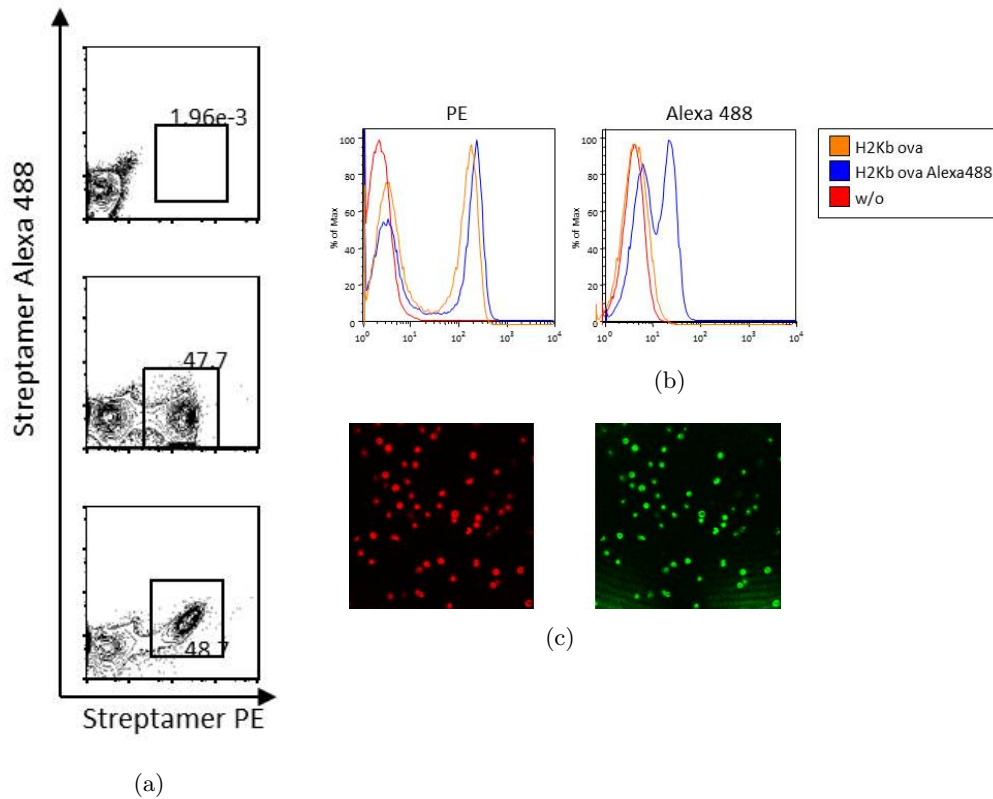
Figure 4.3: **_Strep_tamer staining of T cell specific for H2-k^b Ova$_{256-264}$**: Splenocytes from OT-1 mice were mixed with B6 splenocytes in a 1:1 ratio to obtain a _Strep_tamer negative population as an internal control. $5*10^6$ cells were stained with an αCD8 PB antibody or in combination with H2-k^b Ova$_{256-264}$ _Strep_tamer or the dichromatic _Strep_tamer H2-k^b Ova$_{256-264}$ Alexa488 respectively. (a) shows the staining of _Strep_tamer dyes PE and alexa488, gated on CD8$^+$ living T cells. Numbers indicate the percentage of _Strep_tamer$^+$ T cells in the plot. The PE and Alexa488 fluorescence intensitiy of all CD8$^+$ T cells is additionally shown in histograms (b). The fluorescence intensity of PE (left) and Alexa488 (right) of FACS sorted, CD8$^+$ _Strep_tamer$^+$ T cells detected by confocal microscopy (c).

Refolding of the mutated β_2 microglobulin with the HLA B8 heavy chain was successful and after subsequent dye conjugation, refolded proteins were purified by gel filtration (data not shown). Alexa488 conjugated MHC molecules were incubated with *Strep*-Tactin, forming dichromatic *Strep*tamers, termed HLA B8 IE1$_{199-207K}$-Alexa488 in the following. PBMCs were isolated from a donor ("Donor 1") with a substantial T cell population specific for HLA B8 IE1$_{199-207K}$ and stained with αCD8 antibodies alone or in combination with the monochromatic *Strep*tamer HLA B8 IE1$_{199-207K}$ or the dichromatic *Strep*tamer HLA B8 IE1$_{199-207K}$-Alexa488. Comparable to the staining of mouse cells (Figure 4.3), human T cells stained with the HLA B8 IE1$_{199-207K}$ *Strep*tamer formed a distinct population with bright PE staining intensity (Figure 4.4(a)). However, T cells incubated with the dichromatic *Strep*tamer HLA B8 IE1$_{199-207K}$-Alexa488 showed no Alexa488 fluorescence. In addition, the PE staining was almost lost, resulting in a shift of the specific T cells towards the negative polulation. The absence of Alexa488 fluorescence and the substantially lower PE staining intensity compared to T cells stained with HLA B8 IE1$_{199-207K}$ *Strep*tamer was also clearly visible in the histogram of fluorescence intensities (Figure 4.4(b)). In line with the results obtained by flow cytometry, sorted HLA B8 IE1$_{199-207K}$ specific T cells stained with the dichromatic *Strep*tamer showed no detectable Alexa488 fluorescence and only a very weak PE fluorescence under the microscope (Figure 4.4, lower panel).

4.3.2   Successful dye conjugation to β_2 microglobulin

Due to the low fluorescence intensities of PE and Alexa488, it was not possible to perform k$_{off}$-rate assays with the Alexa488 conjugated MHC molecules. The missing Alexa488 fluorescence of the "dichromatic" *Strep*tamers could be explained by ineffective dye conjugation to the β_2 microglobulin. To test this, human MHC molecules which should be Alexa488 conjugated were incubated with small beads coated with *Strep*-Tactin. Analogue to the multimerization described for *Strep*tamers, recombinant MHCs can bind the *Strep*-Tactin on the beads via their *Strep*-tag sequences(Figure 4.5(b)). MHC loaded beads were subsequently analyzed for their Alexa488 fluorescence. As controls, beads loaded with murine, Alexa488 conjugated MHCs and unloaded beads were analyzed.

The histogram in Figure 4.5 shows the Alexa488 staining intensity of the MHC loaded beads. All beads coated with human MHCs that had been incubated with Alexa488, showed a clear shift in the Alexa488 fluorescence intensity compared to the unloaded beads. Furthermore, this shift was comparable to the shift obtained with the beads loaded with murine Alexa488 conjugated MHCs (Figure 4.5(a)). This indicates that the human MHC molecules were successfully conjugated with Alexa488.

4.3.3   Dye conjugation on β_2 microglobulin is very specific

An unsuccessful dye conjugation could be excluded as reason for the absent Alexa488 fluorescence of T cells that were stained with the dichromatic *Strep*tamers. We then hypothesized that the dye might also bind to a different site than the β_2 mi-
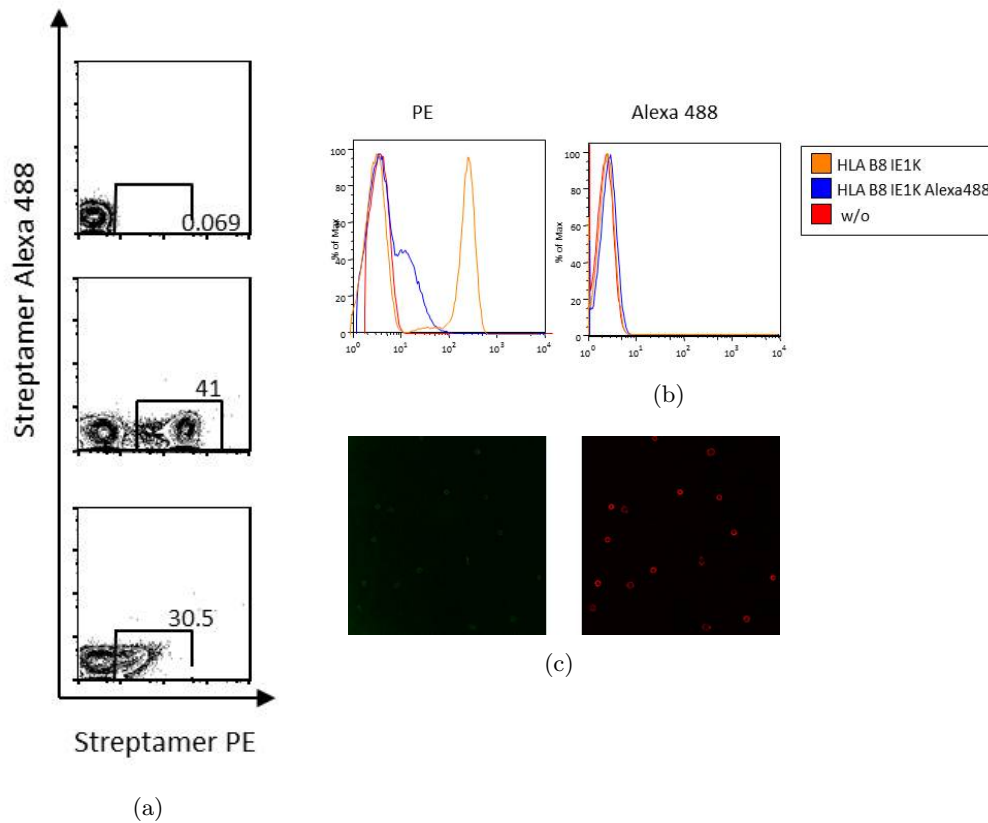
Figure 4.4: ***Strep*tamer staining of T cell specific for HLA B8 IE1**$_{199-207K}$: Lymphocytes were obtained from whole blood (1:1 diluted with PBS) by Ficoll purification. $5*10^6$ cells were stained with αCD8 PB antibody or in combination with HLA B8 IE1$_{199-207K}$ *Strep*tamer or the dichromatic *Strep*tamerHLA B8 IE1$_{199-207K}$ Alexa488 respectively. (a) shows the staining of *Strep*tamer dyes PE and Alexa488, gated on CD8$^+$ living T cells. Numbers indicate the percentage of *Strep*tamer$^+$ T cells in the plot. The PE and Alexa488 fluorescence intensitiy of all CD8$^+$ T cells is additionally shown in histograms (b). The fluorescence intensity of PE (left) and Alexa488 (right) of FACS sorted, CD8$^+$ *Strep*tamer$^+$ T cells detected by confocal microscopy (c).

(a)   (b)
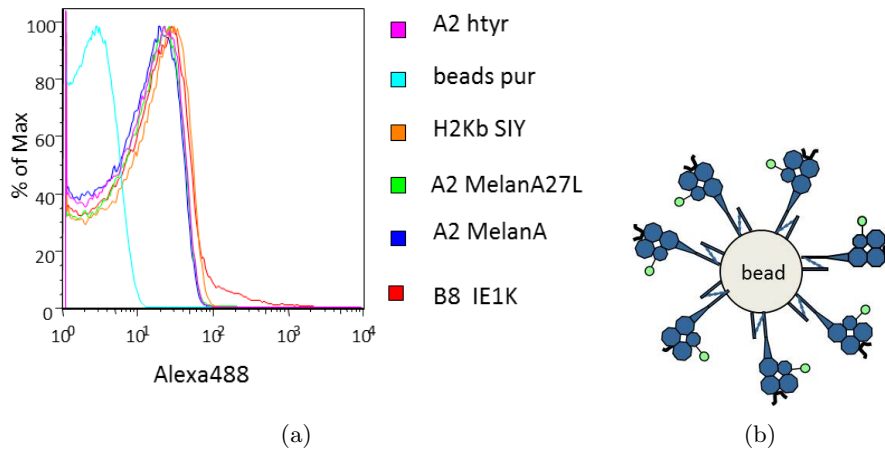
Figure 4.5: Test of fluorescently labeled human MHCs on *Strep*-Tactin coated magnetic beads: 7 μl *Strep*-Tactin coated beads were incubated with 1 μg of the respective MHC molecules for 30min and subsequently analyzed by flowcytometry. Scheme of the MHC loaded *Strep*-Tactin beads is shown in (b) and histrogram of the Alexa488 fluorescence of pure beads as a control or beads loaded with Alexa488 conjugated MHCs is shown in(a).

croglobulin in the human MHC molecule. This could lead to interference with the TCR binding, which could potentially explain the weak staining of the dichromatic *Strep*tamers.

As the dye should only be conjugated to the inserted cysteine at position 67 of the mutated β_2 microglobulin, the dye should not bind to a pMHC complex containing the unmutated β_2 microglobulin with tyrosin at position 67. Therefore, a HLA B8 IE1$_{199-207K}$ molecule containing the unmutated β_2 microglobulin (Figure 4.6 (a), (b)) was incubated with Alexa488 to test the specificity of the dye conjugation.

After the incubation with Alexa488 and the following purification of the MHC molecules by gel filtration, *Strep*tamers were generated with these MHCs and tested for staining of specific T cells. Figure 4.6 shows that the population size and the fluorescence intensity of the *Strep*-Tactin backbone was highly comparable when T cells were stained with either unconjugated HLA B8 IE1$_{199-207K}$ *Strep*tamers (middle panel) or HLA B8 IE1$_{199-207K}$ that was incubated with the dye (lower panel). Furthermore, there was no shift in the Alexa488 fluorescence intensity of the T cells stained with the dye incubated HLA B8 IE1$_{199-207K}$ *Strep*tamer (Figure 4.6(c)). In summary, the dye incubation of an MHC molecule containing the unmutated β_2m seemed not to result in dye conjugation to the MHC molecules and thus does not affect the ability of generated *Strep*tamers to stain specific T cells. This suggests that the dye is very specifically conjugated to the cystein67 in the mutated β_2m. This is in line with analyses of the crystal structure of the human MHC I molecule, where it could be oberserved that all cystein residues are located inside the immunoglobuline domains of the heavy chain and the barrel structure of the β_2m respectively. Only the cysteine inserted at the position 67 in the β_2m is surface accessible and therefore available for dye conjugation.

(a)

(b)

(c)
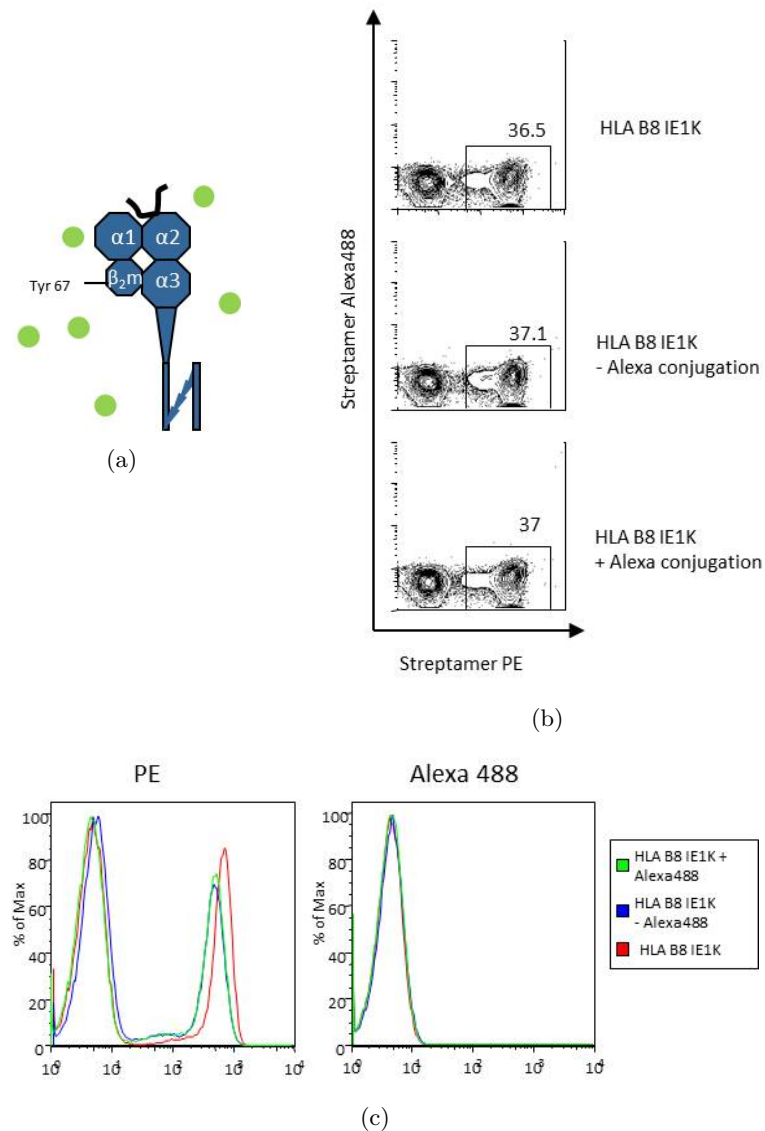
Figure 4.6: **Incubation with fluorescent dye leaves the human MHC molecules unconjugated and intact:** $5*10^6$ purified human lymphocytes were stained with αCD8 PB antibody and HLA B8 IE1$_{199-207K}$ *Strep*tamers or HLA B8 IE1$_{199-207K}$ *Strep*tamers consisting of MHC molecules pretreated with mercaptoethanol or Alexa488 and mercaptoethanol respectively. A schematic illustration of the "wildtype" MHC molecule containing a tyrosine at position 67 of the β_2m is shown in (a). (b) shows the staining of *Strep*tamer dyes PE and Alexa488, gated on CD8$^+$ living T cells. Numbers indicate the percentage of *Strep*tamer$^+$ T cells in the plot. PE and Alexa488 fluorescence intensitiy of all CD8$^+$ T cells is additionally shown in histograms (c).

4.3.4 Generation of chimeric MHC molecules

The previous experiments showed that the dye conjugation on the human β_2m is successful and very specific. However, staining of specific T cells with dye-conjugated dichromatic *Strep*tamers resulted in a strongly reduced PE fluorescence and no detectable Alexa488 fluorescence. A possible reason could be that the dye conjugated human β_2m interfered with the binding of the whole pMHC complex to the TCR.

To test the effect of the dye conjugated β_2m on the TCR binding, we generated a chimeric MHC molecule, consisting of the murine heavy chain and the human β_2m (Figure 4.7(a), (b)). As the complex of murine heavy chain and dye-conjugated murine β_2m was able to form functional dichromatic *Strep*tamers, the failure of *Strep*tamer staining with the chimeric MHC complex would pinpoint to the staining problems to the dye-conjugated human β_2m. H2-k^b loaded with the peptide Ova$_{256-264}$ was chosen as murine pMHC complex, as transgenic T cells specific for this pMHC combination could be easily obtained from OT1 mice. In addition, a large amount of data on *Strep*tamer stainings and k$_{off}$-rates has already been aquired with these cells and allowed for comparison to newly generated data.

The refolding of the chimeric MHC complex resulted in protein complexes with the expected size and produced a protein yield comparable to the murine MHC complex, indicating that the refolding was very efficient. After dye conjugation, OT1 cells were stained with αCD8 antibodies and the dichromatic murine H2-k^b Ova$_{256-264}$ *Strep*tamer or the dichromatic chimeric H2-k^b Ova$_{256-264}$ + Hβ_2m *Strep*tamer. Figure 4.7(c) shows that the staining with the two different *Strep*tamers was highly comparable concerning the PE and the Alexa488 fluorescence intensity. This revealed that it was possible to generate functional dichromatic *Strep*tamers with dye conjugated human β_2m and indicated that the human β_2m was not the main reason for the failing of dye conjugated human MHC molecules.

In parallel, the inverse chimeric MHC molecule, consisting of a human heavy chain and the murine β_2m, was generated to test if the staining capability of the human dichromatic *Strep*tamer could be rescued by dye conjugation to the murine β_2m (Figure 4.8(a), 4.8(b)). Regarding this chimeric MHC complex, the refolding and the subsequent dye conjugation worked with the expected protein yield and complexes of correct size could be purified (data not shown). To see if the refolding of a murine β_2m with a human heavy chain would produce functional MHC molecules, the human heavy chain was additionally refolded with the unmutated murine β_2m. PBMCs from Donor 1 were stained with αCD8 antibodies alone or in combination with HLA B8 IE1$_{199-207K}$ *Strep*tamer, the chimeric HLA B8 IE1$_{199-207K}$ with murine β_2m or the chimeric HLA B8 IE1$_{199-207K}$ with Alexa488 conjugated murine β_2m respectively (Figure 4.8(c)).

Population size and fluorescence intensity of the *Strep*tamer PE staining of the chimeric HLA B8 IE1$_{199-207K}$ with murine β_2m or the human HLA B8 IE1$_{199-207K}$ *Strep*tamer were comparable. This indicated that the human heavy chain that was refolded with a murine β_2m was able to form functional pMHC complexes that were recognized by specific human T cells. However, after dye conjugation on the murine β_2m, the dichromatic *Strep*tamer with the chimeric MHC molecule also lost the ability to bind to specific T cells.
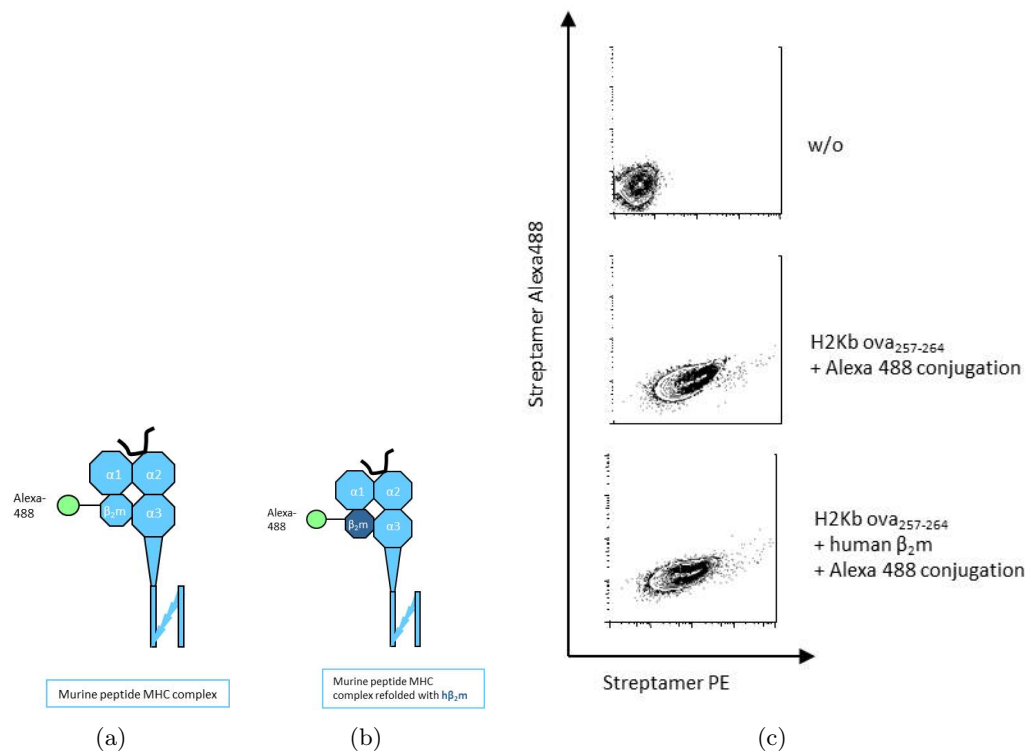
Figure 4.7: ***Strep*tamer staining with chimeric MHC molecules, consisting of a murine heavy chain and a human β_2 microglobulin:** Schematic illustration of a murine pMHC-*Strep*-tag fusion protein (a) and the chimeric protein (b) containing the murine heavy chain (light blue) and the humane β_2m (dark blue). $5*10^6$ splenocytes from OT1 mice were stained with αCD8 PB antibody or in addition with H2-k^b Ova$_{256-264}$-Alexa488 *Strep*tamer or the chimeric *Strep*tamer H2-k^b hβ_2m Ova$_{256-264}$-Alexa488. (c) shows the staining of *Strep*tamer dyes PE and Alexa488, gated on CD8$^+$ living T cells.
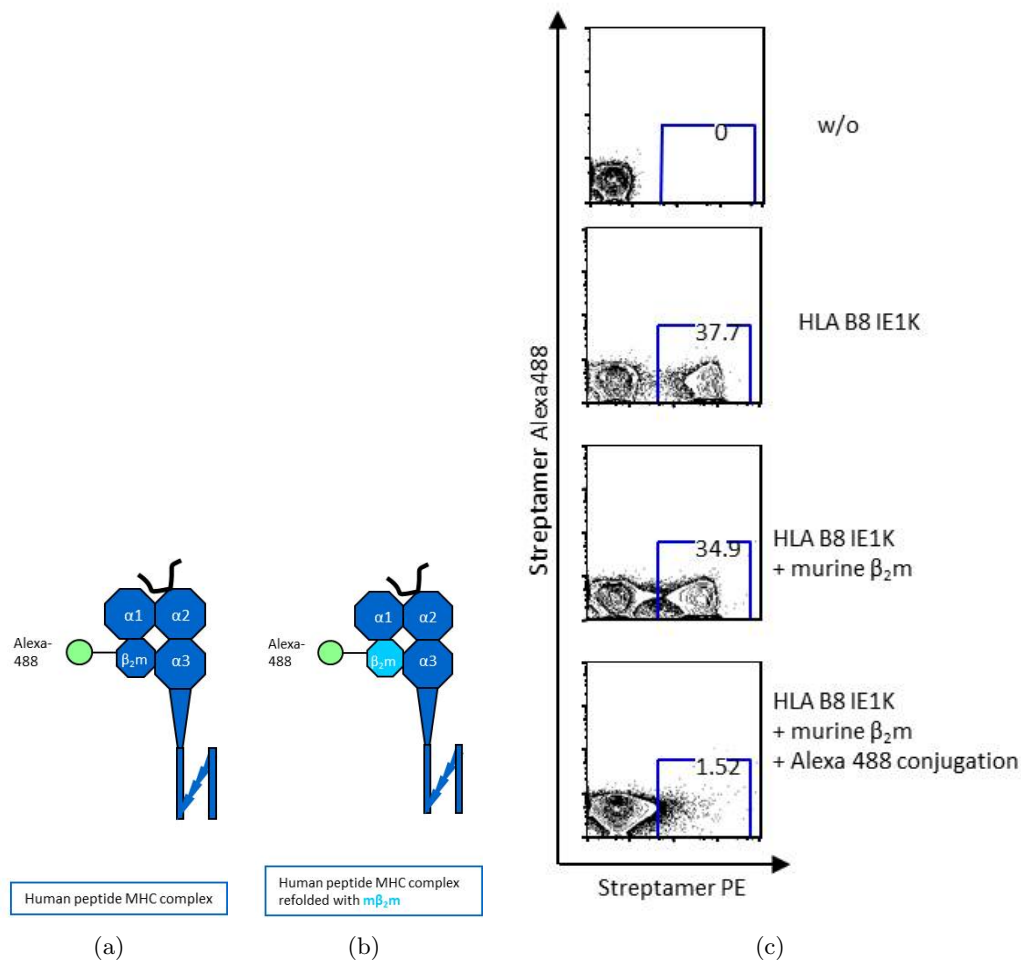
Figure 4.8: ***Strep*tamer staining with chimeric MHC molecules, consisting of a human heavy chain and a murine β_2 microglobulin:** Schematic illustration of a human pMHC-*Strep*-tag fusion protein (a) and the chimeric protein (b) containing the human heavy chain (dark blue) and the murine β_2m (light blue). $5*10^6$ purified human lymphocytes were stained with αCD8 PB antibody or in addition with HLA B8 IE1$_{199-207K}$ *Strep*tamer or the chimeric *Strep*tamers HLA B8 mβ_2m IE1$_{199-207K}$ and HLA B8 mβ_2m IE1$_{199-207K}$-Alexa488 respectively. (c) shows the staining of *Strep*tamer dyes PE and Alexa488, gated on CD8$^+$ living T cells. Numbers indicate the percentage of *Strep*tamer$^+$ T cells in the plot.

The data obtained from experiments with chimeric pMHC complexes showed that it was possible to form a functional pMHC complex with a human β_2m conjugated with Alexa488. However, if the murine β_2m was refolded with the human heavy chain and conjugated to Alexa488, this chimeric complex behaved similar to the human dye conjugated pMHC complex and lost the ability to stain specific T cells. These experiments suggested that the dye conjugation on the β_2m was responsible for the inability of human dichromatic *Strep*tamers to stain cells. This was unexpected, as the crystal structures of the human and the murine MHC I molecules are very similar and the dye conjugation on the murine β_2m did not interfere with the binding of the murine pMHC complex to specific TCRs. However, there were slight structural differences compared to the murine pMHC complex, like the slightly closer proximity of the human β_2m to the human heavy chain. These minor differences might be the reason that dye conjugation on β_2m in the human heavy chain could cause alterations in the MHC molecule that potenially lead to the loss of TCR binding capacity.

4.4 New setup for human k$_{off}$-rate assay

The expriments described in section 4.2 showed that it was not possible to directly transfer the setup for the murine k$_{off}$-rate assay to human MHC molecules, as the dye conjugation on the human β_2m abolished the binding of the pMHC complexes to specific TCRs. For the conducting of the k$_{off}$-rate assay however, the dye conjugation of MHC molecules was an essential prerequisite to be able to observe the dissociation of monomeric MHC molecules from surface bound TCRs by realtime microscopy. Consequently, a different site for dye conjugation within the human pMHC complex had to be found to enable k$_{off}$-rate measurements for human T cells.

4.4.1 Introduction of a new conjugation site

The new conjugation site for the fluorescent dye should not interfere with the binding of the pMHC complex to the TCR. By locating the conjugation site at a position with highest distance to the pMHC-TCR interface, any influence of the dye on TCR binding should be unlikely.

As the *Strep*-tag III region is a flexible polypeptide chain fused to the C-term of the MHC molecule, new conjugation sites within this region should be generated and tested. Figure 4.9 illustrates the binding of the MHC-*Strep*-tag fusion protein to its binding partner, here *Strep*tavidin [202]. The *Strep*-tag III region contains two *Strep*-tag II sequences, which can bind to *Strep*tavidin or *Strep*-Tactin. Flexible peptide chains mainly built of glycine and serine residues, so-called GS-linker, are used to link the C-term of the MHC molecule to the first *Strep*-tag II sequence and connect the two *Strep*-tag II sequences.

To generate a new conjugation site, a cysteine residue had to be introduced at the chosen position by mutagenesis PCR. A fluorescent dye can bind to the free -SH group of this cysteine for example over a maleimide reaction, which links the dye cOvalently to the MHC molecule. In separate approaches, three different conjugation sites were tested. A cysteine was inserted either in the GS-linker region between the
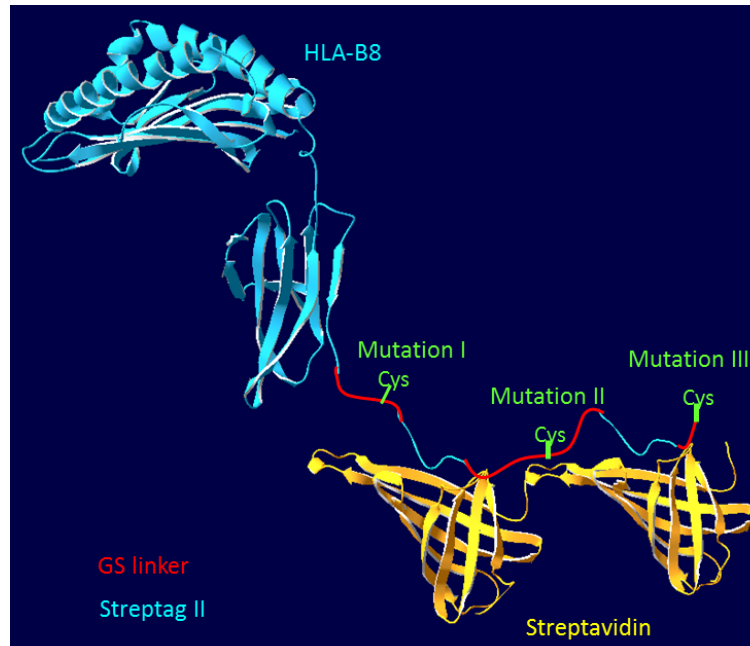
Figure 4.9: **Model of the structure of the MHC-*Strep*-tag fusion protein bound to *Strep*avidin:** Schematic combination of the crystal structures of HLA B8 (adapted from 1M05, [203]) and two *Strep*-tag affinity peptides each bound to *Strep*avidin (adapted from 1RSU, [202]), linked with GS peptide sequences (red). This model illustrates the interaction of the *Strep*-tag III region in the MHC fusion protein with its cognate target, here *Strep*avidin. Approximate positions in the *Strep*-tagIII, at which a cysteine was inserted to create conjugation sites for the fluorochrome, are indicated in green.

MHC C-term and the first *Strep*-tag, in the GS-linker region between the *Strep*-tag II regions or after the second *Strep*-tag II sequence (Figure 4.9). To prevent any influence of the dye on the binding of the *Strep*-tag II sequence to *Strep*-Tactin, an additional GS linker was introduced between the *Strep*-tag II sequence and the third conjugation site.

Figure 4.10 shows the sequence of the *Strep*-tag III region fused to the HLA B8 molecule. The three different conjugation sites with the residues that were introduced by mutagenesis PCR are indicated.

The mutagenesis PCR and the subsequent cloning were successfully performed for mutations I and III. However, even after repeated mutagenesis PCRs with different primers, mutation II could never be generated. Therefore, subsequent expression and refolding of the mutated MHC molecules were done for mutations I and III. Both mutations could be expressed and refolded with the expected protein yield (data not shown). After conjugation with Alexa488, the newly generated MHC molecules were tested in *Strep*tamer stainings.

PBMCs from Donor 1 were purified and stained with αCD8 antibodies alone or in addition with HLA B8 IE1$_{199-207K}$ *Strep*tamer, or with the dichromatic *Strep*tamers HLA B8 IE1$_{199-207K}$ Mutation I or HLA B8 IE1$_{199-207K}$ Mutation III, respectively. As Figure 4.11 shows, the PE fluorescence intensity and the population size of the
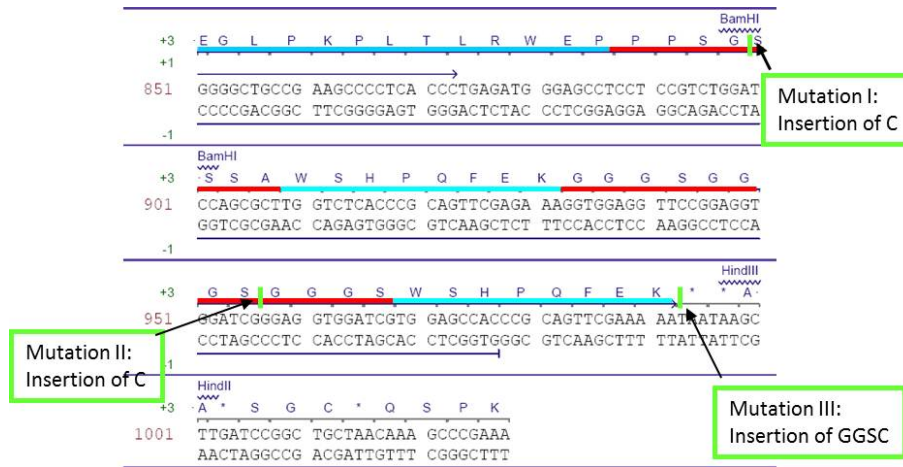
Figure 4.10: **Sequence of the *Strep*-tag III region:** The C-terminus of the human heavy chain is marked with a blue line, GS-linker sequences with red lines and the *Strep*-tagII sequences with light blue lines. Positions and amino acids of planned insertions are indicated.

stained T cells were comparable between the three different *Strep*tamer stainings. This indicates that both dichromatic *Strep*tamers are able to bind efficiently to the TCRs of specific T cells. In addition, both T cell populations stained with the dichromatic *Strep*tamers show a shift in the Alexa488 staining (Figure 4.11 (a), (b)). Hence, the dye conjugation at the two different sites in the *Strep*-tag region was successful and did not interfere with the binding of the pMHC complex to the TCR. As the Alexa488 shift was slightly stronger for T cells stained with HLA B8 IE1$_{199-207K}$ Mutation III, we decided to continue the experiments with those *Strep*tamers. All dye conjugated MHC I molecules described in the following sections contained this cysteine mutation III, if not indicated differently.

To test if the Alexa488 fluorescence of the *Strep*tamer stained T cells were bright enough to perform k$_{off}$-rate assays, living CD8$^+$ *Strep*tamer$^+$ T cells were sorted from PBMCs and the fluorescence intensity was analyzed by confocal microscopy. The Alexa488 fluorescence was detectable and after addition of d-biotin, the k$_{off}$-rates of several cells could be calculated (Figure 4.12). However, in most of the experiments, the Alexa488 fluorescence intensity was very low and could hardly be distinguished from background fluorescence. In these cases, no k$_{off}$-rates could be calculated after addition of d-biotin.

Hence, with the insertion of a new conjugation site at the end of the *Strep*-tag III region, interference of the fluorescent dye with the pMHC-TCR binding could be prevented. For the first time, stable staining of specific T cells was achieved with human dichromatic *Strep*tamers. However, the fluorescence intensity of Alexa488 at this position was very low. Minor changes in the intensity of the *Strep*tamer staining, e.g. due to slight fluctuations of the temperature, resulted in an Alexa488 fluorescence intensity under the detection limit of the confocal microscope. Thus, a new fluorescent dye had to be found, which was bright enough to ensure reliable k$_{off}$-rate measurements.

(a)   (b)
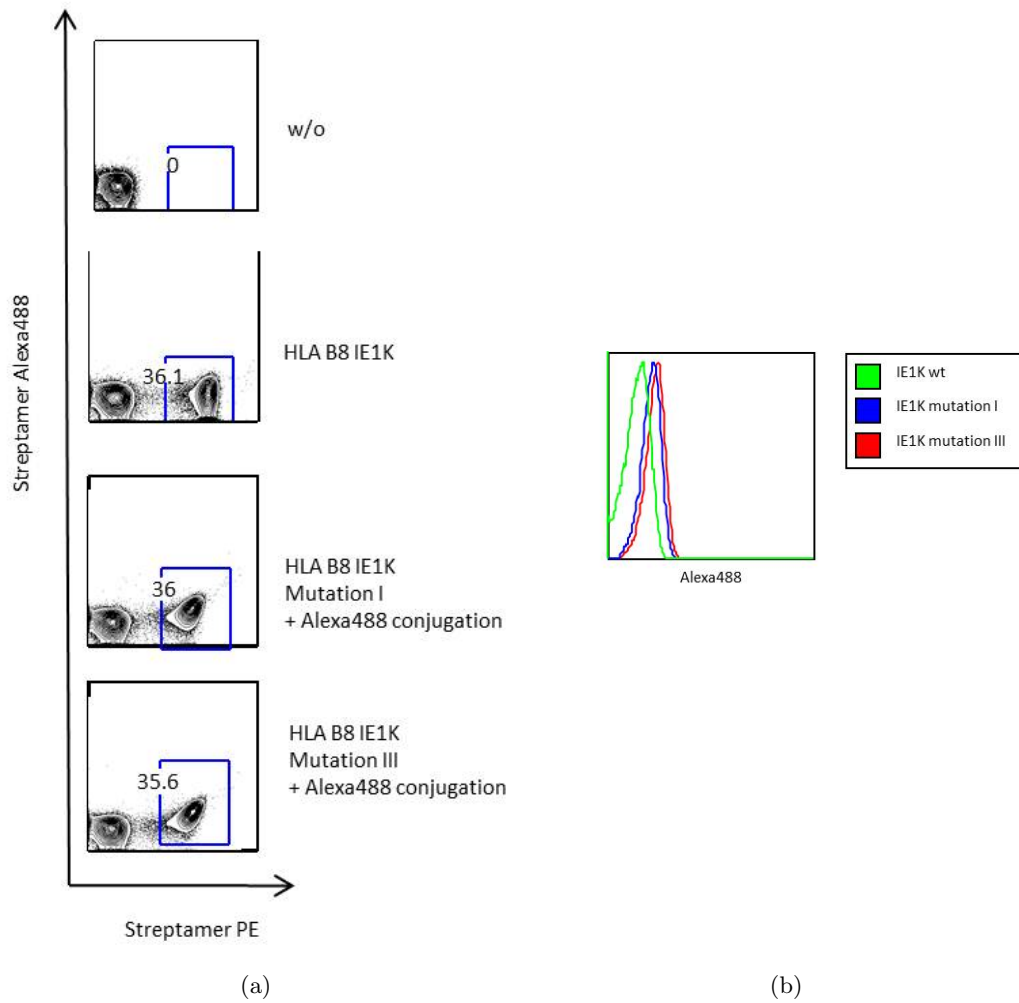
Figure 4.11: **_Strep_tamer staining with HLA B8 molecules containing the indicated mutations in the _Strep_-tag sequence:** $5*10^6$ purified human lymphocytes were stained with αCD8 PB antibody or in addition with HLA B8 IE1$_{199-207K}$ _Strep_tamer or the _Strep_tamers HLA B8 IE1$_{199-207K}$ Mutation I-Alexa488 and HLA B8 IE1$_{199-207K}$ Mutation III-Alexa488 respectively. (a) shows the staining of _Strep_tamer dyes PE and Alexa488, gated on CD8$^+$ living T cells. Numbers indicate the percentage of _Strep_tamer$^+$ T cells in the plot. The histogram in (b) shows the Alexa488 fluorescence intensitiy of the _Strep_tamer$^+$ T cells.

(a)   (b)
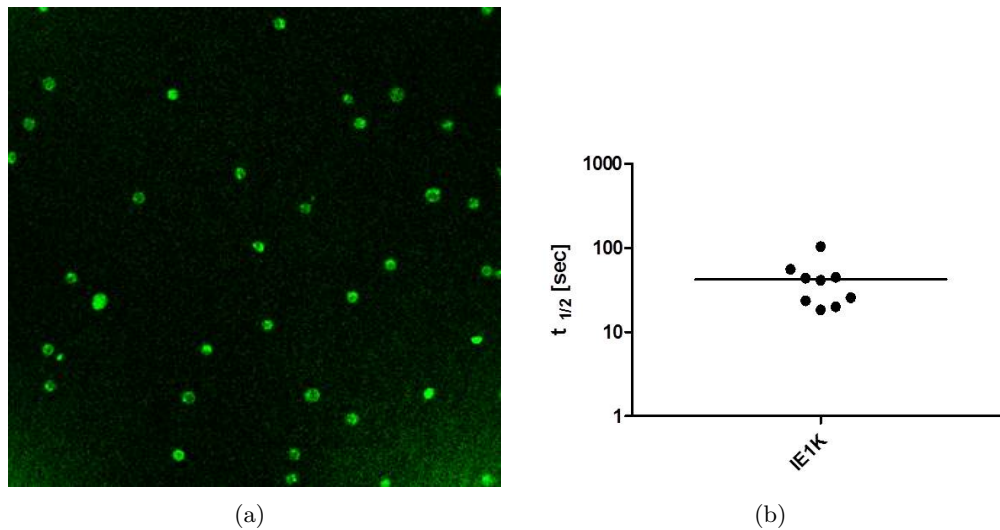
Figure 4.12: **k$_{\text{off}}$-rate assay with T cells stained with HLA B8 IE1K *Strep*tamers, containing Mutation III and Alexa488 conjugation:** Ficoll purified human lymphocytes were stained with αCD8 PB antibody and HLA B8 IE1$_{199-207K}$-Alexa488 *Strep*tamer and sorted for CD8$^+$ *Strep*tamer$^+$ living lymphocytes. k$_{\text{off}}$-rate assays were subsequently performed under microscopic control. (a) Picture of the Alexa488 fluorescence of the sorted cells. (b) Half-life times obtained from several k$_{\text{off}}$-rate assays.

4.4.2   Selection of a new fluorescent dye

Looking for a new fluorescent dye, three criteria were of major importance: the size, the quantum yield and the photobleaching restistance.

The **size** was of obvious importance, as interference of the dye with the binding to the TCR or the *Strep*-Tactin becomes more probable with increasing size of the dye. Alexa488, which could be shown to interfere neither with the TCR nor the *Strep*-Tactin binding when conjugated to the end of the *Strep*-tag III region, has a size of 720.66 g/mol. Hence, the size of a new dye should lie in a similar range. The **quantum yield** of a dye is defined by the ratio of emitted photons to absorbed photons. The higher the quantum yield, the more absorbed photons are emitted as fluorescent light resulting in higher fluorescence intensity of the dye. **Photobleaching** can be described as the destruction of a fluorescent dye during exposure to the excitation (laser) light. As the dissociation of the monomeric MHC molecules was observed by realtime microscopy, the fluorescent dye conjugated to the MHC molecule had to be quite stable during the k$_{\text{off}}$-rate assay. The decay of fluorescence due to photobleaching can be included into the calculations of the k$_{\text{off}}$-rate (s. section 4.4.3) and causes no problems as long as the photobleaching is slow. In contrast, fast photobleaching of the dye would not allow for longer k$_{\text{off}}$-rate measurements and thus limit the range of detectable half life times. As the level of photobleaching is strongly influenced by the molecular structure of the fluorescent dye, a dye with high resistance to photobleaching should be chosen.

The company Atto-tec was found to offer a broad range of small fluorophores with sufficient photobleaching resistance. First, the three different dyes Atto488, Atto532
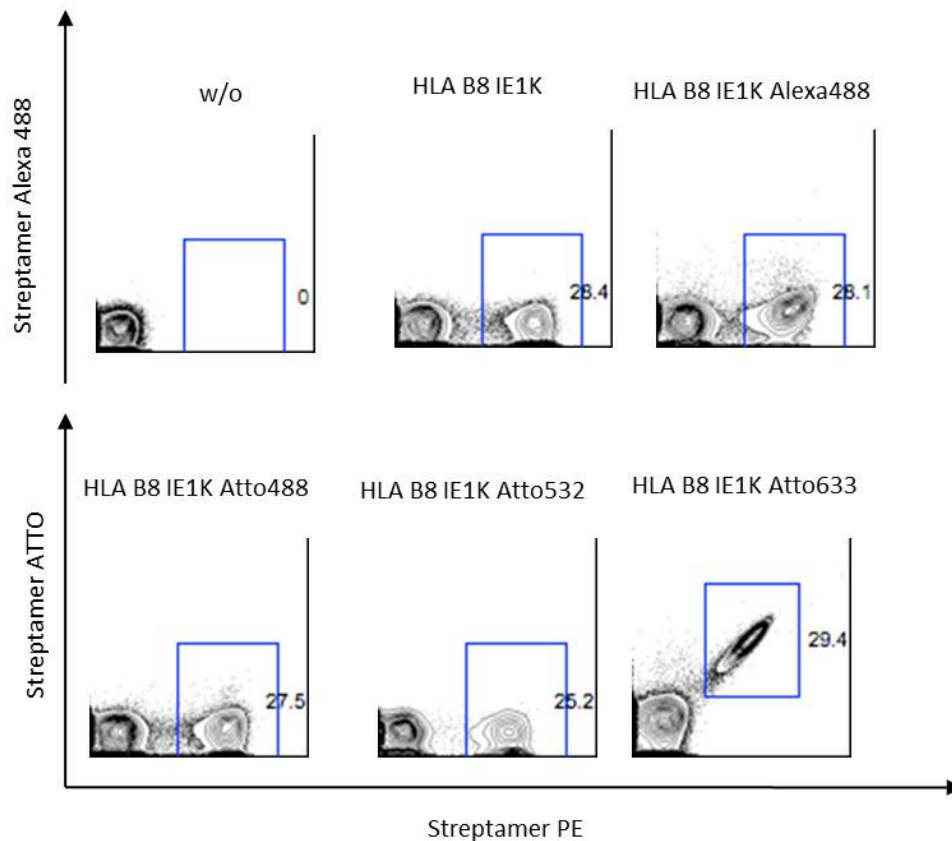
Figure 4.13: **Test staining with HLA B8 IE1K *Strep*tamers conjugated with different fluorescent Atto dyes:** $5*10^6$ purified human lymphocytes were stained with αCD8 PB antibody or in addition with HLA B8 IE1$_{199-207K}$ *Strep*tamer or the *Strep*tamers HLA B8 IE1$_{199-207K}$ conjugated with Alexa488, Atto488, Atto532 or Atto633. Dotplots show the staining of *Strep*-Tactin PE versus the fluorescent dyes on the MHCs, gated on CD8$^+$ living T cells. Numbers indicate the percentage of *Strep*tamer$^+$ T cells in the plot.

and Atto633 were tested. Atto488 was chosen, as it should be 10% brighter than Alexa488 and would allow for microscope settings that are comparable to former murine k$_{\text{off}}$-rate settings. Atto532 is described as the brightest Atto dye. However, available laser settings restrict the detection of Atti532 to microscopy, while analysis by flow cytometry is not possible by conventional analyzers. In contrast, Atto633 is detectable by both flowcytometry and microscopy, as it has a similar excitation wavelength than the widely used APC dye.

PBMCs from Donor 1 were stained with αCD8 antibodies alone or in addition with HLA B8 IE1$_{199-207K}$ *Strep*tamer or with the dichromatic *Strep*tamers HLA B8 IE1$_{199-207K}$-Alexa488, -Atto488, -Atto532 or -Atto633 respectively. As shown in Figure 4.13 all *Strep*tamer stainings showed distinct populations of specific T cells with a comparable population size. This indicated that all *Strep*tamers could bind stably to specific TCRs. However, the *Strep*tamer staining with the MHCs conjugated with Atto488, which should be 10% brighter than Alexa488 according to

(a)   (b)
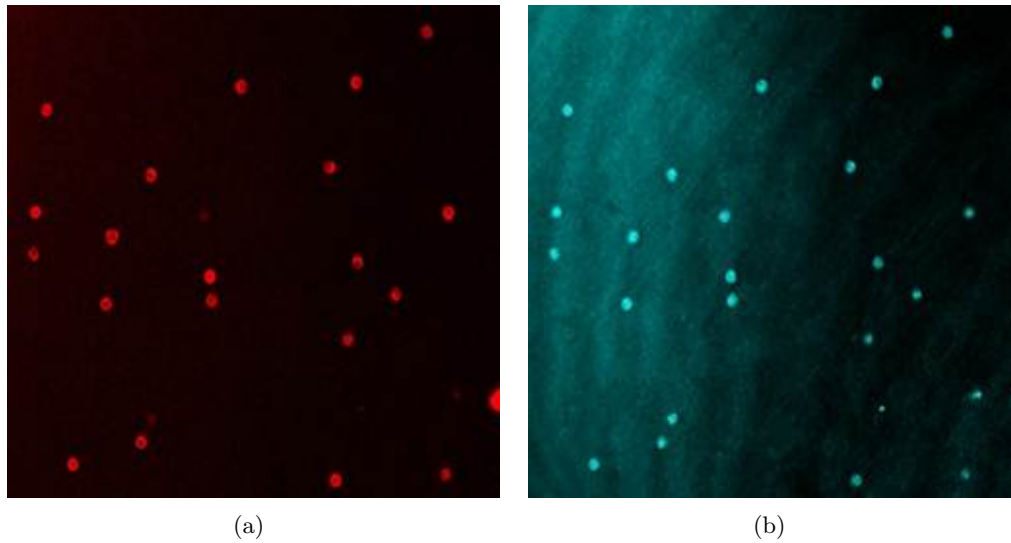
Figure 4.14: **Fluorescence of T cells stained with HLA B8 IE1K Atto633 *Strep*tamer under the microscope:** Ficoll purified human lymphocytes were stained with αCD8 PB antibody and HLA B8 IE1$_{199-207K}$-Atto633 *Strep*tamer and sorted for CD8$^+$ *Strep*tamer$^+$ living lymphocytes. Fluorescence intensity of *Strep*-Tactin PE (a) and Atto633 (b) on the surface of the stained cells is shwon.

manufacturer information, resulted in no detectable Atto488 fluorescence. The fluorescence of Atto532 was not detectable by flow cytometry with the used machine, therefore, specific T cells showed only the *Strep*tamer-PE fluorescence. The fluorescence intensity of the dye was tested later with MHC coated *Strep*-Tactin beads under the microscope (principle s. section 4.4.3), but turned out to be too weak to continue experiments with this dye (data not shown). The fluorescence intensitiy of the Atto633 *Strep*tamer staining seemed to be very promising and specific T cells showed a clear double staining for PE and Atto633. Hence, further microscopic examinations were performed to reveal if Atto633 is a suitable dye for the k$_{\text{off}}$-rate assay.

4.4.2.1 Atto633

Staining with the dichromatic HLA B8 IE1$_{199-207K}$ -Atto633 *Strep*tamer resulted in a high Atto 633 and PE fluorescence intensity of the specific T cell population analyzed by flow cytometry. To be able to perform k$_{\text{off}}$-rate assays with these *Strep*tamers, it had to be tested if the fluorescence intensity of the *Strep*tamer staining was also detectable by fluorescence microscopy.

CD8$^+$ *Strep*tamer$^+$ T cells were sorted by FACS and subsequently analyzed by fluorescence microscopy for Atto 633 and PE staining intensity. The emitted fluorescence of both dyes was very high and cells could be nicely distinguished from background fluorescence (Figure 4.14).

The fluorescence of both *Strep*-Tactin PE and Atto633 conjugated to the MHC molecules was detectable by fluorescence microscopy and seemed bright enough
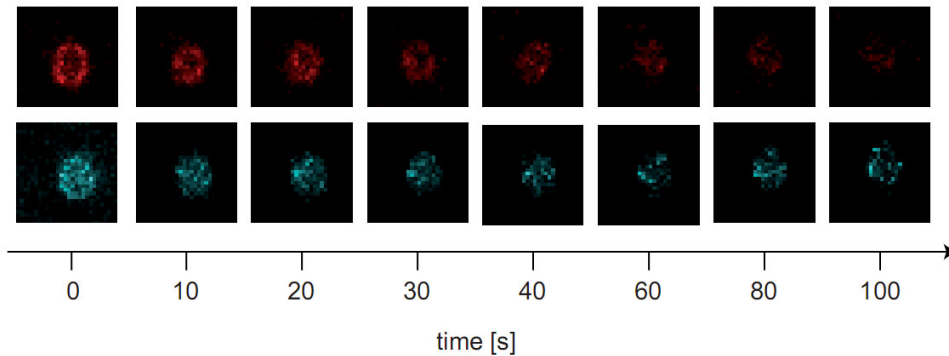
Figure 4.15: **Time series of PE and Atto633 fluorescence after addition of d-biotin:** Ficoll purified human lymphocytes were stained with αCD8 PB antibody and HLA B8 IE1$_{199-207K}$-Atto633 *Strep*tamer and sorted for CD8$^+$ *Strep*tamer$^+$ living lymphocytes. PE and Atto633 fluorescence was monitored before the addition of d-biotin (0s) and in a time series every 10s after the addition.

to perform k$_{\text{off}}$-rate assays. Hence, d-biotin was added to the cells to see, if the *Strep*tamer staining was reversible and if it was possible to calculate the k$_{\text{off}}$-rate from MHC dissociation kinetics.

After addition of d-biotin, a quick dissociation of the *Strep*-Tactin backbone could be observed by the decay of the PE fluorescence (Figure 4.15). A decay of the Atto633 fluorescence intensity was expected due to dissociation of monomeric bound pMHC molecules. However, this decay was also very fast and followed exactly the same kinetics as the decay of the PE fluorescence (Figures 4.15, 4.16(a)). This led to the assumption, that the decay of Atto633 fluorescence intensity is mainly correlated to the decay of the PE fluorescence and not to MHC dissociation.

If there was a correlation between the PE and the Atto633 fluorescence could be tested by leaving the *Strep*tamer associated to the T cells but abolishing the PE fluorescence by photobleaching. Thus, *Strep*tamer stained cells were sequentially exposed to 488nm laser light to destroy the PE fluorescence. As Figure 4.16(b) shows, the decay of the PE fluorescence induced by photobleaching went along with a decay of the Atto633 fluorescence. Control experiments excluded the possibility that Atto633 was also photobleached by 488nm laser light. Taken together, these data suggested, that an intact PE fluorophor was needed to reach sufficient Atto633 fluorescence.

The observed phenotype of the interaction between PE and Atto633 seemed to be typical for FRET (fluorescence energy transfer) between two fluorescent dyes. Two important preconditions for FRET are first that the emission spectrum of the one dye overlaps with the excitation spectrum of the other dye and second that the two dye are located in close proximity. To estimate if FRET could be a possible explanation for the observed correlation of the PE and the Atto633 fluorescence, the emission and excitation spectra of the two dyes were analyzed.

As shown in Figure 4.17, the peak of the PE emission overlaps with a local excitation maximum of Atto633. A part of the photons emitted by PE can be directly

(a)

(b)
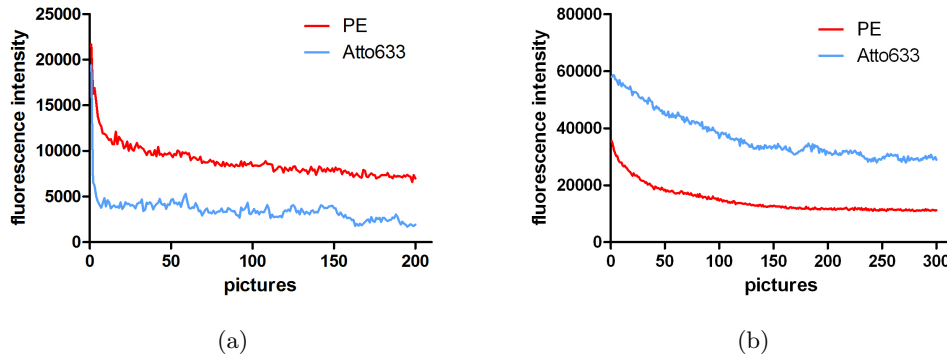
Figure 4.16: **Decay of fluorescence intensity of PE and Atto633 after addition of d-biotin or photobleaching of PE:** Sorted *Strep*tamer stained T cells were mounted under the microscope and the decay of the Atto633 and PE fluorescence observed (a) after the addition of d-biotin or (b) during exposition to laser light. Shown are the plots of the fluorescence intensity of Atto633 and PE over time.
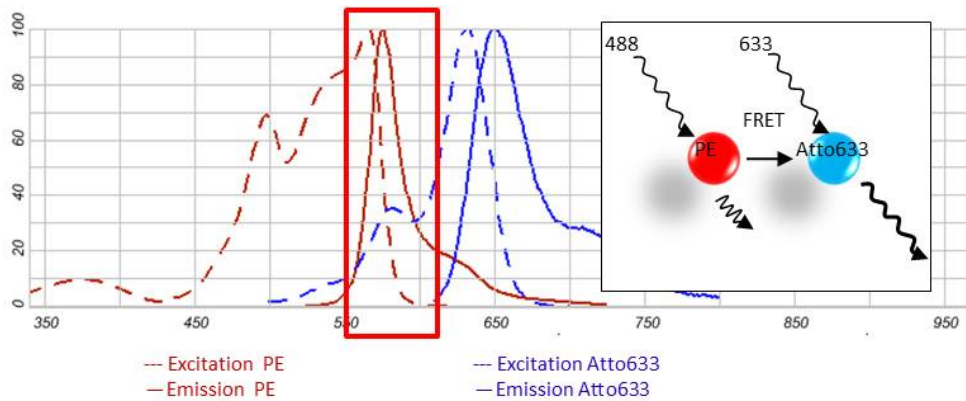
Figure 4.17: **FRET between PE and Atto633 due to close proximity and overlapping spectra:** Shown are the excitation (dashed lines) and emission (solid lines) spectra of PE and Atto633 and a schematic illustration of FRET between Atto633 and PE.

absorbed by Atto633 to excite fluorescence. After dissociation or destruction of the PE fluorophor, Atto633 fluorescence is only induced by 633 laser light excitation. However, this excitation resulted in a fluorescence intensity which is insufficient for the performance of k$_{\text{off}}$-rate assays.

To analyze the Atto633 fluorescence intensity in absence of PE, *Strep*-Tactin beads were coated with HLA B8 IE1$_{199-207K}$ -Atto633 MHCs. With these "bead MHC multimers", PBMCs were stained according to the *Strep*tamer staining protocol and subsequently analyzed by flowcytometry. In line with the data obtained from microscopic examinations, the fluorescence intensity of Atto633 on T cells stained with the MHC-Atto633 coated beads was very low and it was not possible to define a distinct T cell population (data not shown).

In summary, the Atto633 fluorescence intensity was only high enough, if the dye was in close proximity to PE and was excited by FRET. This effect caused the bright

Atto633 fluorescence of T cells stained with the dichromatic *Strep*tamer and analyzed with FACS or fluorescence microscopy (Figures 4.13, 4.14). But for monitoring of the MHCs in the k$_{\text{off}}$-rate assay, a fluorescent dye was needed which was bright enough without other dyes in proximity. As Atto633 could not fulfill these condition, another dye had to be found.

4.4.2.2 Atto565

After extensive testing it turned out that the ordered set of Atto dyes contained no suitable dye for the k$_{\text{off}}$-rate assay. Hence, another set of dyes that fulfilled the preconditions discussed in the first paragraph of this section (4.4.2) were tested. The fluorescent dyes Atto565, Atto594 and Atto647N were chosen. To first test the brightness of the dyes after laser light excitation under the confocal microscope, pMHC molecules conjugated with one of the fluorescent dyes respectively, were incubated with sepharose beads coated with *Strep*-Tactin. Those beads had a size of 45-160nm, showed no autofluorescence after laser light excitation (Figure 4.18) and therefore offered a suitable, cell-free testing system for dye conjugated MHC molecules under the microscope.

Beads coated with pMHC molecules conjugated with Atto 594 and Atto647N respectively, showed only a very weak fluorescence intensity under the microscope (data not shown). As the concentration of pMHC on beads is much higher than the concentration of pMHC bound to surface expressed TCRs on living cells, also the fluorescence intensity of *Strep*tamer stained T cells was expected to be even lower. According to that, Atto594 and Atto647N would not have the capacitiy to reach a sufficient fluorescence intensity in T cell stainings to perform the k$_{\text{off}}$-rate assay.

In contrast, the fluorescence intensity of *Strep*-Tactin beads coated with Atto565 conjugated MHCs was very high (Figure 4.18(a)) and it could be assumed that also the *Strep*tamer staining intensity on living T cells would be bright enough to perform k$_{\text{off}}$-rate assays. With the addition of d-biotin to MHC loaded *Strep*-Tactin beads, also the reversibility of the *Strep*-tag-*Strep*-Tactin binding could be easily tested. As Atto565 is conjugated at the end of the *Strep*-tag sequence of the MHC molecule, an interaction of the dye with *Strep*-Tactin could be possible and would potentially interfere with the reversibility of the *Strep*tamer staining. However, after the addition of d-biotin, complete dissociation of Atto565 conjugated MHC molecules could be observed (data not shown).

After preliminary testings, Atto565 seemed to be a promising candidate for the performance of k$_{\text{off}}$-rate assays. In the next step, it had to be examined if it was possible to stably stain specific T cells with dichromatic *Strep*tamers containing Atto565 conjugated MHC molecules. Hence, PBMCs from donor 1 were stained with αCD3 antibodies alone or in addition with HLA B8 IE1$_{199-207K}$ *Strep*tamer or with the dichromatic *Strep*tamer HLA B8 IE1$_{199-207K}$ -Atto565 (Figure 4.19). In former *Strep*tamer stainings, *Strep*-Tactin PE was used to multimerize the pMHC molecules. However, Atto565 cannot be used in combination with PE, as the emission spectra of both dyes overlap to a high extent. Therefore, *Strep*-Tactin conjugated with APC was chosen, as it basically has the same properties concerning *Strep*-tag binding as *Strep*-Tactin PE, but could be used in combination with Atto565 conjugated MHC
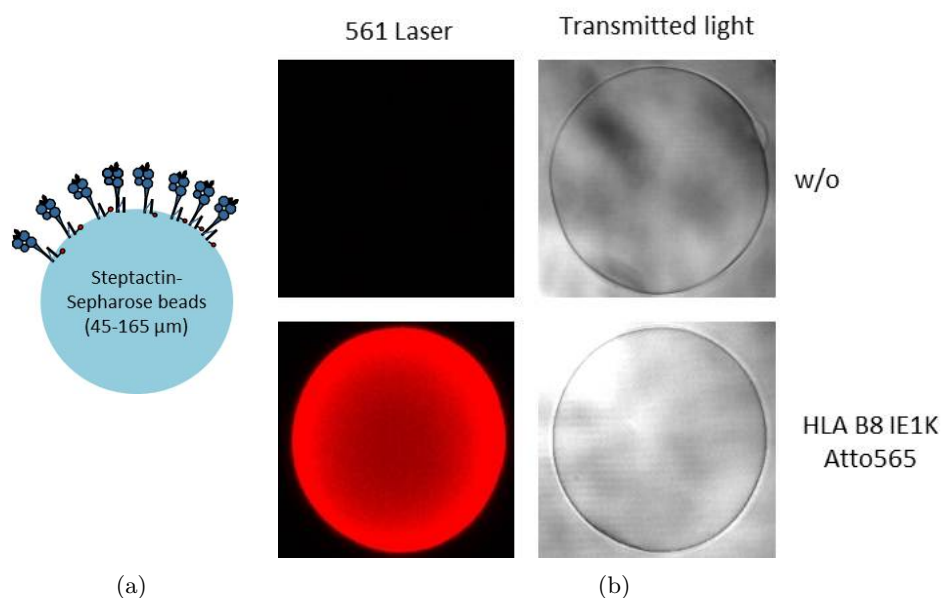
Figure 4.18: **Test of Atto565 conjugated MHCs on *Strep*atctin beads for visibility under the microscope:** (a) Schematic illustration of MHC conjugation to *Strep*-Tactin coated sepharose beads. (b) *Strep*-Tactin beads were incubated with Atto565 conjugated MHC molecules and Atto565 fluorescence was analyzed under the microscope. Unconjugated beads were analyzed for autofluorescence as a control.

molecules. *Strep*tamer stained T cells were analyzed directly by flow cytometry, or after additional incubation with d-biotin to test the reversibility of the staining. As there was no suitable laser available to excite Atto565 fluorescence, only the staining of the *Strep*-Tactin backbone was compared. Both the population size of specific T cells and the fluorescence intensity of the *Strep*-Tactin APC were highly comparable between the HLA B8 IE1$_{199-207K}$ *Strep*tamer and the dichromatic Atto565 *Strep*tamer (Figure 4.19). After addition of d-biotin, stainings of both *Strep*tamers could be reversed.

Thus, it was possible to stably stain specific T cells with *Strep*tamers containing Atto565 conjugated MHCs, and the staining was completely reversible. But to be finally able to perform k$_{\text{off}}$-rate assays, it had to be tested if the fluorescence intensity of Atto565 was sufficiently high in the context of *Strep*tamer staining. PBMCs were stained with antibodies and the dichromatic *Strep*tamer and subsequently FACS sorted for the CD8$^+$ *Strep*tamer$^+$ population. Figure 4.20 shows the fluorescence intensities of APC and Atto565 of sorted T cells under the microscope. While the APC staining of the cells was very bright and distinct (4.20(a)), there is hardly any Atto565 fluorescence detectable (4.20(b)).

After the dissociation of the *Strep*-Tactin-APC backbone by adding d-biotin, the Atto565 fluorescence of the cells became detectable (Figure 4.21). The fluorescence intensity of Atto565 reached a maximum at the point of complete APC dissociation, followed by a decay of Atto565 fluorescence.

Also in this case, FRET between the two *Strep*tamer dyes was a possible explanation
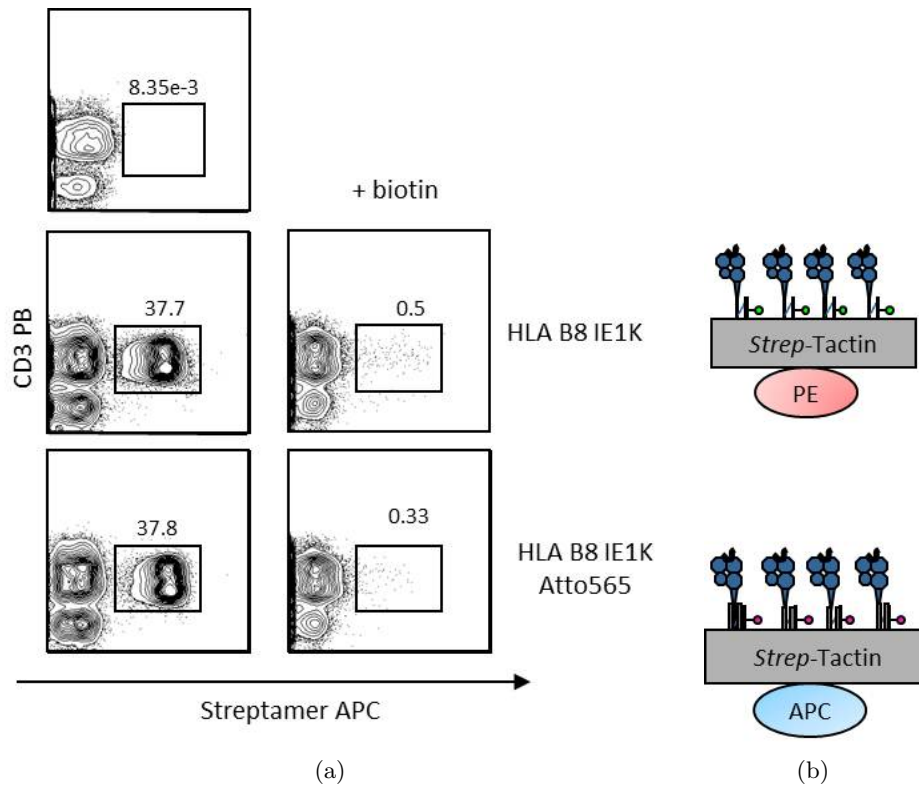
Figure 4.19: **Staining of specific T cells with HLA B8 IE1K Atto565 *Strep*tamers:** (a) $5*10^6$ purified human lymphocytes were stained with αCD3 PB antibody or in addition with HLA B8 IE1$_{199-207K}$ *Strep*tamer or the *Strep*tamers HLA B8 IE1$_{199-207K}$-Atto565 and analyzed directly or incubated with d-biotin. Dot plots show the staining of *Strep*-Tactin PE versus the fluorescent dyes on the MHCs, gated on living T cells. Numbers indicate the percentage of *Strep*tamer$^+$ T cells in the plot. (b) Schematic illustration of the *Strep*tamer used for the murine k$_{off}$-rate assays (upper panel) or the new setup used for human k$_{off}$-rate assay (lower panel).

(a) (b)
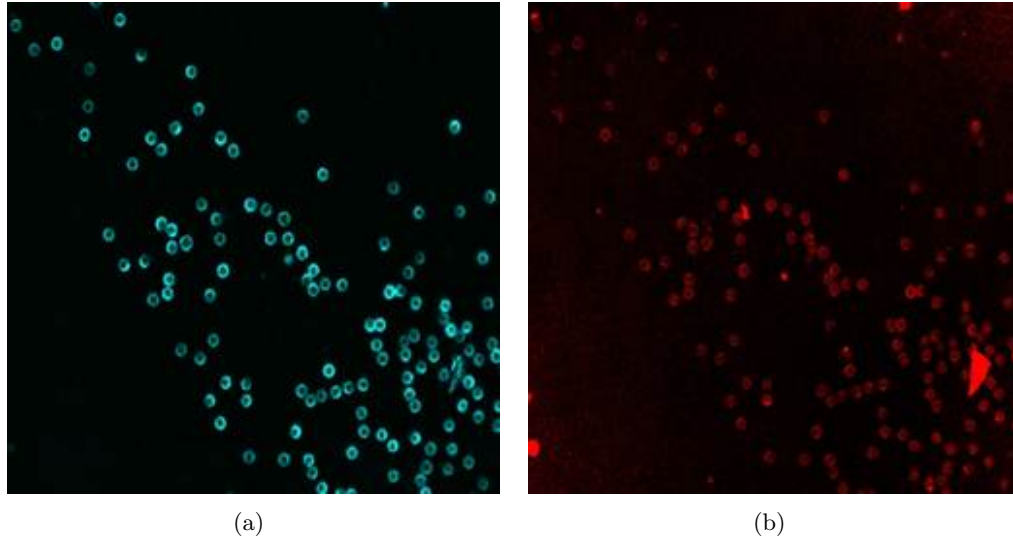
Figure 4.20: **Fluorescence of T cells stained with HLA B8 IE1K Atto565 *Strep*tamer under the microscope:** Ficoll purified human lymphocytes were stained with αCD8 PB antibody and HLA B8 IE1$_{199-207K}$-Atto565 *Strep*tamer and sorted for CD8$^+$ *Strep*tamer$^+$ living lymphocytes. Fluorescence of *Strep*-Tactin APC (a) and Atto565 (b) on the surface of the stained cells is shown.
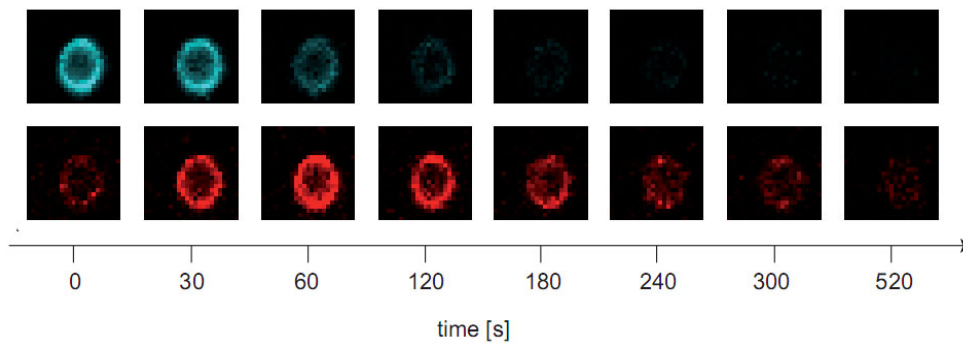
Figure 4.21: **Time series of APC and Atto565 fluorescence after addition of d-biotin:** Ficoll purified human lymphocytes were stained with αCD8 PB antibody and HLA B8 IE1$_{199-207K}$-Atto633 *Strep*tamer and sorted for CD8$^+$ *Strep*tamer$^+$ living lymphocytes. APC and Atto565 fluorescence was monitored before the addition of d-biotin (0s) and in a time series every 10s after the addition.
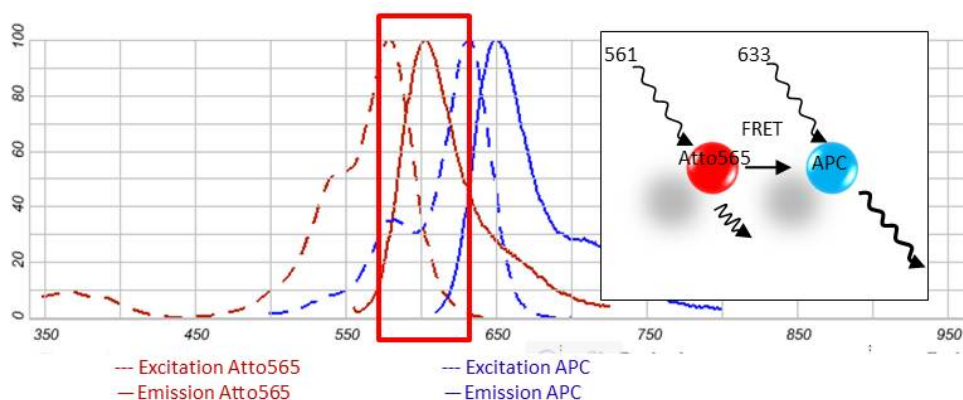
Figure 4.22: **FRET between Atto565 and APC due to close proximity and overlapping spectra:** Shown are the excitation (dashed lines) and emission (solid lines) spectra of Atto565 and APC and a schematic illustration of FRET between Atto565 and APC.

for the observed effect. In contrast to the setup described in 4.4.2.1, Atto565 conjugated to the MHC molecule was the donor of the FRET pair and transferred its emitted photons to the acceptor APC as long as both dyes were in close proximity. With dissociation of the *Strep*-Tactin backbone and thereby of the FRET acceptor, the emitted photons of Atto565 became visible as fluorescent light. The dissociation of the Atto565 conjugated MHC molecules could be subsequently observed as a decay of the Atto565 fluorescence intensity.

The analysis of the emission and excitation spectra of Atto565 and APC confirmed this theory (Figure 4.22). The emission spectrum of Atto565 overlapped strongly with the excitation spectrum of APC and thus allowed for the efficient transfer of photons from the FRET donor to the acceptor.

Similarly to the setup with Atto633, the dye conjugated to the MHC molecule and the dye conjugated to *Strep*-Tactin interacted with each other. However, this time, the intensity of the MHC dye Atto565 was increased after the dissociation of the FRET partner. This effect not only made it possible to continue k$_{\text{off}}$-rate measurements with Atto565 conjugated MHC molecules, it even facilitated the analysis of the fluorescent decay. Figure 4.23 shows the plot of the fluorescence intensities of APC and Atto565 over the time after addition of d-biotin. As already visible in Figure 4.21, the intensity of Atto565 peaked when APC intensity reached the minimum. After this peak, the loss of the fluorescence intensity followed an exponential decay. As the exponent of this decay contained the k$_{\text{off}}$-rate, the data points of the decay had to be fitted with an exponential curve to allow for the calculation of the k$_{\text{off}}$-rate. In the early phase after addition of d-biotin, simultaneous dissociation of the *Strep*-Tactin backbone and pMHC molecules might complicate the analysis of the dissociation kinetics. At the peak of the Atto565 fluorescence, however, the *Strep*-Tactin backbone is about to reach complete dissociation and has therefore no significant influence on the pMHC dissociation kinetics. Hence, the peak of Atto565 fluorescence marks the starting point of the exponential decay and indicates the range of data points for the correct fitting of the exponential decay.

(a)   (b)
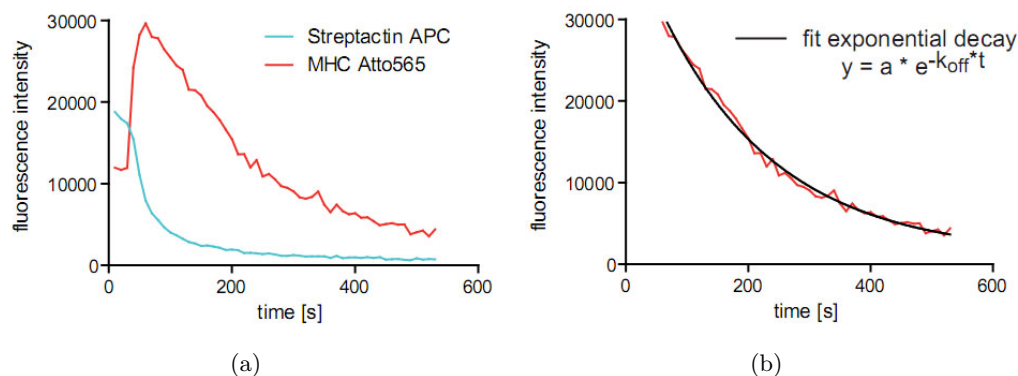
Figure 4.23: **Decay of fluorescence intensity of APC and Atto565 after addition of d-biotin:** Sorted *Strep*tamer stained T cells were mounted under the microscope and the decay of the Atto633 and PE fluorescence observed after the addition of d-biotin. Shown are the plots of the fluorescence intensity (a) of Atto633 and PE over time and (b) the range of data selected for the fit of the exponential decay.

4.4.3   Photobleaching of Atto565 - determination and subtraction

First experiments with T cells showed that the staining with Atto565 *Strep*tamers is well detectable by confocal microscopy and that the dissociation of labeled MHC molecules can be monitored after addition of d-biotin. To finally setup the k$_{off}$-rate assay, photobleaching of Atto565 with the microscope settings (e.g. laser intensity, pinhole, scan speed) adjusted for the measurements of cells, had to be determined. To achieve this, the dye is exposed to laser light for a series of pictures usually taken in the k$_{off}$-rate assay, and the decay of fluorescence during this time was observed. Due to FRET between Atto565 and APC, the Atto565 fluorescence is very low in the presence of APC. Hence, measurements of photobleaching could not be performed with *Strep*tamer stained cells, as the binding of the Atto565 labeled MHCs is only stable in the presence of the *Strep*-Tactin APC backbone. Therefore, photobleaching of Atto565 was determined in the cell free testing system using MHC coated sepharosebeads as described in 4.4.2.2.

Figure 4.24 shows the *Strep*-Tactin beads coated with biotinylated APC (upper row) or Atto565 conjugated MHC molecules (lower row) at different time points in a time series of 300 pictures. While the fluorescence intensities of both dyes decline, the fluorescence intensity of Atto565 seemed to be much more stable than the intensity of APC.

According to the decay law, photo bleaching follows a negative exponential curve that contains the decay coefficient in its exponent. In Figure 4.25, the fluorescence intensities of both dyes are plotted over the time series of pictures and exponential curves are fitted into the data points. Atto565 had a very low decay coefficient, which demonstrated the good photostability of the fluorophor. The bleaching coefficient was subtracted from the decay coefficient of the raw data of the MHC dissociation to calculate the final k$_{off}$-rate.
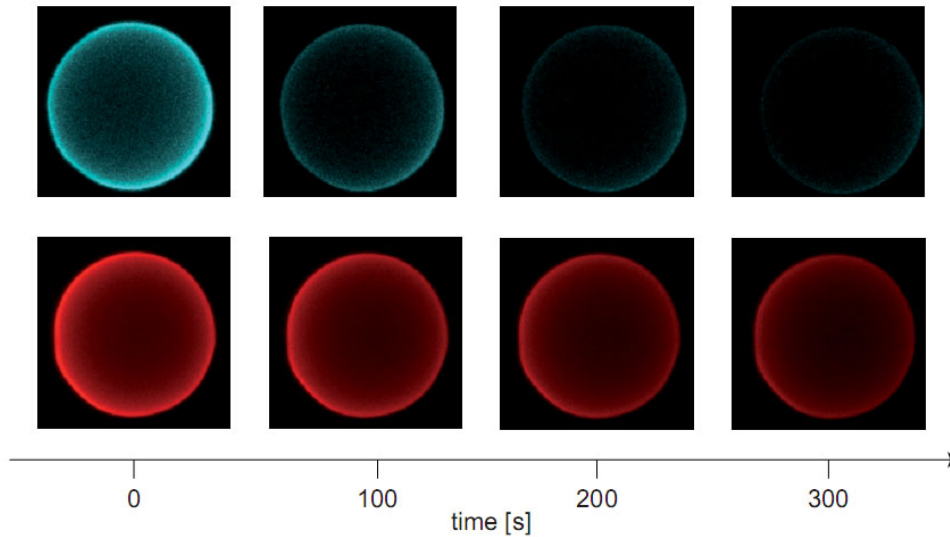
Figure 4.24: **Photobleaching of the fluorescent dye APC and Atto565 in the k$_{\text{off}}$-rate setup on *Strep*-Tactin beads:** *Strep*-Tactin beads were loaded with biotinylated APC (upper row) or with Atto565 (lower row) conjugated MHC molecules. Pictures were taken every 10s with the laser intensities corresponding to the setup of the k$_{\text{off}}$-rate assay.
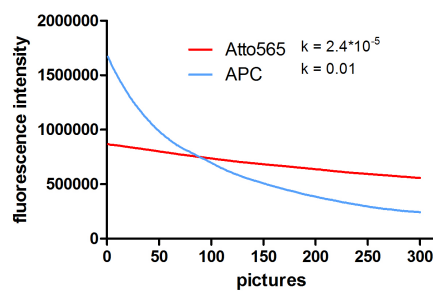
Figure 4.25: **Time plot of photobleaching of the fluorescent dye APC and Atto565 in the k$_{\text{off}}$-rate setup:** Shown are two exemplary decay curves of Atto565 and APC after photobleaching of dye-loaded *Strep*-Tactin beads. k values in the graph indicate the bleaching constants of the dyes, calculated from the exponential fit of the curves.

4.4.4   New analyzer software

As already mentioned, the dissociation of the MHC molecules follows an exponential decay and k$_{\text{off}}$-rate and half life-time (t$_{1/2}$) of the binding can be calculated from the exponent of a curve fitted into the data points. For the analysis, the fluorescence intensity of single cells as well as the background fluorescence is measured for each picture. With the analyzing software analyzer.nt, the background correction of the fluorescence intensity and the plotting of the corrected values over time are carried out automated. To ensure optimal fitting of the data points to an exponential curve, the software allows for the adaption of the area of data points included for fitting. Thereby, fitting of each cell is controlled directly and incorrect fittings e.g. due to variations at the end of the assay can be avoided.

The software "analyzer.nt" was developed by Sebastian Nauerth, Department of Physics, LMU München. Data evaluation is done using R[http://www.r-project.org/], a language for statistical computing. It allows for data import and analyzes using state of the art fitting methods. The basic principles of the model function and the data analysis of this software are describe in the following.

4.4.4.1   Model function

The evaluation of the intensity development is done against an exponential decay model. This is motivated as followed: For every time step dt the probability for every pMHC molecule to dissolve is believed to be equal and constant. The change in fluorescence or in this context the change in the number of dye-conjugated pMHC molecules dN in a time interval dt is therefore expected to be proportional to the absolute number of dye-conjugated pMHC molecules $N(t)$ left after a time t, the probability p_t for a single pMHC molecule to dissolve in dt and the width of the time step:

$$dN = -N(t)p_t dt \tag{4.1}$$

Integrating then gives:

$$\int_{N_{t_0}}^{N(t)} \frac{dN}{N(t)} = -\int_{t_0}^{t} p_t dt \tag{4.2}$$

$$\frac{\ln(N(t))}{\ln(N_{t_0})} = -p_t(t - t_0) \tag{4.3}$$

Choosing $t_0 = 0$ for convenience and eliminating the logarithm, the well known exponential decay law is obtained:

$$N(t) = N_0 \, e^{-p_t t} \tag{4.4}$$

The experimental data sometimes additionally shows a linear decrease of the fluorescence intensity with a varying slope a. While this process has yet to be explained, the model function has to reflect this behavior in order to obtain sensible fit results. The final model function thus reads:

$$N(t) = N_0 \, e^{-p_t t} - at \tag{4.5}$$

The half-value period $\tau_{1/2}$ is calculated from the somehow less illustrative parameter p_t by solving

$$\frac{N_0}{2} = N_0 \, e^{-p_t \tau_{1/2}}. \tag{4.6}$$

One yields

$$\tau_{1/2} = \frac{ln(2)}{p_t} \tag{4.7}$$

or substituted into (4.5):

$$N(t) = N_0 \exp\left(-\frac{ln(2)t}{\tau_{1/2}}\right) - at = N_0 \, 2^{\left(-\frac{t}{\tau_{1/2}}\right)} - at \tag{4.8}$$

4.4.4.2 Correction for photobleaching

The effects of laser induced photobleaching of the fluorescent dyes are integrated into the model by modifying the rate equation (4.9) with a second decay probability p_b:

$$dN = -N(t)p_t dt - N(t)p_b dt = -N(t)(p_t + p_b)dt \tag{4.9}$$

As the two probabilities add up, one can substitute the sum with a effective probability p which is actually observed when performing the k$_{\text{off}}$-rate experiment. The grade of bleaching has to be quantified beforehand in dedicated measurements obtaining p_b. From (4.7), the relation of the half-value periods can be derived:

$$p = p_t + p_b \quad \Leftrightarrow \quad \frac{1}{\tau} = \frac{1}{\tau_{t1/2}} + \frac{1}{\tau_{b1/2}} \tag{4.10}$$

4.4.4.3 Work flow

The R evaluation script starts by prompting the user for a data file. This has to be provided properly formatted in an Microsoft Excel document. For every cell in the file, the following steps are executed:

A Plot of the signal and background intensities over time is displayed and the user is asked to specify the first and last valid data point (Figure 4.26(a), Figure 4.26(b)). The model function is fitted to the data (signal - background) and the result is plotted together with the experimental data points. Note that so far, no numerical values are revealed but an indicator value for the fit quality (i.e. degree of matching). In case, the fit is not convincing, this step can be repeated choosing slightly different start and end points (Figure 4.26(c)). Finally the user has to decide whether the fit is to be considered successful and matching the experimental data or there is no reasonable fit possible for this particular data set and the respective cell is to be discarded. For the latter case there is a number of possible causes including low signal intensity compared to the background and excessive noise obscuring the actual effect. Both these conditions can be easily identified from the plotted data.

When all cells are processed, the results are plotted showing (1) all data points with the points accounted for in the fit marked, (2) the model function plotted with the obtained parameters and (3) the numeric values of the obtained parameters.
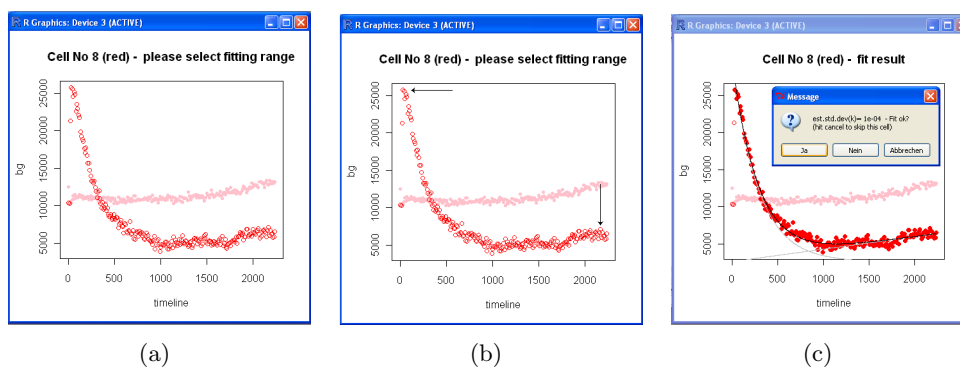
Figure 4.26: **Data analysis with the analyzer.nt software:** (a) Plot of signal (red circles) and background (light red dots) fluorescence intensities. (b) First and last valid data points in the plot (indicated by arrows) have to be chosen. (c) The model function is fitted to the data and the resulting curve is plotted over the raw data. The fit can be either accepted or repeated with slightly different start and end points.

4.5 Validation of the k$_{\text{off}}$-rate assay

With the introduction of a new conjugation site at the C-term of the MHC molecule and the choice of a new dye, the k$_{\text{off}}$-rate assay could be established for the measurement of human T cells. For the first time, the dissociation of monomeric pMHC molecules from surface bound TCR could be reliable monitored. However, several questions had to be addressed to validate the k$_{\text{off}}$-rate assay for human T cells.

4.5.1 Reproducibility and comparability

To prove the reliability of the k$_{\text{off}}$-rate data, it had to be shown that the measured values were reproducible in different experiments. As T cell clones, which all bear an identical TCR, should produce very similar k$_{\text{off}}$-rates , the measurement of such T cell clones provided a suitable system to analyze the reproducibility of the k$_{\text{off}}$-rate assay. Figure 4.27(a) shows the measurement of one T cell clone in different dissociation assays and on different days. The mean half-life time of the measured cells was very stable in the different assays, demonstrating the reliability of the measured values.

In the next step, it should be analyzed if the k$_{\text{off}}$-rate is influenced by culture conditions or if it mainly depends on the TCR. For these experiments, T cell clones were either kept in culture or frozen in liquid nitrogen and later thawed for the performance of the k$_{\text{off}}$-rate assay. The k$_{\text{off}}$-rates of cultured and frozen T cell clones are compared in Figure 4.27(b) . The half-life times of the analyzed T cell clones were very similar, indicating that the k$_{\text{off}}$-rate is independent of the current culture conditions.

In k$_{\text{off}}$-rate assays with murine T cells, Robert Knall could reveal a remarkable correlation between the functional avidity, the k$_{\text{off}}$-rate and the protective capacity of a T cell. However, all those murine k$_{\text{off}}$-rate data were generated with a setup different from the human k$_{\text{off}}$-rate setup (described in 4.2). The newly established

(a) (b)
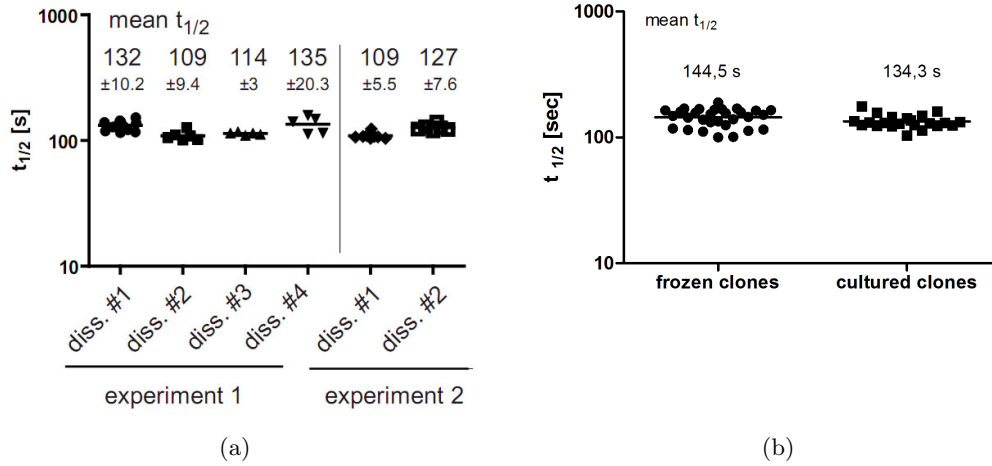
Figure 4.27: **Reproducibility of k$_{\text{off}}$-rate values:** (a) CMV spec. T cell clones were stained with HLA B8 IE1$_8$8 − 96-Atto565 *Strep*tamer and k$_{\text{off}}$-rates of the same clones were measured in different dissociations and on different days. Shown are the half-life times with mean for each dissociation, with mean values and standard deviation indicated in the diagram. (b) HLA B8 IE1$_8$8 − 96 specific T cell clones were either *Strep*tamer stained and analyzed in k$_{\text{off}}$-rate assays directly after culture or frozen stocks were thawed for the analysis in the k$_{\text{off}}$-rate assay. Shown are the half-life times with mean of the frozen and the cultured clones in comparison.

(a) (b)
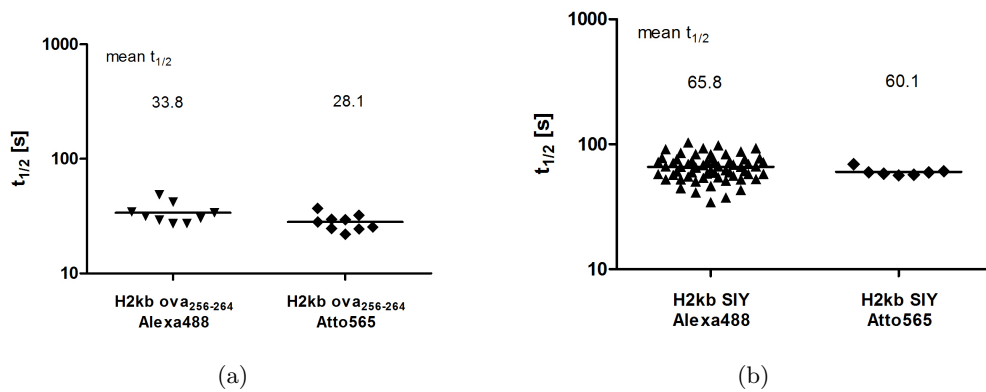
Figure 4.28: **Comparison of data produced with the murine and the human k$_{\text{off}}$-rate assay setup:** (a) Comparison of half-life times calculated from the k$_{\text{off}}$-rate assay with OT1 T cells stained with H2-k^b Ova$_{256−264}$ *Strep*tamers either conjugated at the β_2m with Alexa488 or at the end of the *Strep*-tagIII with Atto565. (b) As in A, half-life times obtained after k$_{\text{off}}$-rate assay with the different dye conjugations were compared for 2C T cells and H2-k^b SIY *Strep*tamers. In both diagrams, half-life times with mean are shown. Numbers indicate mean half life time for each column.

"human k$_{\text{off}}$-rate setup" with the conjugation of Att565 to the end of the *Strep*-tag was transferred to the murine MHC I molecule H2-k^{b} to address two questions: first, how do the two setups perform in comparison and second, does the new dye or the conjugation site influence the k$_{\text{off}}$-rate. The comparison of the different k$_{\text{off}}$-rate setups was performed with two well characterized TCR transgenic mouse cells, OT1 T cells and the 2C T cell line. As shown in Figure 4.28, the half-life times assessed with the different k$_{\text{off}}$-rate setups were highly comparable for the two TCR transgenic T cells. This demonstrated that the changes for the human k$_{\text{off}}$-rate setup had no influence on the calculated half-life time, which allowed for a direct comparison of both systems.

4.5.2   k$_{\text{off}}$-rate is maintained after transfer of the TCR

TCR tranfer experiments suggest that an important part of T cell avidity is hard wired in the TCR [204], pointing out that the structure of the TCR is a critical parameter for T cell functionality. The k$_{\text{off}}$-rate is determined by the binding strength between pMHC and TCR and should be highly dependent on the structure of the TCR.

To test if the measured k$_{\text{off}}$-rates are actually determined by the structure of the TCR, the TCRs of two CMV-specific T cell clones were each transferred to non-specific Jurkat cells and the k$_{\text{off}}$-rates of the T cell clones and the respective TCR transgenic Jurkat cells were compared. The work for this project was done in collaboration with Bianca Weißbrich and Georg Dössinger.

The transferred TCR was highly expressed in about 50% of the transgenic Jurkat cells transduced with TCR from clone A or clone B respectively. TCR expressing Jurkat cells could be FACS sorted with a high purity of over 99% *Strep*tamer^{+} cells (Figure 4.29(a)). k$_{\text{off}}$-rate data obtained from the different cell types showed that the half-life times of the T cell clones and the transgenic Jurkat cells were highly comparable (Figure 4.29(b)). This indicated that the k$_{\text{off}}$-rate indeed dependes to an important part on the structure of the TCR and not mainly on other components expressed on the cell surface.

4.5.3   k$_{\text{off}}$-rate assay of four CMV-specific *ex vivo* populations

After showing that the k$_{\text{off}}$-rate assay provided reliable data that depended on the structure of the TCR, *ex vivo* T cell populations were analyzed in the next step. Data should reveal if different k$_{\text{off}}$-rates could be detected and give information about the range of k$_{\text{off}}$-rates occurring under physiological conditions.

Besides the T cell population specific for HLA B8 IE1$_{199-207K}$, which was used during the whole work to test the k$_{\text{off}}$-rate setup, a second T cell population from Donor 1 specific for HLA B8 IE1$_{88-96}$ was analyzed. In addition, two further T cell populations specific for HLA B7 pp65$_{417-426}$ or HLA A2 pp65$_{495-503}$ from Donor 2 or Donor 3, respectively, were analyzed. Remarkably, the four T cell populations differed strongly in size. The HLA A2 pp65$_{495-503}$ specific population made up only 0.1% of CD8^{+} T cells and was rather small compared to the HLA B8 IE1$_{199-207K}$

(a)

(b)

(c)
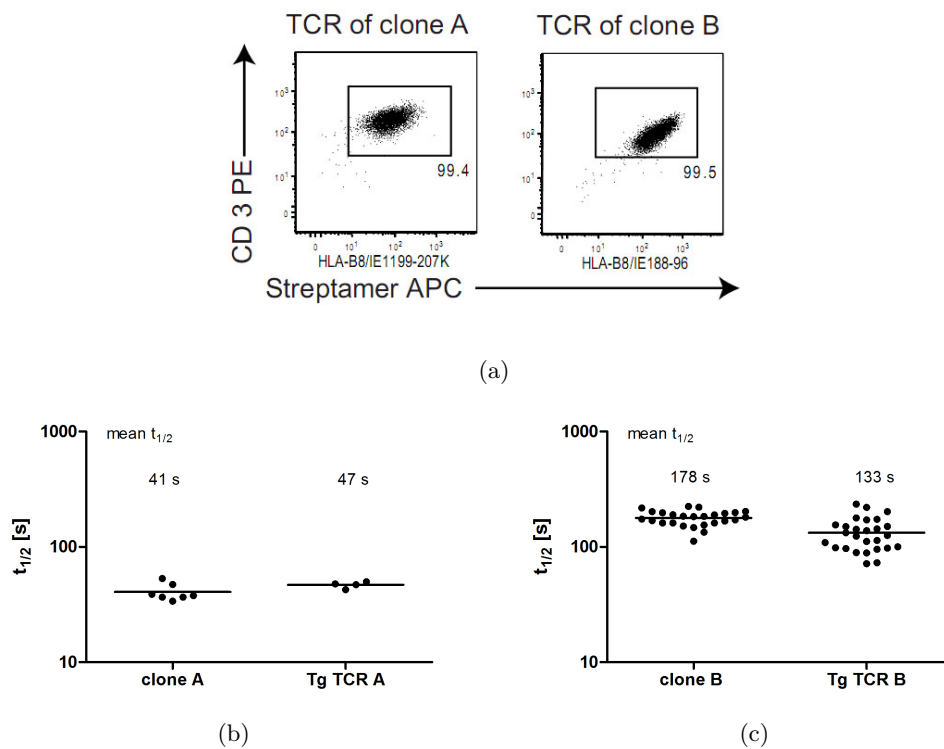
Figure 4.29: **k$_{off}$-rate assay with two different T cell clones and Jurkat cells transduced with the respective TCRs:** The TCRs of two different CMV spec. T cell clones were each transferred to Jurkat 67 cells by retroviral transduction (a) *Strep*tamer staining of transgenic Jurkat cells expressing the TCR of T cell clone A (left panel) or of T cell clone B (right panel). Shown is the *Strep*tamer APC staining versus CD3 antibody staining, gated on living cells. Comparison of the half-life times obtained from k$_{off}$-rate assays with either (b) T cell clone A and the transgenic Jurkat cell bearing TCR A or (c) T cell clone B and the transgenic Jurkat cells bearing TCR B. Shown are half-life times with mean, numbers in the diagrams indicate mean half-life times.
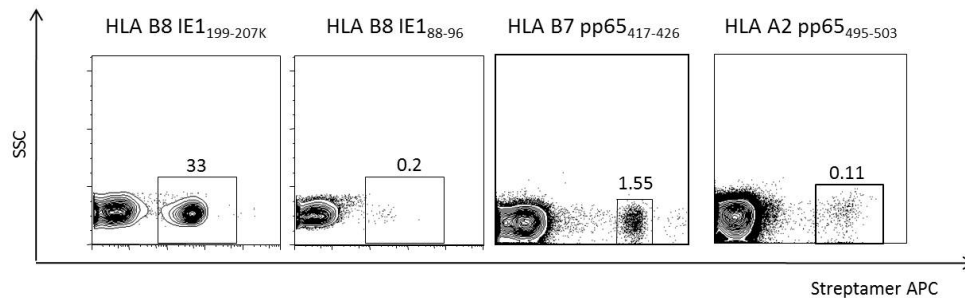
(a)
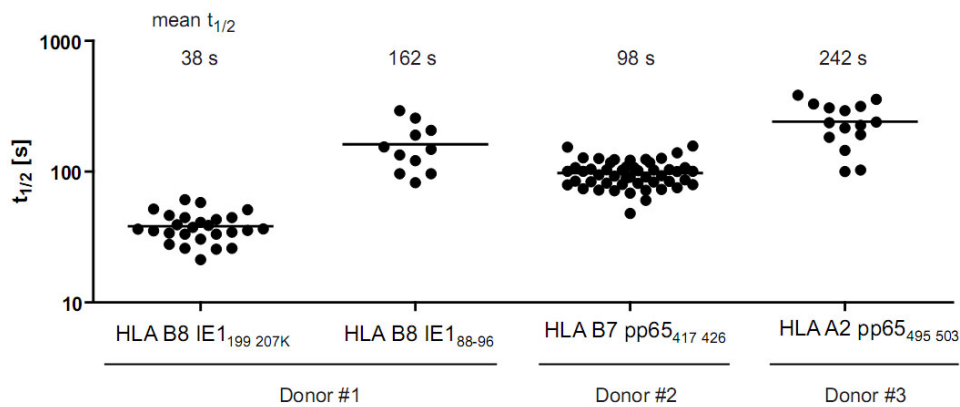
(b)

Figure 4.30: **k_{off}-rate assay with four different CMV-specific *ex vivo* T cell populations:**(a) Staining of PBMCs from three different donors with *Strep*tamers with four different HLA peptide combinations, indicated at the top of the plots. Shown is the *Strep*tamer APC staining of the T cells versus sideward scatter. Cells are gated on living, $CD8^+$ lymphocytes, numbers in the plot indicate the frequency of $CD8^+$ *Strep*tamer$^+$ T cells. (b) Results obtained from the k_{off}-rate assays with the four different CMV-specific *ex vivo* populations. Shown are the $t_{1/2}$ with mean, numbers in the diagram indicate mean $t_{1/2}$ of each population.

specific population with a frequency of over 30% among all CD8$^+$ T cells (Figure 4.30(a)).

The four T cell populations were analyzed in the k$_{off}$-rate assay and revealed strong differences of both the mean half-life times and the variation of half-life time within one population (Figure 4.30(b)). Mean half-life times ranging from 38s up to 242s were obtained, demonstrating that it is possible to determine a wide range of k$_{off}$-rates with the k$_{off}$-rate assay. Interestingly, a correlation between the population size and the k$_{off}$-rate occurred in this group, where upon the biggest T cell population (30% of CD8$^+$) had the fastes half-life time (38s) and the smallest population (0.1% of CD8$^+$) the slowest half-life time (242s).

4.5.4 k$_{off}$-rate assays of CMV-specific T cell clones

A further approach to validate the k$_{off}$-rate assay was done by generating T cell clones of each of the CMV-specific *ex vivo* populations. The generation and culturing of the T cell clones was done by Jeannette Bet and Paulina Paszkiewicz under the supervision of Prof. Stan Riddell. They obtained the clones by sorting *Strep*tamer$^+$ CD8$^+$ PBMC out of the blood of healthy CMV$^+$ donors and cloning the sorted cells by limiting dilution. As each clone and its respective TCR originates from the *ex vivo* populations, the different k$_{off}$-rates of the T cell clones should reflect the range of k$_{off}$-rates found in the respective *ex vivo* population. The k$_{off}$-rate analysis of the T cell clones was done in close cooperation with Bianca Weißbrich.

In Figure 4.31, the k$_{off}$-rates of the four analyzed *ex vivo* populations and their respective clones are shown in four separated diagrams. Each clone had only very low variation in its k$_{off}$-rates , and the clones were settled in the range of k$_{off}$-rates of their originating populations. One exception was found for two T cell clones specific for HLA B8 IE1$_{88-96}$, which had half-life times that were below the range of the *ex vivo* populations (Figure 4.31(b)). However, with a frequency of 0.11% *Strep*tamer$^+$ CD8$^+$ cells, the *ex vivo* population was very small and only few cells could be isolated for the k$_{off}$-rate assays. Therefore, it is likely that the k$_{off}$-rates of the *ex vivo* population did not reflect the whole repertoire of different HLA B8 IE1$_{88-96}$ specific TCRs contained in this population, explaining why the k$_{off}$-rates of the two T cell clones were not contained in the *ex vivo* population. The T cell clones of the two other *ex vivo* populations, specific for HLA B7 pp65$_{417-426}$ and HLA A2 pp65$_{495-503}$ respectively, were again settled within the range of the k$_{off}$-rates of the originating populations Altogether, these data demonstrated again the reliability of the values obtained from the k$_{off}$-rate assay.
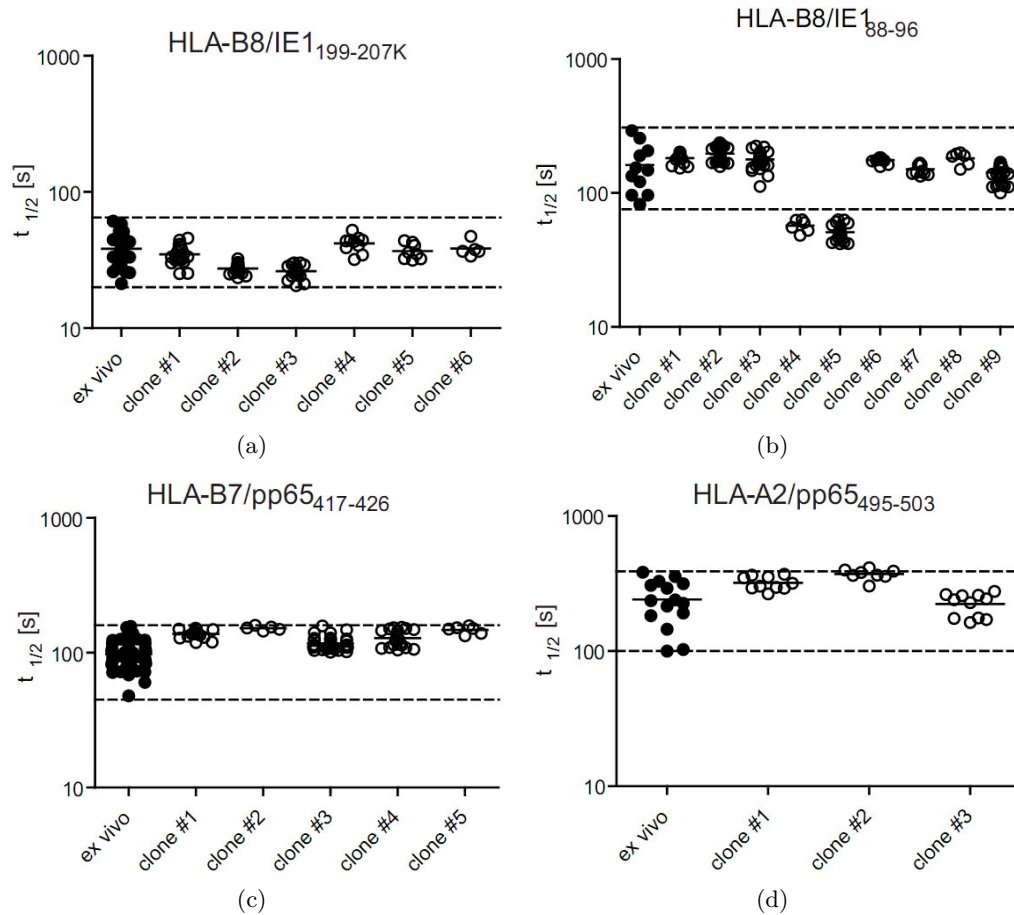
Figure 4.31: **k_{off}-rate assay with T cell clones originating from different *ex vivo* populations:**k_{off}-rate assay were performed with four *ex vivo* populations and their respective T cell clones, generated by limiting dilution. (a)-(d) $t_{1/2}$ with mean of the *ex vivo* population (filled circles) and of the T cell clones (open circles) are compared in each diagram. Dashed lines indicate the range of $t_{1/2}$ found in the *ex vivo* population.

Chapter 5

Discussion

T cells within a certain range of high avidity for their cognate ligand are believed to be most effective for adoptive immunotherapy. T cell receptor (TCR) transfer experiments indicate that a major part of avidity is hard wired within the structure of the TCR. Unfortunately, structural avidity is difficult to assess on living T cells. In the laboratory of Prof. Busch, a novel avidity assay has been developed, where dissociation of truly monomeric pMHC bound to surface expressed TCRs can be monitored by realtime microscopy. This allows measurement of k_{off}-rates, an important component of structural avidity. The k_{off}-rate assay has been established for murine T cells by Robert Knall. His data revealed a clear correlation between the functional avidity and the k_{off}-rate of murine T cells. Most importantly, with adoptive T cell transfer experiments in preclinical mouse models for *Listeria monocytogenes* and mCMV infection, respectively, it could be shown that only specific T cells with a slow k_{off}-rate were able to protect the mice against pathogen infection. These data suggested that the k_{off}-rate might also provide an important parameter for rating T cell quality for adoptive T cell therapy in humans.

Hence, in this PhD work, the k_{off}-rate assay should be established for the measurement of human T cells. Different experiments revealed that the murine k_{off}-rate setup could not be directly transfered to human cells, even though the involved murine and human molecules showed high structural homology. The problem was pointed to the conjugation site of the fluorescent dye and new conjugation sites and subsequently stronger fluorescent dyes were tested. Finally, a new setup for human T cells could be established that enabled reproducible k_{off}-rate measurements. T cell transfer experiments revealed that the k_{off}-rate was highly dependent on the structure of the TCR. Furthermore, four *ex vivo* populations specific for different CMV epitopes were analyzed in more detail with the new setup. These experiments served not only as validation for the method but provided also the possibility to characterize T cell populations with high impact on T cell therapy.

5.1 k_{off}-rate assay to determine T cell avidity

The hypothesis that an important part of T cell avidity is hard wired in the structure of the TCR was supported by T cell transfer experiments. Rosenberg and colleagues

could show that by introducing a TCR to nonspecific PBMCs, both the tumor reactivity and the high avidity of the originating T cells could be transfered [204]. Therefore, the measurement of the structural avidity of T cells via the strength of TCR-ligand interaction seems to be a valid approach to get information on a quality parameter, which is hard wired within the T cells and independent of external influences as e.g. culturing conditions.

Several assays to measure structural avidity have been established in the past. Multimer-based avidity assays measure the MHC-multimer k_{off}-rate from surface expressed TCRs. However, several factors complicate the correct determination of the TCR-pMHC binding strength in these assays. First, a blocking reagent is needed to prevent rebinding of newly dissociated MHC molecules and its concentration can have a strong influence on the dissociation kinetics. Second, due to the multimeric nature of MHC reagents, the k_{off}-rate might not only depend on the TCR avidity but also on other factors like organization of the TCR in the membrane. And third, it is difficult to standardize the generation MHC multimer reagents concerning the level of MHC multimerization. Taken together, the kinetics of multimer k_{off}-rates are influenced by various factors and do not allow for exact analysis of the monomeric TCR-pMHC interaction.

The Biacore assay, based on the phenomenon of surface plasmon resonance, is a very sensitive method to accurately determine the monomeric TCR-pMHC interaction including the calculation of k_{on}-rate and k_{off}-rate . However, both the pMHC complex and the TCR have to be expressed recombinantly to perform the measurements. The expression of an active, soluble TCR has been achieved by different approaches, but there is no expression protocol applicable for all TCRs, which turns the preparations into a difficult and time consuming process. Furthermore, the assay does not reflect physiological conditions, as none of the binding partners is embedded in a physiological membrane and therefore, the contribution of coreceptors as CD8 can not be taken into account. Recent technical innovations of the Biacore method could address these problems. Alterations in the setup now allow for the transport of living cells in the sample flow. Thus it is possible to analyze the interaction of cell surface bound molecules with interaction partners immobilized on the sensor chip surface. Although no experiments measuring TCR-pMHC interaction with this setup have been (to our knowledge) published until now, in theory it should be possible to immobilize the pMHC molecules on the chip surface and let living T cells flow through the chip. The interaction of TCR-pMHC could then be analyzed without the prerequisite of soluble TCRs and with the contribution of CD8. However, this setup no longer allows for the analysis of the monomeric TCR-pMHC interaction, as several TCRs on the T cell surface would probably bind to immobilized MHC molecules. It would be difficult to analyze the statistics on the number of bindings per T cell and in addition, a blocking reagent would become necessary to prevent rebinding of single detached TCRs. Hence, this "physiological" Biacore setup would no longer allow for the accurate calculation of the k_{on}-rate and k_{off}-rate of TCR-pMHC interactions and therefore does not provide a valid approach that could improve T cell avidity assays.

In order to be able to measure monomeric TCR-pMHC interactions in the context

of a living T cell, we developed a novel T cell avidity assay providing the k_{off}-rate of the TCR-pMHC binding. However, there is a vivid discussion in the field if the k_{off}-rate is the determinant factor of T cell avidity or if the k_{on}-rate has an equal or even more important influence. Different new assays to measure TCR avidity and to determine the contribution of k_{on}-rate and k_{off}-rate have been recently published. Huang et al. developed an assay to measure the kinetics of the two dimensional TCR-pMHC interaction with both partners anchored in two dimensional membranes [205]. They claim that this assay would be closer to physiological conditions than most other avidity assays, where at least one of the binding partners is in solution and thus able to move in three dimensions. Analyzing the interaction of the OT1 TCR with a panel of different pMHC ligands with their two dimensional assay, they found fast k_{on}-rate and, compared two three dimensional assays, a broader dynamic range of affinities and k_{on}-rate. The 2D k_{off}-rates were also found to be up to 8 fold faster. It is difficult to estimate the physiological relevance of this model, as the TCR, held with a micropipette, is directed towards the MHC molecules bound to the membrane of a red blood cell (RBC) with controlled contact time and contact area. The TCR-pMHC interaction is observed visually by elongation of the RBC and an adhesion frequency is calculated. This adhesion frequency serves then to determine the k_{off}-rate and k_{on}-rate. Whether this mathematical model is able to provide k_{on}-rates comparable to physiological conditions is debatable. Hence, the basic idea to observe two dimensional interaction of TCR and pMHC is closer to the situation of CTL-target cell contact. The setup of the assay, however, does not seem to reflect the physiological situation.

Another two dimensional approach was developed by Huppa et al.. In order to analyze the TCR-pMHC interaction "in situ", they observed the binding of T cells to pMHCs embedded in a modified planar bilayer system as a surrogate antigen presenting cell surface by fluorescence microscopy [206]. The interaction was visualized by coupling of FRET partners to the TCR and the pMHC, respectively, and monitoring the duration of the FRET signal. With this setup, they found that synaptic TCR-pMHC binding dynamics were significantly different from TCR-pMHC binding in solution, as they observed a 4-12 fold higher dissociation. Also the TCR affinity for pMHCs was elevated as a consequence of a large increase in the association rate. This effect, however, was reversed by disrupting actin polymers inside the T cell, indicating that cytoskeletal components are involved in the stabilization of TCR-pMHC interaction. Based on these results, they proposed the theory that TCR islands on the T cell surface efficiently scan the surface of an adjacent cell. Thus, a high local density of TCRs surrounding a ligand would be provided, in order to keep the TCR continually engaged to generate the maximum possible signal. The findings from this study provide interesting information on the influence of the immunological synapse and the associated cytoskeletal components on the interaction of TCR-pMHC. They claim to measure TCR-pMHC affinity, which should only be dependent on the binding of these two components. In the study of Huppa et al., however, a multitude of components involved in the immunological synapse can potentially influence the duration of the TCR-pMHC interaction. Therefore, it is questionable, if the affinity that depends on the structure of the TCR is really measured in this study.
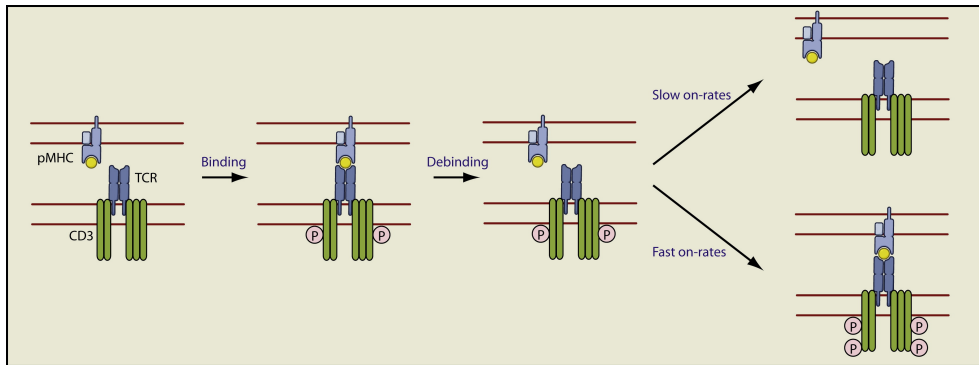
Figure 5.1: **Illustration of the confinement time model:** The confinement time accounts for the multiple rebindings that may occur between pMHC and TCR with fast on-rates. It is a measure of the total time that an individual pMHC and TRC spend together irrespective of interruptions between rebindings. [209]

Not a new method, but new mathematical models were used by two independent publications of Aleksic et al. [207] and Govern et al. [208] to test the two contrasting theories to describe T cell-ligand potency. One theory claims that the ligand potency is a function of TCR-pMHC equilibrium affinity (K_D), i.e. the concentration of available ligand. In the other theory, the half-life time ($t_{1/2}$) of the TCR-pMHC interaction has to be long enough to complete a series of signaling events. An increase in the $t_{1/2}$ raises the probability of a successful signaling and therefore T cell activation. Many studies support the $t_{1/2}$ based model, however, some exceptions challenge this theory, as ligands with a short half-life time can be highly stimulatory if they have fast k_{on}-rates. Aleksic et al. combined theory and experimental approach to elucidate the influence of TCR-pMHC binding parameters on the T cell response in more detail. They analyzed *in vitro* activation of a TCR-trasngenic CD8$^+$ T cell line by a large subset of different cognate pMHC variants to examine the relationship between T cell activation and kinetic measurements. As the data sets contained subsets which differed in the k_{on}-rates, changes in the affinity and in the $t_{1/2}$ could be distinguished. They came to the conclusion that affinity or $t_{1/2}$ alone are not sufficient to fully explain the stimulatory potency. They postulate a new parameter for TCR-pMHC interaction, which they call "confinement time". It is defined by the total time an individual pMHC and TCR are engaged regardless of interruptions between rebindings. The confinement time is dependent on both the k_{on}-rate and the k_{off}-rate. Thereby, a slow k_{on}-rate leaves T cell activation mainly dependent on the $t_{1/2}$ of the TCR-pMHC interaction, whereas activation is determined by affinity if the k_{on}-rate is fast (illustrated in Figure 5.1).

Determining the stimulatory potency of CD4$^+$ T helper cells, Govern et al. came to very similar results. They identified low-, medium and high-potency ligands that had medium or fast binding kinetics. Using mathematical modeling of the biophysical mechanisms leading to T cell activation, they came to the conclusion that ligands with a short $t_{1/2}$ can be highly stimulatory if they show fast k_{on}-rates. Thereby, fast k_{on}-rates allow an individual TCR to quickly bind and rebind to the same pMHC repeatedly before diffusing away. They create the model of an aggregate $t_{1/2}$ (t_a),

based on which the ligand potency is dependent on the K$_D$ when ligands show fast k$_{on}$-rates and t$_{1/2}$-dependent when they have a slow k$_{on}$-rate [208].

So how can we estimate the relevance of the k$_{off}$-rate assay in this context? Albeit mathematical models emphasize the importance of the k$_{on}$-rate, our data provide evidence that the k$_{off}$-rate is an important parameter for T cell avidity. A clear correlation between functional avidity *in vitro* and k$_{off}$-rate could be shown for both murine and human T cells. Most importantly, adoptive T cell transfer experiments with preclinical mouse models revealed that only T cells with a slow k$_{off}$-rate were able to confer protection. Therefore, we think that the measurement of the k$_{off}$-rate alone already provides important information on the avidity of a T cell. Nevertheless it would be very interesting to additionally assess the k$_{on}$-rate using the described avidity assay. There are several obstacles, however, which complicate this approach. First, to observe the k$_{on}$-rate with real-time microscopy, unstained T cells have to be incubated in the staining solution under microscopic control. This would require both the supply of staining reagents to the microscopic setup and local immobilization of the T cells. The Evotec Cytocon 400 technology (s. section 5.4), a microfluidic chip combined with cage electrodes, is able to fulfill these requirements. The unstained T cell could be trapped in the cage and staining solution could be added to the microfluidic system under microscopic control. At this point, however, we have to face the second and probably more severe obstacle for assessing k$_{on}$-rates with our avidity assay. As the k$_{off}$-rate is calculated based on the dissociation of monomeric pMHC molecules, the measurement of the respective k$_{on}$-rate would require the binding of monomeric pMHCs to surface bound TCRs. This binding, however, is very weak and instable, a fact that we utilize for the analysis of the k$_{off}$-rate. Even with the addition of very high concentrations of monomeric pMHCs to unstained T cells, the effects of MHC-binding and -dissociation would always interfere and thus inhibit an accurate calculation of the k$_{on}$-rate. The k$_{on}$-rate of MHC-*Strep*tamers, however, could be analyzed in the described microfluidic setup. *Strep*tamer solution could be added to a trapped, unstained T cell in the chip and the k$_{on}$-rate could be calculated by the increase in T cell staining intensity. This k$_{on}$-rate would be dependent on the multimeric nature of the *Strep*tamers and could not be set in direct relation to the k$_{off}$-rate of monomeric pMHCs. However, it might provide an additional structural parameter of different TCR-pMHC interactions.

5.2 The human k$_{\text{off}}$-rate assay setup

To enable k$_{off}$-rate measurements for human T cells, several parameters of the setup that worked for murine cells had to be altered. First, extensive experiments revealed that the conjugation site in the MHC molecule for the fluorescent dye had to be changed for the human setup. And second, a new fluorescent dye had to be found which was bright enough to perform k$_{off}$-rate assays.

5.2.1 Murine and human MHC I - high similarity, small differences

Dye conjugation with Alexa488 at cysteine 67 in the murine β_2m did not seem to interfere with TCR binding of the conjugated MHC molecules and allowed for the performance of successful k$_{off}$-rate assays. Although there are diverse alterations in the amino acid sequence, the tertiary structure of murine and human MHC I molecules is largely conserved and very similar. For the setup of the human k$_{off}$-rate assay it seemed therefore reasonable to try the analogous conjugation site at cysteine 67 in the human β_2m. *Strep*tamers containing those dye-conjugated human MHC molecules, however, failed to stably stain specific T cells. Different experiments revealed the reason for the diminished or even absent staining of the conjugated MHC I molecules. As no Alexa488 staining could be observed on human T cells stained with the "dichromatic" *Strep*tamers, it was first tested if the dye-conjugation of human MHC I molecules was successful. Coupling MHC molecules to *Strep*-Tactin coated beads and analyzing the fluorescence intensity of the beads by flow cytometry demonstrated that the dye-conjugation was successful and the fluorescence intensity comparable to the murine setup. But if the dye was really coupled to Cys67 was not clear at this point. Dye conjugation to one or multiple other cysteines in the human MHC I molecule could interfere with TCR binding and would therefore explain the diminished TCR binding. To test the specificity of the dye conjugation to Cys67, a MHC I complex that contained the unmutated β_2m with tyrosine at position 67 was incubated following the common protocol. Staining T cells with *Strep*tamers of these dye-incubated Tyr67 MHC molecules resulted in a specific and stable staining which was comparable to *Strep*tamer staining with Tyr67 MHC molecules that had not been incubated with the fluorescent dye. This led to the conclusion that the dye conjugation happened very specifically at position 67 of β_2m and did not influence the other cysteines present in the MHC complex. A look at the crystal structure of human MHC I molecules shows that the -SH groups of all naturally occurring cysteines are located inside the barrel structures of the heavy chain and the β_2m, respectively, with most of them engaged in disulfid-bonds. These -SH groups are therefore not accessible for dye-conjugation, which allows to direct dye-conjugation specifically to the site of a newly inserted, solvent accessible cysteine.

Experiments with chimeric MHC I molecules revealed that the murine heavy chain combined with a dye conjugated human or murine β_2m achieved good T cell staining. This demonstrated that it was possible to generate functional MHC molecules with dye-conjugated human β_2m and excluded the possibility that the diminished T cell staining of human dichromatic *Strep*tamers was human β_2m intrinsic. In contrast, the combination of the human heavy chain with a dye conjugated human or murine β_2m resulted in absent T cell staining. Taken together, these experiments showed that not the nature of the β_2m, but the combination of a human heavy chain with a dye-conjugated β_2m interfered with T cell staining. Even if the structures of human and murine MHC I molecules are very similar, there have to be differences that cause the altered behavior of dye-conjugated isoforms. In-depth analysis of the crystal structures of murine H2-k^b and human HLA B8 revealed small differences in the location of the β_2m to the heavy chain. Thereby, the human β_2m was located slightly closer to the heavy chain than the murine β_2m (s. Figure 5.2). Due to this closer
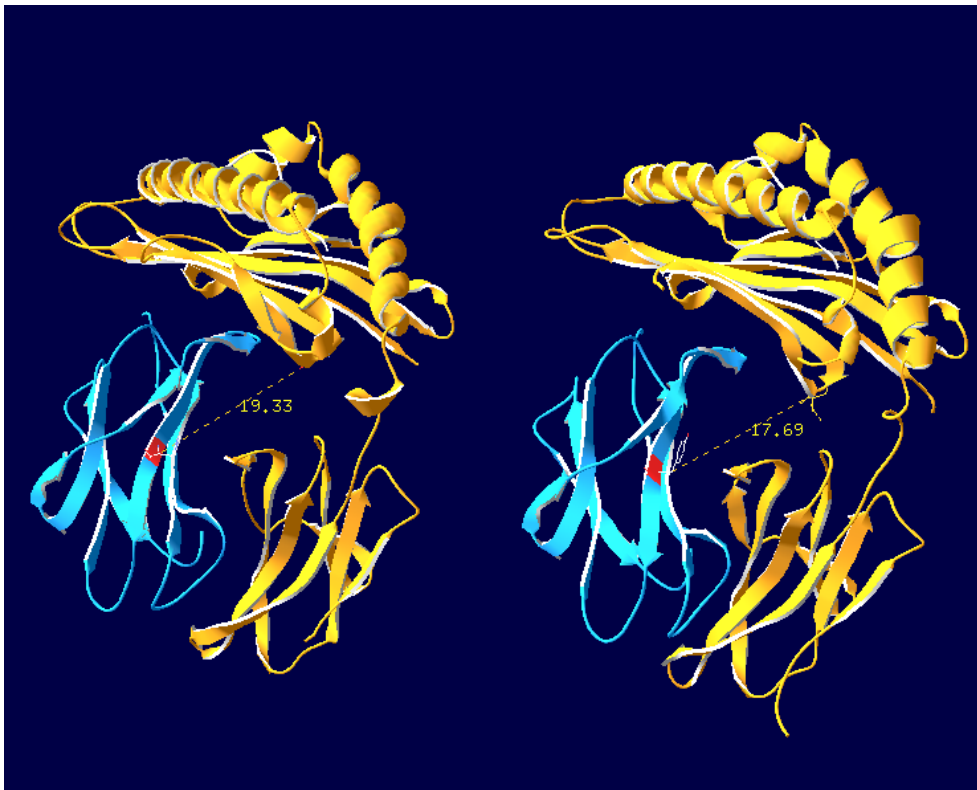
Figure 5.2: **Comparison of β_2m localization in murine and human MHCI molecules:** Crystal structure of H2-k^b with murine β_2m (left, 1N59, [210]) and HLA B8 with human β_2m (right, 1M05, [203]). The distance of the aminoacid at position 67 in β_2m (marked in red) to the closest aminoacid in the heavy chain was calculated with Swiss Prot software.

contact to the heavy chain, dye-conjugation on the β_2m might result in structural alterations of the overall MHC molecule and might also affect the constitution of the MHC-TCR interface. This could weaken the interaction between MHC and TCR and therefore result in diminished staining of those MHC *Strep*tamers. Although we have no proof based on crystal structures, our data strongly support this hypothesis.

5.2.2 Right dye, right place

As different experiments led to the conclusion that dye-conjugation at the β_2m in a human heavy chain interfered with stable TCR binding, new locations for the fluorescent dye conjugation had to be tested. Three sites in the *Strep*-tag III region of the MHC molecule were chosen. This region has maximal distance to the MHC-TCR interface and interference of the conjugated dye with TCR binding of the MHC molecule should therefore be improbable. The first conjugation site should be located in the GS-linker between MHC C-term and the first *Strep*-tag II sequence, the second between the two *Strep*-tag II sequences and the third at the end of the *Strep*-tag III region. The new conjugation sites were generated by insertion of a cysteine for conjugation sites I and II or a cysteine combined with a short GS

linker for conjugation site III by mutagenesis PCR of the MHC vector. Whereas the mutagenesis worked for conjugation sites I and III, we never obtained conjugation site II, even after serial repetitions and alterations of the experimental setup. The reasons for this are not clear. However, dye-conjugation on site III turned out to achieve stable staining of T cells with the respective *Strep*tamers. Furthermore, dye-conjugation at site II could potentially interfere with *Strep*-Tactin binding of both adjacent Stretag II sequences and thus hamper the multimerization of the MHC molecule. For these reasons, attempts to generate conjugation site II were no longer pursued and experiments were continued with dye conjugation at site III.

The fluorescent dye Alexa488 that had been successfully used for murine k$_{\text{off}}$-rate assays was conjugated at the new site. *Strep*tamers of those labeled MHC molecules achieved stable T cell staining and both PE- and Alexa488 fluorescence were detectable by flow cytometry. Analysis of stained T cells under the microscope, however, revealed that the Alexa488 intensity was too low to reliably perform k$_{\text{off}}$-rate assays. But why was Alexa488 bright enough in the murine but not in the human setup? Different TCR expression levels on the surface of murine and human T cells could be a reason. Stainings for the common TCR β chain, however, indicated that the expression levels of the analyzed cells were comparable. The location of the conjugation site could also influence the Alexa488 fluorescence intensity. Located at the end of the *Strep*-tag III, Alexa488 is in close proximity to the backbone dye PE. FRET between the two dyes is due to the emission spectra and the proximity possible. Retrospective analysis of murine k$_{\text{off}}$-rate data revealed that FRET between Alexa488 and PE was also visible in murine experiments. The longer distance of the two dyes in the murine setup might be the reason that the FRET effect is less pronounced and Alexa488 fluorescence also in the presence of PE detectable. Altogether, FRET in the human setup seems to be best explanation for the weak Alexa488 staining. However, no increase in the Alexa488 fluorescence intensity could be observed after dissociation of the *Strep*-Tactin-PE backbone. This suggests that FRET was not the main reason for the weak fluorescence intensity of Alexa488 at conjugation site III. The exact reason for the failure of Alexa488 in the human k$_{\text{off}}$-rate assay setup could not be yet determined, however, we can conclude that location of Alexa488 on the new conjugation site interfered either with the full excitation or emission of Alexa488 fluorescence.

Hence, a new dye had to be found that was small, photobleaching resistant and bright enough to perform k$_{\text{off}}$-rate assays with conjugated MHC molecules. Atto565 conjugated MHC molecules were successfully tested and achieved in combination with APC conjugated *Strep*-Tactin, stable *Strep*tamer staining and successful performance of k$_{\text{off}}$-rate assays. As Atto565 and APC are FRET partners, the full fluorescence intensity of Atto565 can only be detected after dissociation of *Strep*-Tactin APC. This results in a peak of the Atto565 fluorescence that is followed by an exponential decay of the fluorescence due to MHC dissociation. The peak marks the first suitable data point for analysis and allows therefore for an optimal fitting of data points for each analyzed cell. For the correct calculation of the k$_{\text{off}}$-rate, photobleaching of Atto565 has to be subtracted from the overall decay of Atto565 fluorescence. First tests showed that Atto565 was very stable in the laser setup of the k$_{\text{off}}$-rate assay and photobleaching could be neglected. Unexpectedly, same

measurements at later time points revealed small but detectable photobleaching, which was, however, slow enough to allow k$_{\text{off}}$-rate measurements. But the different results of repetitive experiments with the same dye had to be explained. It turned out that in the time between the two experiments, the 561 laser that is used for Atto565 excitation, was exchanged by a new one. The laser power of new and old lasers, which are otherwise identical, can vary significantly. Hence, even if identical percentage of laser power was chosen in the software setups for photobleaching experiments one and two, the absolute laser power might have been much lower in the first experiment with the old laser compared to the second experiment, at which the new laser was already installed. This points out that frequent measurements of the laser power and the resulting Atto565 photobleaching are necessary to ensure accurate analysis of the k$_{\text{off}}$-rate assays (s. section 5.4).

5.3   k$_{\text{off}}$-rate - significance for adoptive T cell therapy

During this PhD work, a k$_{\text{off}}$-rate assay for human cells could be developed that proved to produce reliable and reproducible data. But what is the significance of the k$_{\text{off}}$-rate for T cell quality? Could the k$_{\text{off}}$-rate be an important parameter for the choice of optimal T cells for adoptive transfer? A clear correlation between the k$_{\text{off}}$-rate and the protective capacity of a T cell could be shown in T cell transfer experiments in preclinical mouse models [164]. This strongly indicates that the k$_{\text{off}}$-rate could also be an important parameter for quality of human T cells. Four different *ex vivo* T cell populations with specificities for different CMV epitopes were analyzed. A wide range of k$_{\text{off}}$-rate was calculated, which demonstrated that the populations differed significantly concerning their k$_{\text{off}}$-rates. Functional assays that were performed with the *ex vivo* populations and in addition with T cell clones, revealed a correlation between the k$_{\text{off}}$-rate and the functional avidity of the analyzed cells. These data indicate that CMV specific T cell populations differ in their functionality and thus most probably in their suitability for adoptive T cell transfer. The k$_{\text{off}}$-rate is strongly correlated to the functionality and therefore provides important information on the quality of the T cell populations. Interestingly, we see the tendency that in the case of chronic the population size is negatively correlated with the k$_{\text{off}}$-rate. If the k$_{\text{off}}$-rate and the population size are correlated or if other factors like epitope specificities contribute to this phenotype is object of current investigations. However, there are hints that immune senescence might play an important role. The analyzed *ex vivo* populations originate from three individuals aged 26, 31 and 45. The faster k$_{\text{off}}$-rate and the increasing population size follows an age related pattern. Busch and colleagues propose the following model to explain the change in TCR avidity in an ongoing CMV infection. In the early phase of a CMV infection, T cells with high avidity TCRs receive the strongest signal to proliferate and thus provide the dominant population to control viral replication. With ongoing infection, antigen-driven proliferation results in proliferation associated senescence and dysfunctionality of the high avidity T cells. Recurrence of viral replication induces then antigen driven proliferation in T cell clonotypes with the next highest avidity, starting the cycle of proliferation and senescence again. At the late phase

of CMV infection in elderly people, new naive thymic emigrants are missing and no further T cell clones are available to replace the dysfunctional ones. This results in expansion of the last T cell clone to compensate for its dysfunctionality [211]. The knowledge of CMV and immune senescence is important for the choice of suitable T cell populations for adoptive transfers, as big populations might provide a high number of transferable T cells but with possibly low functionality.

The main goal, however, remains to identify T cells with optimal k_{off}-rate and thus optimal avidity for adoptive T cell therapy. As this project is still basic research and not involved in clinical studies, experimental transfer of T cells with different k_{off}-rates in humans is obviously not possible. However, we are in close collaboration with the group of Dr. Neuenhahn that is involved in an authorized phase I/II adoptive T cell transfer study. In this study, highly immunocompromised patients after allogeneic hematopoietic stem cell transplantation that suffer from CMV complications are treated by *ex vivo* isolated CMV-specific CD8$^+$ T cells. CMV-specific T cells are monitored before, during and after T cell transfer. Through the collaboration, we have the chance to get some patients material and measure an aliquot of the k_{off}-rate of T cells that are going to be transferred. In a retrospective analysis, the k_{off}-rate can be correlated to the clinical outcome after T cell transfer, measured as reduction of viral load and persistence of the T cells. This offers a great opportunity to analyze the *in vivo* functionality of T cells with different k_{off}-rates in humans. But it could also be useful to go in parallel back to the preclinical mouse models to determine optimal T cell avidity for adoptive transfer directly. So far, T cell lines with two different k_{off}-rate rates were transferred into previously infected mice and protective capacity of the T cell was analyzed. Thereby, a clear correlation between a slower k_{off}-rate and a better protectivity could be demonstrated. At this point, however, it would be interesting to go to extremes and test T cell with very low or very high k_{off}-rate and see, wheater the previously found correlation is still valid or if an optimal k_{off}-rate can be identified.

5.4 Applications and further perspectives

In the last section, the significance of k_{off}-rate measurements of specific T cell populations for adoptive T cell transfer was discussed. However, a T cell population is mostly a mix of T cells with different avidities. Even a population with a high mean half-life time and thus slow mean k_{off}-rate will contain also T cells with faster k_{off}-rates. Therefore, we aim to develop a single cell platform to isolate and amplify T cells with optimal avidity. The first step would be the performance of the k_{off}-rate assay with single trapped T cells and the subsequent sorting of T cells with defined avidities. As shortly mentioned in section 5.1, the Evotec Cytocon400 system offers the possibility to trap single cells under microscopic control, add d-biotin and perform the k_{off}-rate assay and subsequently direct the analyzed T cell out of the chip. Figure 5.3 shows the core element of this system, the Evotec Cytocon Loader chip. This microchannel flow through device is equipped with electrodes that allow for contact free cell guidance and trapping via negative dielectrophoresis. Through a detection window in the middle part of the chip, the cell can be

Cytocon™ Loader chip
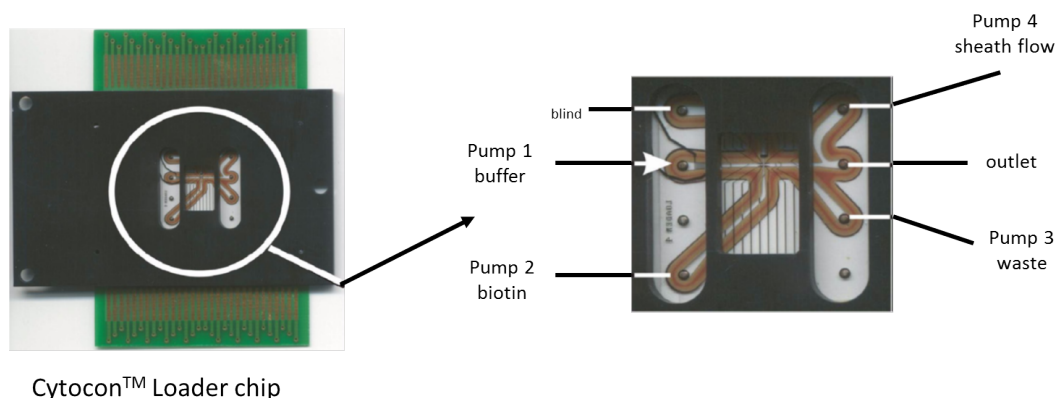
Figure 5.3: **The Evotec Cytocon cell sorter chip:** Picture of the complete cell sorter chip (left) and close-up to the channels and electrodes contained in the microfluidic chip (right). The spots at the top pf the chip, where tubes to the different pumps can be connected, are indicated. The fine dark lines in the chip represent the electrodes that can be software controlled.

directed and trapped under microscopic control. The different channels in the chip are connected to syringe pumps that allow for the addition and flow through of buffer, cells and reagents as d-biotin. To perform the k_{off}-rate assay in the Evotec system, *Strep*tamer stained T cells are added to the buffer flow and guided through the chip. A single cell is trapped in the middle of the chip by switching on the eight cage electrodes. Analogous to the described k_{off}-rate assay, a time series of pictures taken every 10 seconds is started and d-biotin is added after the first picture. After complete MHC-dissociation, the cell is released from the cage and directed to the sort channel of the chip. The cell is released in a small droplet of buffer and can be taken up with a pipette. Here we reach the next step in our single cell platform, the amplification of the T cell with defined avidity. This amplification can achieved either by clonal expansion of the T cell or by identification and sequencing of the TCR with single cell PCR to genetically generate high avidity T cells. The isolation and amplification of T cells with optimal high avidity is reasonable, if the transfer of mixed populations containing high and low avidity T cells would bear any disadvantages. It could be observed that low avidity T cells are able to displace high avidity T cells, in addition they are competing for the same survival factors in the host. However, the described process of the single cell platform is quite time consuming and difficult to realize for each patient individually. This hurdle could be overcome by the generation of TCR data bases, where T cells with optimal avidity for different HLA-peptide combinations could be stored. MHC matched T cells with optimal avidity for adoptive transfer could be individually chosen and transferred into patients.

Beside rating of T cell quality for adoptive transfer, further applications of k_{off}-rate measurements could focus on diagnostic purposes. Thereby, k_{off}-rate measurements could serve to estimate the quality of existing or induced T cell immunity after vaccination. At the moment, such diagnostic procedures are available for the de-

tection of high avidity antibodies, which are clinically correlated with the quality of antibody-mediated immune responses. For T cell responses, such diagnostic measurements have so far not been possible. Analysis of specific T cell with reversible *Strep*tamers allow for the quantification of the T cell immunity, subsequent k_{off}-rate measurements would allow in addition to estimate the quality and perhaps even the further development of those T cells.

Furthermore, the k_{off}-rate assay is also applicable for the measurements of other interactions than TCR-pMHC binding. Virtually, all receptor-ligand interactions with low affinity could be analyzed. The precondition to perform k_{off}-rate measurements is that one of the interaction partners has to be recombinantly expressed and linked to *Strep*-tag III that contains a dye-conjugation site. Analogous to recombinant MHC molecules, the recombinant molecule can be subsequently conjugated with Atto565 and multimerized on *Strep*-Tactin to form dichromatic *Strep*tamers. Preliminary experiments are started with an chimeric antigen receptor (CAR) developed from an anti-ROR1 mAB. ROR1 is an oncofetal tyrosine kinase receptor that is uniformly expressed on chronic lymphocytic leukemia (CLL) and mantle cell lymphoma (MCL). It could be shown that the anti-ROR1 mAb is able to confer specific recognition of malignant, but not mature normal B cells when expressed in $CD8^+$ T cells [212]. ROR1 has now been recombinantly expressed and conjugated with Atto565 to measure the interaction with different ROR1 specific CARs and thereby rate the efficiency of the CAR-transduced T cells.

The k_{off}-rate assay for both murine and human T cells has been found to be a reliable method the measure an important part of T cell avidity and reproducible data can be generated with this assay. However, there are several points that could improve the technique. First, the introduction of an internal bleaching control would help to standardize the k_{off}-rate assay and allow for internal quality control during the determination of MHC dissociation. In the ideal setup, photobleaching would be calculated individually for each dissociation experiment. To achieve this, beads coated with Atto565 spiked to the T cells could be used. The beads could be discriminated by their shape and size and would be exposed to exactly the same conditions concerning laser power and further microscope setup as the stained T cells. However, one problem arises with this setup. Preliminary experiments showed that the fluorescence intensity of those dye-coupled beads is often by a multitude stronger than the fluorescence intensity of *Strep*tamer stained T cells. To perform the k_{off}-rate assay, the detection range of the microscope has to be adjusted to the darkest and the brightest values in the picture to assure optimal resolution and quality of the detection range. If the fluorescence intensity of beads and T cells is very different, the investigator has two possibilities: first, adjust the upper limit of the detection range to the beads, but this would result in less contrast and less amplification of the staining intensity of the T cell and thus hamper the analysis. Second, the upper limit could be adjusted to the intensity of the T cells, providing optimal conditions for the observation of the dissociation, but the staining intensity of the beads would be above the detection range. In this case, changes in the fluorescence intensity would not be detectable until the fluorescence intensity declines to the detection range. Consequently, photobleaching of the beads could not be monitored in this range. To overcome these hurdles, it could be a possibility to conjugate beads with titrated

amounts of fluorescent dye and thus generate beads with different fluorescence intensities. For every k_{off}-rate experiment, beads with the convenient fluorescence intensity could be chosen, which would allow to perform bleaching measurements in a microscope setup optimized for the *Strep*tamer stained T cells.

A second and also very important aspect for further improvements is the reduction of the cell number needed for the k_{off}-rate assay. At the moment, about 10^4 cells are needed to perform one MHC dissociation assay. However, only a small part of the cells can be observed and other cells that lie out of the field of view are lost for further experiments. The reservoir that is currently used to mount the cell under the microscope has a very big diameter compared to the size of the observation field. Thus, a possible improvement could be the reduction the width of this reservoir. This would be useful in combination with smaller membranes, as the diameter of the membrane determines the spreading of the droplet on the glass surface containing the cells. There might be also different chips available to observe cells under the microscope. Many of them make it possible to analyze very limited amounts of T cells. However, cells have to be both locally immobilized and constantly cooled to perform reliable k_{off}-rate measurements. No chip fulfilling these conditions could be found yet, but it has to be examined if modifications of existing chips would make k_{off}-rate measurements possible.

Finally, further automation of data analysis would improve the data though-put. Manuel gating of the cells is quite time consuming, especially when cells move and the gates have to be adjusted for every picture in the dissociation. A possibility could be the integration of a tracking software that detects single cells based on their stronger fluorescence intensity compared to the background. This software could follow these cells automatically through the dissociation. Of course, strict controlling of the resulting curves would be necessary to rule out wrong gates caused e.g. by the interference of two overlapping cells in the same gate.

In conclusion, the established k_{off}-rate assay for human T cells offers a broad range of different applications for the analysis TCR-MHC interaction, but also for the analysis of other molecules. Further improvements of the assay could help to standardize, simplify and accelerate the measurement of different receptor-ligand interactions.

Chapter 6

Summary

In higher vertebrates, the adaptive immune system serves to combat microbial pathogens in a very specific manner and results in many cases in life long protection against reinfection. While antibodies of the humoral immunity directly bind intact antigen fragments of the antigen have to be processed and presented in the context of MHC molecules to be recognized by T cells of the cellular immunity. The T cell antigen receptor (or simply T cell receptor (TCR)) detects foreign peptides, derived from intracellular pathogens, or abnormal proteins by binding both to the peptide and to the MHC molecule presenting the peptide. In addition, several TCR associated molecules as the coreceptors CD3 and CD8 or CD4, and other costimulatory molecules take part in this interaction, creating the immunological synapse. Based on the interactions in this synapse, signaling events are induced, triggering T cell effector functions like lysis of the target cell. The in vivo efficacy of a $CD8^+$ T cell, e.g. the ability to clear viral infections, is strongly influenced by the quality of the T cell. The term T cell avidity is often used to describe this quality. The so called "functional avidity" is measured by determining the amount of peptide needed for a T cell to reach maximal effector function or proliferation and is influenced by many factors like expression of the TCR, costimulatory molecules or efficiency of downstream signaling. The binding strength between the TCR, pMHC and the coreceptors is combined in the term "structural avidity". Remarkably, it could be shown, that by transferring a specific TCR, also the high functional avidity was transferred to newly generated T cells, emphasizing the influence of structural avidity on T cell functionality.

A recently developed method in our laboratory allows for the calculation of an important component of the structural avidity, the k_{off}-rate. This novel technique is based on the binding of reversible pMHC multimers, so called *Strep*tamers, to TCRs on the T cell surface. The addition of d-biotin results in detachment of the multimerizing backbone, leaving monomeric MHC-molecules bound to the T cell. Using pMHCs conjugated to a fluorescent dye allows to observe the dissociation of the monomeric pMHCs from the TCRs by realtime microscopy and thereby assess the k_{off}-rate. The k_{off}-rate assay was established with murine T cells and revealed a strong correlation between the k_{off}-rate and the functional avidity of a T cell. Most importantly, in adoptive T cell transfer experiments, only T cells with a slow k_{off}-rate

were able to confer protection to mice after infection. This led to the assumption that the k_{off}-rate might also provide an important parameter for the quality of human T cells chosen for adoptive transfer. Hence, the k_{off}-rate assay setup was transferred to human molecules to allow for the measurement of human T cells. To achieve this, dye conjugated human pMHC I molecules had to be generated and tested for the ability to form functional *Strep*tamers suited for the assay under the microscope. Due to high structural similarities of human and murine MHC I molecules, the conjugation site for the fluorescent dye was chosen analogous to the murine setup on the β_2 microglobuline. However, even though it could be shown that the dye conjugation on this site was successful and highly specific, no stable staining could be achieved with *Strep*tamers generated from these conjugated pMHC. Experiments with chimeric MHC molecules revealed that dye conjugation on human or murine β_2 microglobuline in a human heavy chain interfered with stable binding to the TCR. As the dye conjugation of the MHC I molecule is an essential requirement for the performance of the k_{off}-rate assay, a suitable conjugation site in the human MHC I molecule had to be found. To prevent interference with TCR binding, three different conjugation sites in the *Strep*-tag sequence at the C-term of the recombinant MHC I molecule were tested. Two of these conjugation sites could be successfully generated with mutagenesis PCR and stable *Strep*tamer staining could be achieved with the dye conjugated MHCs. However, the fluorescent dye Alexa488 that was used for the murine assay turned out not to be bright enough to perform k_{off}-rate assays with this setup. Therefore, a new dye had to be found which had to be small enough to prevent any interference with TCR or *Strep*-Tactin binding, sufficiently bright and resistant to photobleaching. After testing different dyes, Atto565-conjugated MHCs multimerized on an APC-conjugated *Strep*-Tactin backbone turned out to be best suited for the use in k_{off}-rate assays. Fluorescence energy transfer (FRET) of the two dyes, caused by their close proximity and their overlapping spectra, helped to determine the time point at which the APC backbone is detached and the dissociation of the pMHC can be analyzed. First human k_{off}-rate assays were performed with CMV specific T cells, as these cells can be easily obtained from healthy individuals. In addition, it is interesting to examine CMV specific T cells in more detail, as they are used for adoptive T cell therapy of immunocompromised patients with CMV complications. Examination of three populations specific for different CMV epitopes revealed a remarkable difference in the k_{off}-rates. The k_{off}-rates of T cell clones generated by single cell dilution, were found to be in the range of the k_{off}-rates from the originating ex vivo populations, demonstrating the reliability of data generated with the k_{off}-rate assay. T cell transfer experiments, performed in collaboration with Bianca Weißbrich and Georg Dössinger, revealed that the k_{off}-rate was maintained after transfer of the TCR to non-specific Jurkat cells. This strongly indicated that the measured k_{off}-rate is hard wired within the structure of the TCR.

In conclusion, a new k_{off}-rate assay setup was established for the accurate measurement of human T cells. This assay allows for the exact determination of the MHC k_{off}-rate from surface. This offers the possibility to define a new parameter of T cell functionality on a single cell level, which might be of importance for the choice of best suited T cells for adoptive transfer.

Bibliography

[1] C. A. Janeway, P. Travers, M. Walport and M. J.Shlomchik. *Immunobiology*. Garland Publishing, 6 edition, Juli 2004.

[2] T. Korn, E. Bettelli, M. Oukka and V. K. Kuchroo. Il-17 and th17 cells. *Annu Rev Immunol*, **27**:485–517, 2009. doi: 10.1146/annurev.immunol.021908.132710. URL http://dx.doi.org/10.1146/annurev.immunol.021908.132710.

[3] C. R. F. Monks, B. A. Freiberg, H. Kupfer, N. Sciaky and A. Kupfer. Three-dimensional segregation of supramolecular activation clusters in t cells. *Nature*, **395**(6697):82–86, September 1998. ISSN 0028-0836. URL http://dx.doi.org/10.1038/25764.

[4] M. R. Jenkins and G. M. Griffiths. The synapse and cytolytic machinery of cytotoxic t cells. *Current Opinion in Immunology*, **22**(3): 308 – 313, 2010. ISSN 0952-7915. doi: 10.1016/j.coi.2010.02.008. URL http://www.sciencedirect.com/science/article/pii/S0952791510000403. ¡ce:title¿Lymphocyte activation and effector functions ? Vaccines¡/ce:title¿.

[5] G. Berke. The ctl's kiss of death. *Cell*, **81**(1):9 – 12, 1995. ISSN 0092-8674. doi: 10.1016/0092-8674(95)90365-8. URL http://www.sciencedirect.com/science/article/pii/0092867495903658.

[6] P. A. Henkart. Lymphocyte-mediated cytotoxicity: Two pathways and multiple effector molecules. *Immunity*, **1**(5):343 – 346, 1994. ISSN 1074-7613. doi: 10.1016/1074-7613(94)90063-9. URL http://www.sciencedirect.com/science/article/pii/1074761394900639.

[7] V. Kalia, S. Sarkar, T. S. Gourley, B. T. Rouse and R. Ahmed. Differentiation of memory b and t cells. *Current Opinion in Immunology*, **18** (3):255 – 264, 2006. ISSN 0952-7915. doi: 10.1016/j.coi.2006.03.020. URL http://www.sciencedirect.com/science/article/pii/S0952791506000689.

[8] O. Bannard, M. Kraman and D. Fearon. Pathways of memory cd8+ t-cell development. *European Journal of Immunology*, **39**(8):2083–2087, 2009. ISSN 1521-4141. doi: 10.1002/eji.200939555. URL http://dx.doi.org/10.1002/eji.200939555.

[9] F. Sallusto, D. Lenig, R. Forster, M. Lipp and A. Lanzavecchia. Two subsets of memory t lymphocytes with distinct homing potentials and effector functions. *Nature*, **401**(6754):708–712, October 1999. ISSN 0028-0836. URL `http://dx.doi.org/10.1038/44385`.

[10] K. Huster, M. Koffler, C. Stemberger, M. Schiemann, H. Wagner and D. Busch. Unidirectional development of cd8+ central memory tcells into protective listeria-specific effector memory tcells. *European Journal of Immunology*, **36** (6):1453–1464, 2006. ISSN 1521-4141. doi: 10.1002/eji.200635874. URL `http://dx.doi.org/10.1002/eji.200635874`.

[11] G. Lauvau, S. Vijh, P. Kong, T. Horng, K. Kerksiek, N. Serbina, R. A. Tuma and E. G. Pamer. Priming of memory but not effector cd8 t cells by a killed bacterial vaccine. *Science*, **294** (5547):1735–1739, 2001. doi: 10.1126/science.1064571. URL `http://www.sciencemag.org/content/294/5547/1735.abstract`.

[12] A. Cerwenka, T. M. Morgan and R. W. Dutton. Naive, effector, and memory cd8 t cells in protection against pulmonary influenza virus infection: Homing properties rather than initial frequencies are crucial. *The Journal of Immunology*, **163**(10):5535–5543, 1999. URL `http://jimmunol.org/content/163/10/5535.abstract`.

[13] M. F. Bachmann, P. Wolint, K. Schwarz, P. Jger and A. Oxenius. Functional properties and lineage relationship of cd8+ t cell subsets identified by expression of il-7 receptor and cd62l. *The Journal of Immunology*, **175**(7):4686–4696, 2005. URL `http://jimmunol.org/content/175/7/4686.abstract`.

[14] C. Stemberger, K. M. Huster, M. Koffler, F. Anderl, M. Schiemann, H. Wagner and D. H. Busch. A single naive cd8+ t cell precursor can develop into diverse effector and memory subsets. *Immunity*, **27**(6):985 – 997, 2007. ISSN 1074-7613. doi: 10.1016/j.immuni.2007.10.012. URL `http://www.sciencedirect.com/science/article/pii/S1074761307005407`.

[15] H. Claman, E. Chaperon and R. Triplett. Thymus-marrow cell combinations. synergism in antibody production. *Proceedings of the society for experimental biology and medicine*, **122**(4), 1966. ISSN 0037-9727.

[16] K. Rajewsky. Carrier effect and cellular cooperation in induction of antibodies. *Proceedings of the royal society of London series B-biological sciences*, **176** (1045), 1971. ISSN 0962-8452. doi: 10.1098/rspb.1971.0002.

[17] P. Marrack, J. P. Scott-Browne, S. Dai, L. Gapin and J. W. Kappler. Evolutionarily conserved amino acids that control TCR-MHC interaction. *ANNUAL REVIEW OF IMMUNOLOGY*, **26**:171–203, 2008. ISSN 0732-0582. doi: 10.1146/annurev.immunol.26.021607.090421.

[18] R. M. ZINKERNAGEL and P. C. DOHERTY. Restriction of in vitro t cell-mediated cytotoxicity in lymphocytic choriomeningitis within a syngeneic

or semiallogeneic system. *Nature*, **248**(5450):701–702, April 1974. URL `http://dx.doi.org/10.1038/248701a0`.

[19] J. Kappler, B. Skidmore, J. White and P. Marrack. Antigen-inducible, h-2-restricted, interleukin-2-producing t cell hybridomas. lack of independent antigen and h-2 recognition. *The Journal of Experimental Medicine*, **153**(5):1198–1214, 1981. doi: 10.1084/jem.153.5.1198. URL `http://jem.rupress.org/content/153/5/1198.abstract`.

[20] J.-M. Claverie, A. Prochnicka-Chalufour and L. Bougueleret. Implications of a fab-like structure for the t-cell receptor. *Immunology Today*, **10**(1): 10 – 14, 1989. ISSN 0167-5699. doi: 10.1016/0167-5699(89)90058-3. URL `http://www.sciencedirect.com/science/article/pii/0167569989900583`.

[21] M. M. Davis and P. J. Bjorkman. T-cell antigen receptor genes and t-cell recognition. *Nature*, **334**(6181):395–402, August 1988. URL `http://dx.doi.org/10.1038/334395a0`.

[22] K. C. Garcia, M. Degano, R. L. Stanfield, A. Brunmark, M. R. Jackson, P. A. Peterson, L. Teyton and I. A. Wilson. An alphabeta t cell receptor structure at 2.5 and its orientation in the tcr-mhc complex. *Science*, **274**(5285):209–219, 1996. doi: 10.1126/science.274.5285.209. URL `http://www.sciencemag.org/content/274/5285/209.abstract`.

[23] D. N. Garboczi, P. Ghosh, U. Utz, Q. R. Fan, W. E. Biddison and D. C. Wiley. Structure of the complex between human t-cell receptor, viral peptide and hla-a2. *Nature*, **384**(6605):134–141, November 1996. URL `http://dx.doi.org/10.1038/384134a0`.

[24] K. S. Campbell, B. Bckstrm, G. Tiefenthaler and E. Palmer. Cart: a conserved antigen receptor transmembrane motif. *Seminars in Immunology*, **6**(6):393 – 410, 1994. ISSN 1044-5323. doi: 10.1006/smim.1994.1049. URL `http://www.sciencedirect.com/science/article/pii/S1044532384710499`.

[25] J. L. Jorgensen, U. Esser, B. Fazekas de St. Groth, P. A. Reay and M. M. Davis. Mapping t-cell receptor-peptide contacts by variant peptide. *Nature*, **355** (6357):224–230, January 1992. URL `http://dx.doi.org/10.1038/355224a0`.

[26] J. L. Jorgensen, P. A. Reay, E. W. Ehrich and M. M. Davis. Molecular components of t-cell recognition. *Annual Review of Immunology*, **10**(1):835–873, 1992. doi: 10.1146/annurev.iy.10.040192.004155. URL `http://www.annualreviews.org/doi/abs/10.1146/annurev.iy.10.040192.004155`.

[27] M. Bouvier. Accessory proteins and the assembly of human class i mhc molecules: a molecular and structural perspective. *Molecular Immunology*, **39**(12):697 – 706, 2003. ISSN 0161-5890. doi: 10.1016/S0161-5890(02)00261-4. URL `http://www.sciencedirect.com/science/article/pii/S0161589002002614`.

[28] P. J. Bjorkman. Mhc restriction in three dimensions: A view of t cell receptor/ligand interactions. *Cell*, **89**(2):167 – 170, 1997. ISSN 0092-8674. doi: 10.1016/S0092-8674(00)80195-6. URL `http://www.sciencedirect.com/science/article/pii/S0092867400801956`.

[29] P. J. Bjorkman, M. A. Saper, B. Samraoui, W. S. Bennett, J. L. Strominger and D. C. Wiley. Structure of the human class i histocompatibility antigen, hla-a2. *Nature*, **329**(6139):506–512, October 1987. URL `http://dx.doi.org/10.1038/329506a0`.

[30] M. Bouvier and D. Wiley. Importance of peptide amino and carboxyl termini to the stability of mhc class i molecules. *Science*, **265**(5170):398–402, 1994. doi: 10.1126/science.8023162. URL `http://www.sciencemag.org/content/265/5170/398.abstract`.

[31] J. Ruppert, J. Sidney, E. Celis, R. T. Kubo, H. M. Grey and A. Sette. Prominent role of secondary anchor residues in peptide binding to hla-a2.1 molecules. *Cell*, **74**(5):929 – 937, 1993. ISSN 0092-8674. doi: 10.1016/0092-8674(93)90472-3. URL `http://www.sciencedirect.com/science/article/pii/0092867493904723`.

[32] J. Hennecke and D. C. Wiley. T cell receptormhc interactions up close. *Cell*, **104**(1):1 – 4, 2001. ISSN 0092-8674. doi: 10.1016/S0092-8674(01)00185-4. URL `http://www.sciencedirect.com/science/article/pii/S0092867401001854`.

[33] M. G. Rudolph, R. L. Stanfield and I. A. Wilson. How tcrs bind mhcs, peptides, and coreceptors. *Annual Review of Immunology*, **24**(1):419–466, 2006. doi: 10.1146/annurev.immunol.23.021704.115658. URL `http://www.annualreviews.org/doi/abs/10.1146/annurev.immunol.23.021704.115658`.

[34] M.-K. Teng, A. Smolyar, A. Tse, J.-H. Liu, J. Liu, R. Hussey, S. Nathenson, H.-C. Chang, E. Reinherz and J.-H. Wang. Identification of a common docking topology with substantial variation among different tcrpeptidemhc complexes. *Current Biology*, **8**(7):409 – 414, 1998. ISSN 0960-9822. doi: 10.1016/S0960-9822(98)70160-5. URL `http://www.sciencedirect.com/science/article/pii/S0960982298701605`.

[35] Y.-H. Ding, K. J. Smith, D. N. Garboczi, U. Utz, W. E. Biddison and D. C. Wiley. Two human t cell receptors bind in a similar diagonal mode to the hla-a2/tax peptide complex using different tcr amino acids. *Immunity*, **8**(4): 403 – 411, 1998. ISSN 1074-7613. doi: 10.1016/S1074-7613(00)80546-4. URL `http://www.sciencedirect.com/science/article/pii/S1074761300805464`.

[36] E. L. Reinherz, K. Tan, L. Tang, P. Kern, J.-h. Liu, Y. Xiong, R. E. Hussey, A. Smolyar, B. Hare, R. Zhang, A. Joachimiak, H.-C. Chang, G. Wagner and J.-h. Wang. The crystal structure of a t cell receptor in complex with peptide and mhc class ii. *Science*,

286(5446):1913–1921, 1999.   doi: 10.1126/science.286.5446.1913.   URL
http://www.sciencemag.org/content/286/5446/1913.abstract.

[37] J. Hennecke, A. Carfi and D. C. Wiley. Structure of a covalently stabilized
complex of a human [alpha][beta] t-cell receptor, influenza ha peptide and mhc
class ii molecule, hla-dr1. *EMBO J*, **19**(21):5611–5624, November 2000. ISSN
0261-4189. URL http://dx.doi.org/10.1093/emboj/19.21.5611.

[38] E. S. Huseby, F. Crawford, J. White, P. Marrack and J. W. Kappler.
Interface-disrupting amino acids establish specificity between t cell re-
ceptors and complexes of major histocompatibility complex and peptide.
Nat Immunol, **7**(11):1191–1199, November 2006.   ISSN 1529-2908.   URL
http://dx.doi.org/10.1038/ni1401.

[39] K. C. Garcia, L. Teyton and I. A. Wilson.   Structural ba-
sis of t cell recognition.   *Annual Review of Immunology*, **17**(1):
369–397, 1999.   doi: 10.1146/annurev.immunol.17.1.369.   URL
http://www.annualreviews.org/doi/abs/10.1146/annurev.immunol.17.1.369.

[40] J. Sloan-Lancaster and P. M. Allen. Altered peptide ligandinduced partial t
cell activation: Molecular mechanisms and role in t cell biology. *Annual Review
of Immunology*, **14**(1):1–27, 1996. doi: 10.1146/annurev.immunol.14.1.1. URL
http://www.annualreviews.org/doi/abs/10.1146/annurev.immunol.14.1.1.

[41] Y.-H. Ding, B. M. Baker, D. N. Garboczi, W. E. Biddison and D. C.
Wiley.   Four a6-tcr/peptide/hla-a2 structures that generate very dif-
ferent t cell signals are nearly identical.   *Immunity*, **11**(1):45 – 56,
1999.   ISSN 1074-7613.   doi: 10.1016/S1074-7613(00)80080-1.   URL
http://www.sciencedirect.com/science/article/pii/S1074761300800801.

[42] M. Degano, K. Garcia, V. Apostolopoulos, M. G. Rudolph, L. Tey-
ton and I. A. Wilson.   A functional hot spot for antigen recogni-
tion in a superagonist tcr/mhc complex.   *Immunity*, **12**(3):251 – 261,
2000.   ISSN 1074-7613.   doi: 10.1016/S1074-7613(00)80178-8.   URL
http://www.sciencedirect.com/science/article/pii/S1074761300801788.

[43] M. M. Davis, J. J. Boniface, Z. Reich, D. Lyons, J. Hampl, B. Arden and Y.-h.
Chien. Ligand recognition by alpha beta t cell receptors. *Annual Review of Im-
munology*, **16**(1):523–544, 1998. doi: 10.1146/annurev.immunol.16.1.523. URL
http://www.annualreviews.org/doi/abs/10.1146/annurev.immunol.16.1.523.

[44] D. M. Kranz. Incompatible differences: view of an allogeneic pmhc-tcr com-
plex. *Nat Immunol*, **1**(4):277–278, October 2000. ISSN 1529-2908. URL
http://dx.doi.org/10.1038/79716.

[45] J.-B. Reiser, C. Darnault, A. Guimezanes, C. Gregoire, T. Mosser, A.-
M. Schmitt-Verhulst, J. C. Fontecilla-Camps, B. Malissen, D. Housset and
G. Mazza. Crystal structure of a t cell receptor bound to an allogeneic mhc
molecule. *Nat Immunol*, **1**(4):291–297, October 2000. ISSN 1529-2908. URL
http://dx.doi.org/10.1038/79728.

[46] J. A. Speir, K. Garcia, A. Brunmark, M. Degano, P. A. Peterson, L. Teyton and I. A. Wilson. Structural basis of 2c tcr allorecognition of h-2ld peptide complexes. *Immunity*, **8**(5):553 – 562, 1998. ISSN 1074-7613. doi: 10.1016/S1074-7613(00)80560-9. URL `http://www.sciencedirect.com/science/article/pii/S1074761300805609`.

[47] N. Manolios, F. Letourneur, J. Bonifacino and R. Klausner. Pairwise, cooperative and inhibitory interactions describe the assembly and probable structure of the t-cell antigen receptor. *EMBO J.*, **10(7)**:1643–51, 1991.

[48] F. Koning, W. Lee Maloy and J. E. Coligan. The implications of subunit interactions for the structure of the t cell receptor-cd3 complex. *European Journal of Immunology*, **20**(2):299–305, 1990. ISSN 1521-4141. doi: 10.1002/eji.1830200211. URL `http://dx.doi.org/10.1002/eji.1830200211`.

[49] D. Gil, W. W. Schamel, M. Montoya, F. Snchez-Madrid and B. Alarcn. Recruitment of nck by cd3 reveals a ligand-induced conformational change essential for t cell receptor signaling and synapse formation. *Cell*, **109**(7): 901 – 912, 2002. ISSN 0092-8674. doi: 10.1016/S0092-8674(02)00799-7. URL `http://www.sciencedirect.com/science/article/pii/S0092867402007997`.

[50] D. J. Kappes, B. Alarcn and J. Regueiro. T lymphocyte receptor deficiencies. *Current Opinion in Immunology*, **7**(4):441 – 447, 1995. ISSN 0952-7915. doi: 10.1016/0952-7915(95)80086-7. URL `http://www.sciencedirect.com/science/article/pii/0952791595800867`.

[51] N. Wang, B. Wang, M. Salio, D. Allen, J. She and C. Terhorst. Expression of a cd3 epsilon transgene in cd3 epsilon(null) mice does not restore cd3 gamma and delta expression but efficiently rescues t cell development from a subpopulation of prothymocytes. *International Immunology*, **10**(12):1777–1788, 1998. doi: 10.1093/intimm/10.12.1777. URL `http://intimm.oxfordjournals.org/content/10/12/1777.abstract`.

[52] U. Moebius, G. Kober, A. L. Griscelli, T. Hercend and S. C. Meuer. Expression of different cd8 isoforms on distinct human lymphocyte subpopulations. *European Journal of Immunology*, **21**(8):1793–1800, 1991. ISSN 1521-4141. doi: 10.1002/eji.1830210803. URL `http://dx.doi.org/10.1002/eji.1830210803`.

[53] D. de Totero, P. Tazzari, J. DiSanto, P. di Celle, D. Raspadori, R. Conte, M. Gobbi, G. Ferrara, N. Flomenberg and F. Lauria. Heterogeneous immunophenotype of granular lymphocyte expansions: differential expression of the cd8 alpha and cd8 beta chains [see comments]. *Blood*, **80**(7):1765–1773, 1992. URL `http://bloodjournal.hematologylibrary.org/content/80/7/1765.abstract`.

[54] G. F. Gao, J. Tormo, U. C. Gerth, J. R. Wyer, A. J. McMichael, D. I. Stuart, J. I. Bell, E. Y. Jones and B. K. Jakobsen. Crystal structure of the complex be-

tween human cd8[alpha][alpha] and hla-a2. *Nature*, **387**(6633):630–634, June 1997. ISSN 0028-0836. URL `http://dx.doi.org/10.1038/42523`.

[55] P. S. Kern, M. kun Teng, A. Smolyar, J. huan Liu, J. Liu, R. E. Hussey, R. Spoerl, H.-C. Chang, E. L. Reinherz and J. huai Wang. Structural basis of cd8 coreceptor function revealed by crystallographic analysis of a murine cd8 ectodomain fragment in complex with h-2kb. *Immunity*, **9**(4): 519 – 530, 1998. ISSN 1074-7613. doi: 10.1016/S1074-7613(00)80635-4. URL `http://www.sciencedirect.com/science/article/pii/S1074761300806354`.

[56] H.-C. Chang, K. Tan and Y.-M. Hsu. Cd8 alpha beta has two distinct binding modes of interaction with peptide-major his- tocompatibility complex class i. *Journal of Biological Chemistry*, **281**(38):28090–28096, 2006. doi: 10.1074/jbc.M604931200. URL `http://www.jbc.org/content/281/38/28090.abstract`.

[57] H.-C. Chang, K. Tan, J. Ouyang, E. Parisini, J. huan Liu, Y. Le, X. Wang, E. L. Reinherz and J. huai Wang. Structural and mutational analyses of a cd8 heterodimer and comparison with the cd8 homodimer. *Immunity*, **23** (6):661 – 671, 2005. ISSN 1074-7613. doi: 10.1016/j.immuni.2005.11.002. URL `http://www.sciencedirect.com/science/article/pii/S1074761305003754`.

[58] R. Koenig. Interactions between mhc molecules and co-receptors of the tcr. *Current Opinion in Immunology*, **14**(1):75 – 83, 2002. ISSN 0952-7915. doi: 10.1016/S0952-7915(01)00300-4. URL `http://www.sciencedirect.com/science/article/pii/S0952791501003004`.

[59] G. F. Gao, Z. Rao and J. I. Bell. Molecular coordination of t- cell receptors and coreceptors cd8 and cd4 in their recognition of peptide-mhc ligands. *Trends in Immunology*, **23**(8):408 – 413, 2002. ISSN 1471-4906. doi: 10.1016/S1471-4906(02)02282-2. URL `http://www.sciencedirect.com/science/article/pii/S1471490602022822`.

[60] L. Wooldridge, B. Laugel, J. Ekeruche, M. Clement, H. A. van den Berg, D. A. Price and A. K. Sewell. Cd8 controls t cell cross-reactivity. *The Journal of Immunology*, **185**(8):4625–4632, 2010. doi: 10.4049/jimmunol.1001480. URL `http://jimmunol.org/content/185/8/4625.abstract`.

[61] V. Renard, P. Romero, E. Vivier, B. Malissen and I. F. Luescher. Cd8beta increases cd8 coreceptor function and participation in tcrligand binding. *The Journal of Experimental Medicine*, **184**(6):2439–2444, 1996. doi: 10.1084/jem.184.6.2439. URL `http://jem.rupress.org/content/184/6/2439.abstract`.

[62] A. Arcaro, C. Grgoire, T. R. Bakker, L. Baldi, M. Jordan, L. Goffin, N. Boucheron, F. Wurm, P. A. van der Merwe, B. Malissen and I. F. Luescher. Cd8 endows cd8 with efficient coreceptor function by coupling t cell recep- tor/cd3 to raft-associated cd8/p56lck complexes. *The Journal of Experimen- tal Medicine*, **194**(10):1485–1495, 2001. doi: 10.1084/jem.194.10.1485. URL `http://jem.rupress.org/content/194/10/1485.abstract`.

[63] M. A. Purbhoo, J. M. Boulter, D. A. Price, A.-L. Vuidepot, C. S. Hourigan, P. R. Dunbar, K. Olson, S. J. Dawson, R. E. Phillips, B. K. Jakobsen, J. I. Bell and A. K. Sewell. The human cd8 coreceptor effects cytotoxic t cell activation and antigen sensitivity primarily by mediating complete phosphorylation of the t cell receptor chain. *Journal of Biological Chemistry*, **276**(35):32786–32792, 2001. doi: 10.1074/jbc.M102498200. URL http://www.jbc.org/content/276/35/32786.abstract.

[64] A. Veillette, M. A. Bookman, E. M. Horak and J. B. Bolen. The cd4 and cd8 t cell surface antigens are associated with the internal membrane tyrosine-protein kinase p56lck. *Cell*, **55**(2):301 – 308, 1988. ISSN 0092-8674. doi: 10.1016/0092-8674(88)90053-0. URL http://www.sciencedirect.com/science/article/pii/0092867488900530.

[65] L. Wooldridge, H. A. van den Berg, M. Glick, E. Gostick, B. Laugel, S. L. Hutchinson, A. Milicic, J. M. Brenchley, D. C. Douek, D. A. Price and A. K. Sewell. Interaction between the cd8 coreceptor and major histocompatibility complex class i stabilizes t cell receptor-antigen complexes at the cell surface. *Journal of Biological Chemistry*, **280**(30):27491–27501, 2005. doi: 10.1074/jbc.M500555200. URL http://www.jbc.org/content/280/30/27491.abstract.

[66] K. C. Garcia, C. A. Scott, A. Brunmark, F. R. Carbone, P. A. Peterson, I. A. Wilson and L. Teyton. Cd8 enhances formation of stable t-cell receptor/mhc class i molecule complexes. *Nature*, **384**(6609):577–581, December 1996. URL http://dx.doi.org/10.1038/384577a0.

[67] I. F. Luescher, E. Vivier, A. Layer, J. Mahiou, F. Godeau, B. Malissen and P. Romero. Cd8 modulation of t-cell antigen receptor-ligand interactions on living cytotoxic t lymphocytes. *Nature*, **373**(6512):353–356, January 1995. URL http://dx.doi.org/10.1038/373353a0.

[68] H. A. van den Berg, L. Wooldridge, B. Laugel and A. K. Sewell. Coreceptor cd8-driven modulation of t cell antigen receptor specificity. *Journal of Theoretical Biology*, **249**(2):395 – 408, 2007. ISSN 0022-5193. doi: 10.1016/j.jtbi.2007.08.002. URL http://www.sciencedirect.com/science/article/pii/S0022519307003621.

[69] D. M. Gakamsky, I. F. Luescher, A. Pramanik, R. B. Kopito, F. Lemonnier, H. Vogel, R. Rigler and I. Pecht. Cd8 kinetically promotes ligand binding to the t-cell antigen receptor. *Biophysical Journal*, **89**(3):2121 – 2133, 2005. ISSN 0006-3495. doi: 10.1529/biophysj.105.061671. URL http://www.sciencedirect.com/science/article/pii/S0006349505728563.

[70] B. Laugel, H. A. van den Berg, E. Gostick, D. K. Cole, L. Wooldridge, J. Boulter, A. Milicic, D. A. Price and A. K. Sewell. Different t cell receptor affinity thresholds and cd8 coreceptor dependence govern cytotoxic t lymphocyte activation and tetramer binding properties. *Journal of Biological*

Chemistry, **282**(33):23799–23810, 2007. doi: 10.1074/jbc.M700976200. URL http://www.jbc.org/content/282/33/23799.abstract.

[71] G. J. Kersh, E. N. Kersh, D. H. Fremont and P. M. Allen. High- and low-potency ligands with similar affinities for the tcr: The importance of kinetics in tcr signaling. *Immunity*, **9**(6):817–826, 1998.

[72] J. D. Rabinowitz, C. Beeson, D. S. Lyons, M. M. Davis and H. M. McConnell. Kinetic discrimination in t-cell activation. *Proceedings of the National Academy of Sciences*, **93**(4):1401–1405, 1996. URL http://www.pnas.org/content/93/4/1401.abstract.

[73] H. A. Van Den Berg and D. A. Rand. Quantitative theories of t-cell responsiveness. *Immunological Reviews*, **216**(1):81–92, 2007. ISSN 1600-065X. doi: 10.1111/j.1600-065X.2006.00491.x. URL http://dx.doi.org/10.1111/j.1600-065X.2006.00491.x.

[74] M. A. Alexander-Miller, G. R. Leggatt and J. A. Berzofsky. Selective expansion of high- or low-avidity cytotoxic t lymphocytes and efficacy for adoptive immunotherapy. *Proceedings of the National Academy of Sciences*, **93**(9):4102–4107, 1996.

[75] V. Dutoit, V. Rubio-Godoy, P.-Y. Dietrich, A.-L. Quiqueres, V. Schnuriger, D. Rimoldi, D. Linard, D. Speiser, P. Guillaume, P. Batard, J.-C. Cerottini, P. Romero and D. Valmori. Heterogeneous t-cell response to mage-a10(254-262). *Cancer Research*, **61**(15):5850–5856, 2001.

[76] C. Sedlik, G. Dadaglio, M. F. Saron, E. Deriaud, M. Rojas, S. I. Casal and C. Leclerc. In vivo induction of a high-avidity, high-frequency cytotoxic t-lymphocyte response is associated with antiviral protective immunity. *Journal of Virology*, **74**(13):5769–5775, 2000. doi: 10.1128/JVI.74.13.5769-5775.2000. URL http://jvi.asm.org/content/74/13/5769.abstract.

[77] C. Yee, P. A. Savage, P. P. Lee, M. M. Davis and P. D. Greenberg. Isolation of high avidity melanoma-reactive ctl from heterogeneous populations using peptide-mhc tetramers. *The Journal of Immunology*, **162**(4):2227–2234, 1999. URL http://jimmunol.org/content/162/4/2227.abstract.

[78] I. Messaoudi, J. A. G. Patio, R. Dyall, J. LeMaoult and J. Nikolich-ugich. Direct link between mhc polymorphism, t cell avidity, and diversity in immune defense. *Science*, **298**(5599):1797–1800, 2002. doi: 10.1126/science.1076064. URL http://www.sciencemag.org/content/298/5599/1797.abstract.

[79] M. Alexander-Miller. High-avidity cd8+ t cells. *Immunologic Research*, **31**:13–24, 2005. ISSN 0257-277X. URL http://dx.doi.org/10.1385/IR:31:1:13. 10.1385/IR:31:1:13.

[80] J. G. Houbiers, H. W. Nijman, S. H. van der Burg, J. W. Drijfhout, P. Kenemans, C. J. van de Velde, A. Brand, F. Momburg, W. M. Kast

and C. J. Melief. In vitro induction of human cytotoxic t lymphocyte responses against peptides of mutant and wild-type p53. *Eur J Immunol*, **23**(9):2072–2077, Sep 1993. doi: 10.1002/eji.1830230905. URL `http://dx.doi.org/10.1002/eji.1830230905`.

[81] S. Walter, L. Herrgen, O. Schoor, G. Jung, D. Wernet, H.-J. Bhring, H.-G. Rammensee and S. Stevanovi? Cutting edge: predetermined avidity of human cd8 t cells expanded on calibrated mhc/anti-cd28-coated microspheres. *J Immunol*, **171**(10):4974–4978, Nov 2003.

[82] M. A. Derby, M. A. Alexander-Miller, R. Tse and J. A. Berzofsky. High-avidity ctl exploit two complementary mechanisms to provide better protection against viral infection than low-avidity ctl. *The Journal of Immunology*, **166** (3):1690–1697, 2001.

[83] A. Gallimore, T. Dumrese, H. Hengartner, R. M. Zinkernagel and H. G. Rammensee. Protective immunity does not correlate with the hierarchy of virus-specific cytotoxic t cell responses to naturally processed peptides. *J Exp Med*, **187**(10):1647–1657, May 1998.

[84] H. J. Zeh, D. Perry-Lalley, M. E. Dudley, S. A. Rosenberg and J. C. Yang. High avidity ctls for two self-antigens demonstrate superior in vitro and in vivo antitumor efficacy. *The Journal of Immunology*, **162**(2):989–994, 1999.

[85] W. R. Heath and F. R. Carbone. Cross-presentation, dendritic cells, tolerance and immunity. *Annu Rev Immunol*, **19**: 47–64, 2001. doi: 10.1146/annurev.immunol.19.1.47. URL `http://dx.doi.org/10.1146/annurev.immunol.19.1.47`.

[86] E. Palmer. Negative selection–clearing out the bad apples from the t-cell repertoire. *Nat Rev Immunol*, **3**(5):383–391, May 2003. doi: 10.1038/nri1085. URL `http://dx.doi.org/10.1038/nri1085`.

[87] W. L. Redmond and L. A. Sherman. Peripheral tolerance of cd8 t lymphocytes. *Immunity*, **22**(3):275–284, Mar 2005. doi: 10.1016/j.immuni.2005.01.010. URL `http://dx.doi.org/10.1016/j.immuni.2005.01.010`.

[88] S. C. Jameson, K. A. Hogquist and M. J. Bevan. Positive selection of thymocytes. *Annu Rev Immunol*, **13**:93–126, 1995. doi: 10.1146/annurev.iy.13.040195.000521. URL `http://dx.doi.org/10.1146/annurev.iy.13.040195.000521`.

[89] J. Sprent. Central tolerance of t cells. *Int Rev Immunol*, **13**(2):95–105, 1995.

[90] J. Sprent and H. Kishimoto. The thymus and negative selection. *Immunol Rev*, **185**:126–135, Jul 2002.

[91] R. N. Germain, E. H. Levine and J. Madrenas. *Immunologist*, **3/4**:113–121, 1995.

[92] C. A. Janeway. Ligands for the t-cell receptor: hard times for avidity models. *Immunology Today*, **16**(5):223 – 225, 1995. ISSN 0167-5699. doi: 10.1016/0167-5699(95)80163-4. URL http://www.sciencedirect.com/science/article/pii/0167569995801634.

[93] S. M. Alam, P. J. Travers, J. L. Wung, W. Nasholds, S. Redpath, S. C. Jameson and N. R. J. Gascoigne. T-cell-receptor affinity and thymocyte positive selection. *Nature*, **381**(6583):616–620, 1996. 10.1038/381616a0.

[94] T. W. McKeithan. Kinetic proofreading in t-cell receptor signal transduction. *Proc Natl Acad Sci U S A*, **92**(11):5042–5046, May 1995.

[95] A. M. Mowat. Anatomical basis of tolerance and immunity to intestinal antigens. *Nat Rev Immunol*, **3**(4):331–341, Apr 2003. doi: 10.1038/nri1057. URL http://dx.doi.org/10.1038/nri1057.

[96] G. Y. Liu, P. J. Fairchild, R. M. Smith, J. R. Prowle, D. Kioussis and D. C. Wraith. Low avidity recognition of self-antigen by t cells permits escape from central tolerance. *Immunity*, **3**(4):407–415, Oct 1995.

[97] P. S. Ohashi, S. Oehen, K. Buerki, H. Pircher, C. T. Ohashi, B. Odermatt, B. Malissen, R. M. Zinkernagel and H. Hengartner. Ablation of "tolerance" and induction of diabetes by virus infection in viral antigen transgenic mice. *Cell*, **65**(2):305–317, Apr 1991.

[98] S. Sakaguchi. Naturally arising cd4+ regulatory t cells for immunologic self-tolerance and negative control of immune responses. *Annu Rev Immunol*, **22**:531–562, 2004. doi: 10.1146/annurev.immunol.21.120601.141122. URL http://dx.doi.org/10.1146/annurev.immunol.21.120601.141122.

[99] M. S. Jordan, A. Boesteanu, A. J. Reed, A. L. Petrone, A. E. Holenbeck, M. A. Lerman, A. Naji and A. J. Caton. Thymic selection of cd4+cd25+ regulatory t cells induced by an agonist self-peptide. *Nat Immunol*, **2**(4):301–306, Apr 2001. doi: 10.1038/86302. URL http://dx.doi.org/10.1038/86302.

[100] T. Takahashi, Y. Kuniyasu, M. Toda, N. Sakaguchi, M. Itoh, M. Iwata, J. Shimizu and S. Sakaguchi. Immunologic self-tolerance maintained by cd25+cd4+ naturally anergic and suppressive t cells: induction of autoimmune disease by breaking their anergic/suppressive state. *Int Immunol*, **10**(12):1969–1980, Dec 1998.

[101] A. M. Thornton and E. M. Shevach. Cd4+cd25+ immunoregulatory t cells suppress polyclonal t cell activation in vitro by inhibiting interleukin 2 production. *J Exp Med*, **188**(2):287–296, Jul 1998.

[102] S. Read, S. Mauze, C. Asseman, A. Bean, R. Coffman and F. Powrie. Cd38+ cd45rb(low) cd4+ t cells: a population of t cells with immune regulatory activities in vitro. *Eur J Immunol*, **28**(11):3435–3447, Nov 1998.

[103] L. Cederbom, H. Hall and F. Ivars. Cd4+cd25+ regulatory t cells down-regulate co-stimulatory molecules on antigen-presenting cells. *Eur J Immunol*, **30**(6):1538–1543, Jun 2000.

[104] R. M. Steinman, D. Hawiger and M. C. Nussenzweig. Tolero-genic dendritic cells. *Annu Rev Immunol*, **21**:685–711, 2003. doi: 10.1146/annurev.immunol.21.120601.141040. URL http://dx.doi.org/10.1146/annurev.immunol.21.120601.141040.

[105] L. H. Boise, A. J. Minn, P. J. Noel, C. H. June, M. A. Accavitti, T. Lindsten and C. B. Thompson. Cd28 costimulation can promote t cell survival by enhancing the expression of bcl-xl. *Immunity*, **3**(1):87–98, Jul 1995.

[106] E. R. Kearney, K. A. Pape, D. Y. Loh and M. K. Jenkins. Visualization of peptide-specific t cell immunity and peripheral tolerance induction in vivo. *Immunity*, **1**(4):327–339, Jul 1994.

[107] J. Hernandez, S. Aung, W. L. Redmond and L. A. Sherman. Phenotypic and functional analysis of cd8(+) t cells undergoing peripheral deletion in response to cross-presentation of self-antigen. *J Exp Med*, **194**(6):707–717, Sep 2001.

[108] T. C. Manning and D. M. Kranz. Binding energetics of t-cell receptors: corre-lation with immunological consequences. *Immunol Today*, **20**(9):417–422, Sep 1999.

[109] R. N. Germain and I. Stefanov. The dynamics of t cell receptor signaling: complex orchestration and the key roles of tempo and cooperation. *Annu Rev Immunol*, **17**:467–522, 1999. doi: 10.1146/annurev.immunol.17.1.467. URL http://dx.doi.org/10.1146/annurev.immunol.17.1.467.

[110] S. C. Jameson and M. J. Bevan. T cell receptor antagonists and partial ago-nists. *Immunity*, **2**(1):1–11, Jan 1995.

[111] G. J. Kersh and P. M. Allen. Essential flexibility in the t-cell recognition of antigen. *Nature*, **380**(6574):495–498, Apr 1996. doi: 10.1038/380495a0. URL http://dx.doi.org/10.1038/380495a0.

[112] C. Rosette, G. Werlen, M. A. Daniels, P. O. Holman, S. M. Alam, P. J. Travers, N. R. Gascoigne, E. Palmer and S. C. Jameson. The impact of duration versus extent of tcr occupancy on t cell activation: a revision of the kinetic proofreading model. *Immunity*, **15**(1):59–70, Jul 2001.

[113] A. E. Denton, R. Wesselingh, S. Gras, C. Guillonneau, M. R. Olson, J. D. Mintern, W. Zeng, D. C. Jackson, J. Rossjohn, P. D. Hodgkin, P. C. Doherty and S. J. Turner. Affinity thresholds for naive cd8+ ctl activation by peptides and engineered influenza a viruses. *J Immunol*, **187**(11):5733–5744, Dec 2011. doi: 10.4049/jimmunol.1003937. URL http://dx.doi.org/10.4049/jimmunol.1003937.

[114] D. S. Lyons, S. A. Lieberman, J. Hampl, J. J. Boniface, Y. Chien, L. J. Berg and M. M. Davis. A tcr binds to antagonist ligands with lower affinities and faster dissociation rates than to agonists. *Immunity*, **5**(1):53–61, Jul 1996.

[115] J. Madrenas and R. N. Germain. Variant tcr ligands: new insights into the molecular basis of antigen-dependent signal transduction and t-cell activation. *Semin Immunol*, **8**(2):83–101, Apr 1996.

[116] E. Corse, R. A. Gottschalk and J. P. Allison. Strength of tcr-peptide/mhc interactions and in vivo t cell responses. *J Immunol*, **186**(9):5039–5045, May 2011. doi: 10.4049/jimmunol.1003650. URL http://dx.doi.org/10.4049/jimmunol.1003650.

[117] C. Wlfing, J. D. Rabinowitz, C. Beeson, M. D. Sjaastad, H. M. McConnell and M. M. Davis. Kinetics and extent of t cell activation as measured with the calcium signal. *J Exp Med*, **185**(10):1815–1825, May 1997.

[118] J.-L. Chen, A. J. Morgan, G. Stewart-Jones, D. Shepherd, G. Bossi, L. Wooldridge, S. L. Hutchinson, A. K. Sewell, G. M. Griffiths, P. A. van der Merwe, E. Y. Jones, A. Galione and V. Cerundolo. Ca2+ release from the endoplasmic reticulum of ny-eso-1-specific t cells is modulated by the affinity of tcr and by the use of the cd8 coreceptor. *J Immunol*, **184**(4):1829–1839, Feb 2010. doi: 10.4049/jimmunol.0902103. URL http://dx.doi.org/10.4049/jimmunol.0902103.

[119] P. P. Yachi, J. Ampudia, T. Zal and N. R. J. Gascoigne. Altered peptide ligands induce delayed cd8-t cell receptor interaction–a role for cd8 in distinguishing antigen quality. *Immunity*, **25**(2):203–211, Aug 2006. doi: 10.1016/j.immuni.2006.05.015. URL http://dx.doi.org/10.1016/j.immuni.2006.05.015.

[120] D. Zehn, S. Y. Lee and M. J. Bevan. Complete but curtailed t-cell response to very low-affinity antigen. *Nature*, **458**(7235):211–214, Mar 2009. doi: 10.1038/nature07657. URL http://dx.doi.org/10.1038/nature07657.

[121] L. Malherbe, C. Hausl, L. Teyton and M. G. McHeyzer-Williams. Clonal selection of helper t cells is determined by an affinity threshold with no further skewing of tcr binding properties. *Immunity*, **21**(5):669–679, Nov 2004. doi: 10.1016/j.immuni.2004.09.008. URL http://dx.doi.org/10.1016/j.immuni.2004.09.008.

[122] J. J. Moon, H. H. Chu, M. Pepper, S. J. McSorley, S. C. Jameson, R. M. Kedl and M. K. Jenkins. Naive cd4(+) t cell frequency varies for different epitopes and predicts repertoire diversity and response magnitude. *Immunity*, **27**(2):203–213, Aug 2007. doi: 10.1016/j.immuni.2007.07.007. URL http://dx.doi.org/10.1016/j.immuni.2007.07.007.

[123] D. H. Busch and E. G. Pamer. T cell affinity maturation by selective expansion during infection. *J Exp Med*, **189**(4):701–710, Feb 1999.

[124] J. W. J. van Heijst, C. Gerlach, E. Swart, D. Sie, C. Nunes-Alves, R. M. Kerkhoven, R. Arens, M. Correia-Neves, K. Schepers and T. N. M. Schumacher. Recruitment of antigen-specific cd8+ t cells in response to infection is markedly efficient. *Science*, **325**(5945):1265–1269, Sep 2009. doi: 10.1126/science.1175455. URL `http://dx.doi.org/10.1126/science.1175455`.

[125] C. S. Clements, M. A. Dunstone, W. A. Macdonald, J. McCluskey and J. Rossjohn. Specificity on a knife-edge: the alphabeta t cell receptor. *Curr Opin Struct Biol*, **16**(6):787–795, Dec 2006. doi: 10.1016/j.sbi.2006.09.004. URL `http://dx.doi.org/10.1016/j.sbi.2006.09.004`.

[126] J. D. Stone, A. S. Chervin and D. M. Kranz. T-cell receptor binding affinities and kinetics: impact on t-cell activity and specificity. *Immunology*, **126**(2):165–176, Feb 2009. doi: 10.1111/j.1365-2567.2008.03015.x. URL `http://dx.doi.org/10.1111/j.1365-2567.2008.03015.x`.

[127] L. Malherbe, L. Mark, N. Fazilleau, L. J. McHeyzer-Williams and M. G. McHeyzer-Williams. Vaccine adjuvants alter tcr-based selection thresholds. *Immunity*, **28**(5):698–709, May 2008. doi: 10.1016/j.immuni.2008.03.014. URL `http://dx.doi.org/10.1016/j.immuni.2008.03.014`.

[128] P. A. Savage, J. J. Boniface and M. M. Davis. A kinetic basis for t cell receptor repertoire selection during an immune response. *Immunity*, **10**(4): 485–492, Apr 1999.

[129] S. Ehl, P. Klenerman, P. Aichele, H. Hengartner and R. M. Zinkernagel. A functional and kinetic comparison of antiviral effector and memory cytotoxic t lymphocyte populations in vivo and in vitro. *Eur J Immunol*, **27**(12):3404–3413, Dec 1997. doi: 10.1002/eji.1830271240. URL `http://dx.doi.org/10.1002/eji.1830271240`.

[130] D. C. Jackson, G. L. Ada and R. Tha Hla. Cytotoxic t cells recognize very early, minor changes in ectromelia virus-infected target cells. *Aust J Exp Biol Med Sci*, **54**(4):349–363, Aug 1976.

[131] R. M. Zinkernagel and A. Althage. Antiviral protection by virus-immune cytotoxic t cells: infected target cells are lysed before infectious virus progeny is assembled. *J Exp Med*, **145**(3):644–651, Mar 1977.

[132] R. C. Brower, R. England, T. Takeshita, S. Kozlowski, D. H. Margulies, J. A. Berzofsky and C. Delisi. Minimal requirements for peptide mediated activation of cd8+ ctl. *Mol Immunol*, **31**(16):1285–1293, Nov 1994.

[133] S. J. Brodie, D. A. Lewinsohn, B. K. Patterson, D. Jiyamapa, J. Krieger, L. Corey, P. D. Greenberg and S. R. Riddell. In vivo migration and function of transferred hiv-1-specific cytotoxic t cells. *Nat Med*, **5**(1):34–41, Jan 1999. doi: 10.1038/4716. URL `http://dx.doi.org/10.1038/4716`.

[134] S. Valitutti, S. Mller, M. Cella, E. Padovan and A. Lanzavecchia. Serial triggering of many t-cell receptors by a few peptide-mhc complexes.

Nature, **375**(6527):148–151, May 1995. doi: 10.1038/375148a0. URL http://dx.doi.org/10.1038/375148a0.

[135] A. G. Cawthon and M. A. Alexander-Miller. Optimal colocalization of tcr and cd8 as a novel mechanism for the control of functional avidity. *J Immunol*, **169**(7):3492–3498, Oct 2002.

[136] A. G. Cawthon, H. Lu and M. A. Alexander-Miller. Peptide requirement for ctl activation reflects the sensitivity to cd3 engagement: correlation with cd8alphabeta versus cd8alphaalpha expression. *J Immunol*, **167**(5):2577–2584, Sep 2001.

[137] C. Prussin and D. D. Metcalfe. Detection of intracytoplasmic cytokine using flow cytometry and directly conjugated anti-cytokine antibodies. *J Immunol Methods*, **188**(1):117–128, Dec 1995.

[138] K. T. Brunner, J. Mauel, J. C. Cerottini and B. Chapuis. Quantitative assay of the lytic action of immune lymphoid cells on 51-cr-labelled allogeneic target cells in vitro; inhibition by isoantibody and by drugs. *Immunology*, **14**(2): 181–196, Feb 1968.

[139] B. Liedberg, C. Nylander and L. I. Surface plasmon resonance for gas detection and biosensing. *Sensors and Actuators*, **4**:299–304, 1983.

[140] L. G. Fgerstam, A. Frostell-Karlsson, R. Karlsson, B. Persson and I. Rnnberg. Biospecific interaction analysis using surface plasmon resonance detection applied to kinetic, binding site and concentration analysis. *J Chromatogr*, **597** (1-2):397–410, Apr 1992.

[141] L. Jason-Moller, M. Murphy and J. Bruno. Overview of biacore systems and their applications. *Curr Protoc Protein Sci*, **Chapter 19**: Unit 19.13, Sep 2006. doi: 10.1002/0471140864.ps1913s45. URL http://dx.doi.org/10.1002/0471140864.ps1913s45.

[142] D. H. Margulies, D. Plaksin, S. N. Khilko and M. T. Jelonek. Studying interactions involving the t-cell antigen receptor by surface plasmon resonance. *Curr Opin Immunol*, **8**(2):262–270, Apr 1996.

[143] M. Corr, A. E. Slanetz, L. F. Boyd, M. T. Jelonek, S. Khilko, B. K. al Ramadi, Y. S. Kim, S. E. Maher, A. L. Bothwell and D. H. Margulies. T cell receptor-mhc class i peptide interactions: affinity, kinetics, and specificity. *Science*, **265** (5174):946–949, Aug 1994.

[144] K. C. Garcia, M. D. Tallquist, L. R. Pease, A. Brunmark, C. A. Scott, M. Degano, E. A. Stura, P. A. Peterson, I. A. Wilson and L. Teyton. Alphabeta t cell receptor interactions with syngeneic and allogeneic ligands: Affinity measurements and crystallization. *Proceedings of the National Academy of Sciences*, **94**(25):13838–13843, 1997.

[145] B. K. Al-Ramadi, M. T. Jelonek, L. F. Boyd, D. H. Margulies and A. L. Both-well. Lack of strict correlation of functional sensitization with the apparent affinity of mhc/peptide complexes for the tcr. *J Immunol*, **155**(2):662–673, Jul 1995.

[146] S. M. Alam, G. M. Davies, C. M. Lin, T. Zal, W. Nasholds, S. C. Jameson, K. A. Hogquist, N. R. J. Gascoigne and P. J. Travers. Qualitative and quanti-tative differences in t cell receptor binding of agonist and antagonist ligands. *Immunity*, **10**(2):227–237, 1999. doi: 10.1016/S1074-7613(00)80023-0.

[147] A. Y. Lin, B. Devaux, A. Green, C. Sagerstrm, J. F. Elliott and M. M. Davis. Expression of t cell antigen receptor heterodimers in a lipid-linked form. *Sci-ence*, **249**(4969):677–679, Aug 1990.

[148] P. Schuck. Kinetics of ligand binding to receptor immobilized in a poly-mer matrix, as detected with an evanescent wave biosensor. i. a com-puter simulation of the influence of mass transport. *Biophys J*, **70**(3):1230–1249, Mar 1996. doi: 10.1016/S0006-3495(96)79681-9. URL http://dx.doi.org/10.1016/S0006-3495(96)79681-9.

[149] J. D. Altman, P. A. Moss, P. J. Goulder, D. H. Barouch, M. G. McHeyzer-Williams, J. I. Bell, A. J. McMichael and M. M. Davis. Phenotypic analysis of antigen-specific t lymphocytes. *Science*, **274**(5284):94–96, Oct 1996.

[150] X. L. Wang and J. D. Altman. Caveats in the design of mhc class i tetramer/antigen-specific t lymphocytes dissociation as-says. *Journal of Immunological Methods*, **280**(1-2):25 – 35, 2003. ISSN 0022-1759. doi: 10.1016/S0022-1759(03)00079-6. URL http://www.sciencedirect.com/science/article/pii/S0022175903000796.

[151] F. Crawford, H. Kozono, J. White, P. Marrack and J. Kappler. Detection of antigen-specific t cells with multivalent soluble class ii mhc covalent peptide complexes. *Immunity*, **8**(6):675–682, Jun 1998.

[152] T. M. Fahmy, J. G. Bieler and J. P. Schneck. Probing t cell membrane organi-zation using dimeric mhc-ig complexes. *J Immunol Methods*, **268**(1):93–106, Oct 2002.

[153] W. Rees, J. Bender, T. K. Teague, R. M. Kedl, F. Crawford, P. Marrack and J. Kappler. An inverse relationship between t cell receptor affinity and antigen dose during cd4(+) t cell responses in vivo and in vitro. *Proc Natl Acad Sci U S A*, **96**(17):9781–9786, Aug 1999.

[154] H. Echchakir, G. Dorothe, I. Vergnon, J. Menez, S. Chouaib and F. Mami-Chouaib. Cytotoxic t lymphocytes directed against a tumor-specific mutated antigen display similar hla tetramer binding but dis-tinct functional avidity and tissue distribution. *Proc Natl Acad Sci U S A*, **99**(14):9358–9363, Jul 2002. doi: 10.1073/pnas.142308199. URL http://dx.doi.org/10.1073/pnas.142308199.

[155] T. M. Lawson, S. Man, E. C. Wang, S. Williams, N. Amos, G. M. Gillespie, P. A. Moss and L. K. Borysiewicz. Functional differences between influenza a-specific cytotoxic t lymphocyte clones expressing dominant and subdominant tcr. *Int Immunol*, **13**(11):1383–1390, Nov 2001.

[156] B. Palermo, R. Campanelli, S. Mantovani, E. Lantelme, A. M. Manganoni, G. Carella, G. Da Prada, G. R. della Cuna, F. Romagne, L. Gauthier, A. Necker and C. Giachino. Diverse expansion potential and heterogeneous avidity in tumor-associated antigen-specific t lymphocytes from primary melanoma patients. *Eur J Immunol*, **31**(2):412–420, Feb 2001. doi: 62;3.0.CO;2-4. URL http://dx.doi.org/62;3.0.CO;2-4.

[157] A. Amrani, J. Verdaguer, P. Serra, S. Tafuro, R. Tan and P. Santamaria. Progression of autoimmune diabetes driven by avidity maturation of a t-cell population. *Nature*, **406**(6797):739–742, Aug 2000. doi: 10.1038/35021081. URL http://dx.doi.org/10.1038/35021081.

[158] J. N. Blattman, R. Antia, D. J. D. Sourdive, X. Wang, S. M. Kaech, K. Murali-Krishna, J. D. Altman and R. Ahmed. Estimating the precursor frequency of naive antigen-specific cd8 t cells. *J Exp Med*, **195**(5):657–664, Mar 2002.

[159] V. Dutoit, V. Rubio-Godoy, M.-A. Doucey, P. Batard, D. Linard, D. Rimoldi, D. Speiser, P. Guillaume, J.-C. Cerottini, P. Romero and D. Valmori. Functional avidity of tumor antigen-specific ctl recognition directly correlates with the stability of mhc/peptide multimer binding to tcr. *J Immunol*, **168**(3):1167–1171, Feb 2002.

[160] V. Rubio-Godoy, V. Dutoit, D. Rimoldi, D. Lienard, F. Lejeune, D. Speiser, P. Guillaume, J. C. Cerottini, P. Romero and D. Valmori. Discrepancy between elispot ifn-gamma secretion and binding of a2/peptide multimers to tcr reveals interclonal dissociation of ctl effector function from tcr-peptide/mhc complexes half-life. *Proc Natl Acad Sci U S A*, **98**(18):10302–10307, Aug 2001. doi: 10.1073/pnas.181348898. URL http://dx.doi.org/10.1073/pnas.181348898.

[161] D. Valmori, V. Dutoit, V. Schnuriger, A.-L. Quiquerez, M. J. Pittet, P. Guillaume, V. Rubio-Godoy, P. R. Walker, D. Rimoldi, D. Linard, J.-C. Cerottini, P. Romero and P.-Y. Dietrich. Vaccination with a melan-a peptide selects an oligoclonal t cell population with increased functional avidity and tumor reactivity. *J Immunol*, **168**(8):4231–4240, Apr 2002.

[162] D. Drake, 3rd and T. J. Braciale. Cutting edge: lipid raft integrity affects the efficiency of mhc class i tetramer binding and cell surface tcr arrangement on cd8+ t cells. *J Immunol*, **166**(12):7009–7013, Jun 2001.

[163] P. A. Savage and M. M. Davis. A kinetic window constricts the t cell receptor repertoire in the thymus. *Immunity*, **14**(3):243–252, 2001. doi: 10.1016/S1074-7613(01)00106-6.

[164] R. Knall. *Direct ex vivo identification of individual antigen-specific T cells with optimal avidity for protection.* PhD thesis, TU Muenchen, 2007.

[165] S. R. Riddell and P. D. Greenberg. Principles for adoptive t cell therapy of human viral diseases. *Annu Rev Immunol*, **13**: 545–586, 1995. doi: 10.1146/annurev.iy.13.040195.002553. URL http://dx.doi.org/10.1146/annurev.iy.13.040195.002553.

[166] S. Ehl, P. Klenerman, R. M. Zinkernagel and G. Bocharov. The impact of variation in the number of cd8(+) t-cell precursors on the outcome of virus infection. *Cell Immunol*, **189**(1):67–73, Oct 1998. doi: 10.1006/cimm.1998.1344. URL http://dx.doi.org/10.1006/cimm.1998.1344.

[167] S. R. Riddell, K. S. Watanabe, J. M. Goodrich, C. R. Li, M. E. Agha and P. D. Greenberg. Restoration of viral immunity in immunodeficient humans by the adoptive transfer of t cell clones. *Science*, **257**(5067):238–241, Jul 1992.

[168] M. A. Roskrow, N. Suzuki, Y. Gan, J. W. Sixbey, C. Y. Ng, S. Kimbrough, M. Hudson, M. K. Brenner, H. E. Heslop and C. M. Rooney. Epstein-barr virus (ebv)-specific cytotoxic t lymphocytes for the treatment of patients with ebv-positive relapsed hodgkin's disease. *Blood*, **91**(8):2925–2934, Apr 1998.

[169] E. A. Walter, P. D. Greenberg, M. J. Gilbert, R. J. Finch, K. S. Watanabe, E. D. Thomas and S. R. Riddell. Reconstitution of cellular immunity against cytomegalovirus in recipients of allogeneic bone marrow by transfer of t-cell clones from the donor. *N Engl J Med*, **333** (16):1038–1044, Oct 1995. doi: 10.1056/NEJM199510193331603. URL http://dx.doi.org/10.1056/NEJM199510193331603.

[170] H. Einsele, E. Roosnek, N. Rufer, C. Sinzger, S. Riegler, J. Lffler, U. Grigoleit, A. Moris, H.-G. Rammensee, L. Kanz, A. Kleihauer, F. Frank, G. Jahn and H. Hebart. Infusion of cytomegalovirus (cmv)-specific t cells for the treatment of cmv infection not responding to antiviral chemotherapy. *Blood*, **99**(11): 3916–3922, Jun 2002.

[171] K. S. Peggs. Adoptive t cell immunotherapy for cytomegalovirus. *Expert Opin Biol Ther*, **9**(6):725–736, Jun 2009. doi: 10.1517/14712590902967588. URL http://dx.doi.org/10.1517/14712590902967588.

[172] H. Einsele, M. Kapp and G. U. Grigoleit. Cmv-specific t cell therapy. *Blood Cells Mol Dis*, **40**(1):71–75, 2008. doi: 10.1016/j.bcmd.2007.07.002. URL http://dx.doi.org/10.1016/j.bcmd.2007.07.002.

[173] M. Knabel, T. J. Franz, M. Schiemann, A. Wulf, B. Villmow, B. Schmidt, H. Bernhard, H. Wagner and D. H. Busch. Reversible mhc multimer staining for functional isolation of t-cell populations and effective adoptive transfer. *Nat Med*, **8**(6):631–637, Jun 2002. doi: 10.1038/nm0602-631. URL http://dx.doi.org/10.1038/nm0602-631.

[174] A. M. Leen, C. M. Rooney and A. E. Foster. Improving t cell therapy for cancer. *Annu Rev Immunol*, **25**:243–265, 2007. doi: 10.1146/annurev.immunol.25.022106.141527. URL `http://dx.doi.org/10.1146/annurev.immunol.25.022106.141527`.

[175] C. Berger, C. J. Turtle, M. C. Jensen and S. R. Riddell. Adoptive transfer of virus-specific and tumor-specific t cell immunity. *Curr Opin Immunol*, **21**(2):224–232, Apr 2009. doi: 10.1016/j.coi.2009.02.010. URL `http://dx.doi.org/10.1016/j.coi.2009.02.010`.

[176] S. A. Rosenberg, J. R. Yannelli, J. C. Yang, S. L. Topalian, D. J. Schwartzentruber, J. S. Weber, D. R. Parkinson, C. A. Seipp, J. H. Einhorn and D. E. White. Treatment of patients with metastatic melanoma with autologous tumor-infiltrating lymphocytes and interleukin 2. *J Natl Cancer Inst*, **86**(15): 1159–1166, Aug 1994.

[177] C. M. Rooney, C. A. Smith, C. Y. Ng, S. K. Loftin, J. W. Sixbey, Y. Gan, D. K. Srivastava, L. C. Bowman, R. A. Krance, M. K. Brenner and H. E. Heslop. Infusion of cytotoxic t cells for the prevention and treatment of epstein-barr virus-induced lymphoma in allogeneic transplant recipients. *Blood*, **92**(5): 1549–1555, Sep 1998.

[178] M. E. Dudley, J. C. Yang, R. Sherry, M. S. Hughes, R. Royal, U. Kammula, P. F. Robbins, J. Huang, D. E. Citrin, S. F. Leitman, J. Wunderlich, N. P. Restifo, A. Thomasian, S. G. Downey, F. O. Smith, J. Klapper, K. Morton, C. Laurencot, D. E. White and S. A. Rosenberg. Adoptive cell therapy for patients with metastatic melanoma: evaluation of intensive myeloablative chemoradiation preparative regimens. *J Clin Oncol*, **26**(32):5233–5239, Nov 2008. doi: 10.1200/JCO.2008.16.5449. URL `http://dx.doi.org/10.1200/JCO.2008.16.5449`.

[179] M. E. Dudley, J. R. Wunderlich, P. F. Robbins, J. C. Yang, P. Hwu, D. J. Schwartzentruber, S. L. Topalian, R. Sherry, N. P. Restifo, A. M. Hubicki, M. R. Robinson, M. Raffeld, P. Duray, C. A. Seipp, L. Rogers-Freezer, K. E. Morton, S. A. Mavroukakis, D. E. White and S. A. Rosenberg. Cancer regression and autoimmunity in patients after clonal repopulation with antitumor lymphocytes. *Science*, **298**(5594):850–854, 2002.

[180] M. E. Dudley, J. R. Wunderlich, J. C. Yang, R. M. Sherry, S. L. Topalian, N. P. Restifo, R. E. Royal, U. Kammula, D. E. White, S. A. Mavroukakis, L. J. Rogers, G. J. Gracia, S. A. Jones, D. P. Mangiameli, M. M. Pelletier, J. Gea-Banacloche, M. R. Robinson, D. M. Berman, A. C. Filie, A. Abati and S. A. Rosenberg. Adoptive cell transfer therapy following non-myeloablative but lymphodepleting chemotherapy for the treatment of patients with refractory metastatic melanoma. *Journal of Clinical Oncology*, **23**(10):2346–2357, 2005.

[181] R. Perret and F. Ronchese. Memory t cells in cancer immunotherapy: which cd8 t-cell population provides the best protection against tumours? *Tissue*

Antigens, **72**(3):187–194, Sep 2008. doi: 10.1111/j.1399-0039.2008.01088.x. URL http://dx.doi.org/10.1111/j.1399-0039.2008.01088.x.

[182] B. Ludewig, S. Oehen, F. Barchiesi, R. A. Schwendener, H. Hengartner and R. M. Zinkernagel. Protective antiviral cytotoxic t cell memory is most efficiently maintained by restimulation via dendritic cells. *J Immunol*, **163**(4): 1839–1844, Aug 1999.

[183] A. D. Roberts and D. L. Woodland. Cutting edge: effector memory cd8+ t cells play a prominent role in recall responses to secondary viral infection in the lung. *J Immunol*, **172**(11):6533–6537, Jun 2004.

[184] E. J. Wherry, V. Teichgrber, T. C. Becker, D. Masopust, S. M. Kaech, R. Antia, U. H. von Andrian and R. Ahmed. Lineage relationship and protective immunity of memory cd8 t cell subsets. *Nat Immunol*, **4**(3):225–234, Mar 2003. doi: 10.1038/ni889. URL http://dx.doi.org/10.1038/ni889.

[185] C. Berger, M. C. Jensen, P. M. Lansdorp, M. Gough, C. Elliott and S. R. Riddell. Adoptive transfer of effector cd8+ t cells derived from central memory cells establishes persistent t cell memory in primates. *J Clin Invest*, **118**(1):294–305, Jan 2008. doi: 10.1172/JCI32103. URL http://dx.doi.org/10.1172/JCI32103.

[186] S. M. Kaech, J. T. Tan, E. J. Wherry, B. T. Konieczny, C. D. Surh and R. Ahmed. Selective expression of the interleukin 7 receptor identifies effector cd8 t cells that give rise to long-lived memory cells. *Nat Immunol*, **4**(12):1191–1198, Dec 2003. doi: 10.1038/ni1009. URL http://dx.doi.org/10.1038/ni1009.

[187] C. A. Klebanoff, L. Gattinoni, P. Torabi-Parizi, K. Kerstann, A. R. Cardones, S. E. Finkelstein, D. C. Palmer, P. A. Antony, S. T. Hwang, S. A. Rosenberg, T. A. Waldmann and N. P. Restifo. Central memory self/tumor-reactive cd8+ t cells confer superior antitumor immunity compared with effector memory t cells. *Proc Natl Acad Sci U S A*, **102**(27):9571–9576, Jul 2005. doi: 10.1073/pnas.0503726102. URL http://dx.doi.org/10.1073/pnas.0503726102.

[188] C. A. Klebanoff, L. Gattinoni and N. P. Restifo. Cd8+ t-cell memory in tumor immunology and immunotherapy. *Immunol Rev*, **211**: 214–224, Jun 2006. doi: 10.1111/j.0105-2896.2006.00391.x. URL http://dx.doi.org/10.1111/j.0105-2896.2006.00391.x.

[189] Y. Zhao, Z. Zheng, P. F. Robbins, H. T. Khong, S. A. Rosenberg and R. A. Morgan. Primary human lymphocytes transduced with ny-eso-1 antigen-specific tcr genes recognize and kill diverse human tumor cell lines. *The Journal of Immunology*, **174**(7):4415–4423, 2005.

[190] T. M. Clay, M. C. Custer, J. Sachs, P. Hwu, S. A. Rosenberg and M. I. Nishimura. Efficient transfer of a tumor antigen-reactive tcr to human pe-

ripheral blood lymphocytes confers anti-tumor reactivity. *The Journal of Immunology*, **163**(1):507–513, 1999.

[191] R. A. Morgan, M. E. Dudley, Y. Y. L. Yu, Z. Zheng, P. F. Robbins, M. R. Theoret, J. R. Wunderlich, M. S. Hughes, N. P. Restifo and S. A. Rosenberg. High efficiency tcr gene transfer into primary human lymphocytes affords avid recognition of melanoma tumor antigen glycoprotein 100 and does not alter the recognition of autologous melanoma antigens. *The Journal of Immunology*, **171**(6):3287–3295, 2003.

[192] M. H. M. Heemskerk, M. Hoogeboom, R. Hagedoorn, M. G. D. Kester, R. Willemze and J. H. F. Falkenburg. Reprogramming of virus-specific t cells into leukemia-reactive t cells using t cell receptor gene transfer. *J Exp Med*, **199**(7):885–894, Apr 2004. doi: 10.1084/jem.20031110. URL http://dx.doi.org/10.1084/jem.20031110.

[193] M. H. M. Heemskerk, M. Hoogeboom, R. A. de Paus, M. G. D. Kester, M. A. W. G. van der Hoorn, E. Goulmy, R. Willemze and J. H. F. Falkenburg. Redirection of antileukemic reactivity of peripheral t lymphocytes using gene transfer of minor histocompatibility antigen ha-2-specific t-cell receptor complexes expressing a conserved alpha joining region. *Blood*, **102**(10):3530–3540, Nov 2003. doi: 10.1182/blood-2003-05-1524. URL http://dx.doi.org/10.1182/blood-2003-05-1524.

[194] S.-A. Xue, L. Gao, D. Hart, R. Gillmore, W. Qasim, A. Thrasher, J. Apperley, B. Engels, W. Uckert, E. Morris and H. Stauss. Elimination of human leukemia cells in nod/scid mice by wt1-tcr gene-transduced human t cells. *Blood*, **106**(9):3062–3067, Nov 2005. doi: 10.1182/blood-2005-01-0146. URL http://dx.doi.org/10.1182/blood-2005-01-0146.

[195] T. Stanislawski, R. H. Voss, C. Lotz, E. Sadovnikova, R. A. Willemsen, J. Kuball, T. Ruppert, R. L. Bolhuis, C. J. Melief, C. Huber, H. J. Stauss and M. Theobald. Circumventing tolerance to a human mdm2-derived tumor antigen by tcr gene transfer. *Nat Immunol*, **2**(10):962–970, Oct 2001. doi: 10.1038/ni1001-962. URL http://dx.doi.org/10.1038/ni1001-962.

[196] T. van Meerten, M.-J. Claessen, A. Hagenbeek and S. B. Ebeling. The cd20/alphacd20 'suicide' system: novel vectors with improved safety and expression profiles and efficient elimination of cd20-transgenic t cells. *Gene Ther*, **13**(9):789–797, May 2006. doi: 10.1038/sj.gt.3302705. URL http://dx.doi.org/10.1038/sj.gt.3302705.

[197] C. Berger, M. E. Flowers, E. H. Warren and S. R. Riddell. Analysis of transgene-specific immune responses that limit the in vivo persistence of adoptively transferred hsv-tk-modified donor t cells after allogeneic hematopoietic cell transplantation. *Blood*, **107**(6):2294–2302, Mar 2006. doi: 10.1182/blood-2005-08-3503. URL http://dx.doi.org/10.1182/blood-2005-08-3503.

[198] A. Di Stasi, S.-K. Tey, G. Dotti, Y. Fujita, A. Kennedy-Nasser, C. Martinez, K. Straathof, E. Liu, A. G. Durett, B. Grilley, H. Liu, C. R. Cruz, B. Savoldo, A. P. Gee, J. Schindler, R. A. Krance, H. E. Heslop, D. M. Spencer, C. M. Rooney and M. K. Brenner. Inducible apoptosis as a safety switch for adoptive cell therapy. *N Engl J Med*, **365**(18):1673–1683, Nov 2011. doi: 10.1056/NEJMoa1106152. URL http://dx.doi.org/10.1056/NEJMoa1106152.

[199] E. Kieback, J. Charo, D. Sommermeyer, T. Blankenstein and W. Uckert. A safeguard eliminates t cell receptor gene-modified autoreactive t cells after adoptive transfer. *Proc Natl Acad Sci U S A*, **105**(2):623–628, Jan 2008. doi: 10.1073/pnas.0710198105. URL http://dx.doi.org/10.1073/pnas.0710198105.

[200] K. C. Parker and J. L. Strominger. Localization of the sites of iodination of human .beta.2-microglobulin; quaternary structure implications for histocompatibility antigens. *Biochemistry*, **22**(5):1145–1153, 1983. doi: 10.1021/bi00274a024. URL http://pubs.acs.org/doi/abs/10.1021/bi00274a024.

[201] J. B. Walter, D. N. Garboczi, Q. R. Fan, X. Zhou, B. D. Walker and H. N. Eisen. A mutant human 2-microglobulin can be used to generate diverse multimeric class i peptide complexes as specific probes for t cell receptors. *Journal of Immunological Methods*, **214**(1-2):41 – 50, 1998. ISSN 0022-1759. doi: 10.1016/S0022-1759(98)00035-0. URL http://www.sciencedirect.com/science/article/pii/S0022175998000350.

[202] T. G. Schmidt, J. Koepke, R. Frank and A. Skerra. Molecular interaction between the strep-tag affinity peptide and its cognate target, streptavidin. *J Mol Biol*, **255**(5):753–766, Feb 1996. doi: 10.1006/jmbi.1996.0061. URL http://dx.doi.org/10.1006/jmbi.1996.0061.

[203] L. Kjer-Nielsen, C. S. Clements, A. G. Brooks, A. W. Purcell, M. R. Fontes, J. McCluskey and J. Rossjohn. The structure of hla-b8 complexed to an immunodominant viral determinant: peptide-induced conformational changes and a mode of mhc class i dimerization. *J Immunol*, **169**(9):5153–5160, Nov 2002.

[204] L. A. Johnson, B. Heemskerk, D. J. Powell, C. J. Cohen, R. A. Morgan, M. E. Dudley, P. F. Robbins and S. A. Rosenberg. Gene transfer of tumor-reactive tcr confers both high avidity and tumor reactivity to nonreactive peripheral blood mononuclear cells and tumor-infiltrating lymphocytes. *The Journal of Immunology*, **177**(9):6548–6559, 2006.

[205] J. Huang, V. I. Zarnitsyna, B. Liu, L. J. Edwards, N. Jiang, B. D. Evavold and C. Zhu. The kinetics of two-dimensional tcr and pmhc interactions determine t-cell responsiveness. *Nature*, **464**(7290):932–936, Apr 2010. doi: 10.1038/nature08944. URL http://dx.doi.org/10.1038/nature08944.

[206] J. B. Huppa, M. Axmann, M. A. Mrtelmaier, B. F. Lillemeier, E. W. Newell, M. Brameshuber, L. O. Klein, G. J. Schtz and M. M. Davis. Tcr-peptide-mhc interactions in situ show accelerated kinetics and increased affinity. *Nature*, **463**(7283):963–967, Feb 2010. doi: 10.1038/nature08746. URL `http://dx.doi.org/10.1038/nature08746`.

[207] M. Aleksic, O. Dushek, H. Zhang, E. Shenderov, J.-L. Chen, V. Cerundolo, D. Coombs and P. A. van der Merwe. Dependence of t cell antigen recognition on t cell receptor-peptide mhc confinement time. *Immunity*, **32**(2):163–174, Feb 2010. doi: 10.1016/j.immuni.2009.11.013. URL `http://dx.doi.org/10.1016/j.immuni.2009.11.013`.

[208] C. C. Govern, M. K. Paczosa, A. K. Chakraborty and E. S. Huseby. Fast on-rates allow short dwell time ligands to activate t cells. *Proc Natl Acad Sci U S A*, **107**(19):8724–8729, May 2010. doi: 10.1073/pnas.1000966107. URL `http://dx.doi.org/10.1073/pnas.1000966107`.

[209] C. C. Govern and A. K. Chakraborty. For t cell receptors, some breakups might not last forever. *Immunity*, **32**(2): 141–142, Feb 2010. doi: 10.1016/j.immuni.2010.02.005. URL `http://dx.doi.org/10.1016/j.immuni.2010.02.005`.

[210] A. Achour, J. Michalsson, R. A. Harris, J. Odeberg, P. Grufman, J. K. Sandberg, V. Levitsky, K. Krre, T. Sandalova and G. Schneider. A structural basis for lcmv immune evasion: subversion of h-2d(b) and h-2k(b) presentation of gp33 revealed by comparative crystal structure.analyses. *Immunity*, **17**(6): 757–768, Dec 2002.

[211] V. R. Buchholz, M. Neuenhahn and D. H. Busch. Cd8+ t cell differentiation in the aging immune system: until the last clone standing. *Curr Opin Immunol*, **23**(4):549–554, Aug 2011. doi: 10.1016/j.coi.2011.05.002. URL `http://dx.doi.org/10.1016/j.coi.2011.05.002`.

[212] M. Hudecek, T. M. Schmitt, S. Baskar, M. T. Lupo-Stanghellini, T. Nishida, T. N. Yamamoto, M. Bleakley, C. J. Turtle, W.-C. Chang, H. A. Greisman, B. Wood, D. G. Maloney, M. C. Jensen, C. Rader and S. R. Riddell. The b-cell tumor-associated antigen ror1 can be targeted with t cells modified to express a ror1-specific chimeric antigen receptor. *Blood*, **116**(22):4532–4541, Nov 2010. doi: 10.1182/blood-2010-05-283309. URL `http://dx.doi.org/10.1182/blood-2010-05-283309`.

Danksagung

An dieser Stelle möchte ich mich bei all den Personen bedanken, die mich während meiner Promotion unterstützt und so maßgeblich zum Gelingen der Arbeit beigetragen haben.

Zu allererst möchte ich Prof. Dirk Busch danken. Ich durfte ein sehr anspruchsvolles und interessantes Projekt bearbeiten und meine eigenen Ideen einbringen. Dabei konnte ich mir jedoch jederzeit Rat und Anregungen bei Prof. Busch holen und mir besonders an schwierigen Punkten sicher sein, dass er das Projekt durch neue Ideen in die richtige Richtung weiterführt. Durch diese nahe und fachlich exzellente Betreuung wurde nicht nur das Projekt erfolgreich entwickelt, ich konnte zudem wissenschaftlich viel dazulernen. Desweiteren danke ich Prof. Jörg Durner für die Betreuung meiner Promotion und Prof. Kay Schneitz für den Vorsitz der Prüfungskommission.

Ein ganz großes Dankeschön geht natürlich auch an alle aus dem Busch Labor! Meine Mitstreiter bei dem Projekt, Bianca Weißbrich und Georg Dössinger, haben mir durch angeregte Diskussionen oft weitergeholfen und auch manchmal durch gemeinsamen Galgenhumor schwierige Zeiten während der Promotion leichter gemacht. Sie haben mich außerdem sehr hilfsbereit unterstützt, als ich wegen der kleinen Lucie im Bauch nurnoch eingeschränkt experimentieren konnte. Ein Dankeschön auch an Jeannette Bet und Paulina Paszkiewicz, die mir durch die Generierung und Bereitstellung der T Zellklone sehr weitergeholfen haben. Bei Dr. Christian Stemberger, Florian Anderl, Veit Buchholz und Dr. Stefan Dreher möchte ich mich für ihre Unterstützung und enorm große Hilfsbereitschaft bedanken. Durch ihre Erfahrung und ihre Kompetenz haben sie mir fachlich sehr weitergeholfen, mir aber auch gezeigt, manche Dinge mit der nötigen Gelassenheit zu sehen. Vielen Dank auch an Dr. Matthias Schiemann, Katleen Wild und Lynette Henkel für die Zellsortierungen, die Grundlage vieler Experimente waren. Nicht vergessen möchte ich natürlich auch Anna Hochholzer, Inge Hensel, Tina Goller und Patricia Gräf, die zu einer hilfsbereiten, fachlich kompetenten, aber auch sehr lustigen Arbeitsatmosphäre im Labor beigetragen haben. Weiterhin danke ich Prof. Ulrike Protzer und Karin Krebs für die Unterstützung meiner Arbeit und anregende Diskussionen.

Für das Gelingen meiner Arbeit war aber auch die Unterstützung von Familie und Freunden sehr wichtig. Dabei geht ein besonderer Dank an meine Eltern, die mir nicht nur ein Zimmer zu Verfügung gestellt haben, in dem ich in Ruhe meine Arbeit schreiben konnte, sondern mir die Zeit des Schreibens durch wunderbare Mittagessen, aufbauende Gespräche und nicht zuletzt Kinderbetreuung sehr angenehm gemacht haben. Meinem Mann Sebastian muss ich auf viele Weise danken: Zum